AD-A107 752 GEORGIA INST OF TECH ATLANTA ENGINEERING EXPERIMENT --ETC F/G 19/1
ANTENNA CONSIDERATIONS AND SIGNAL PROCESSING TECHNIQUES FOR THE--ETC(U)
JUN 81 W J STEINWAY, J A FULLER DAAK70-78-C-0081

UNCLASSIFIED NL

1 OF 2
AD
A107752

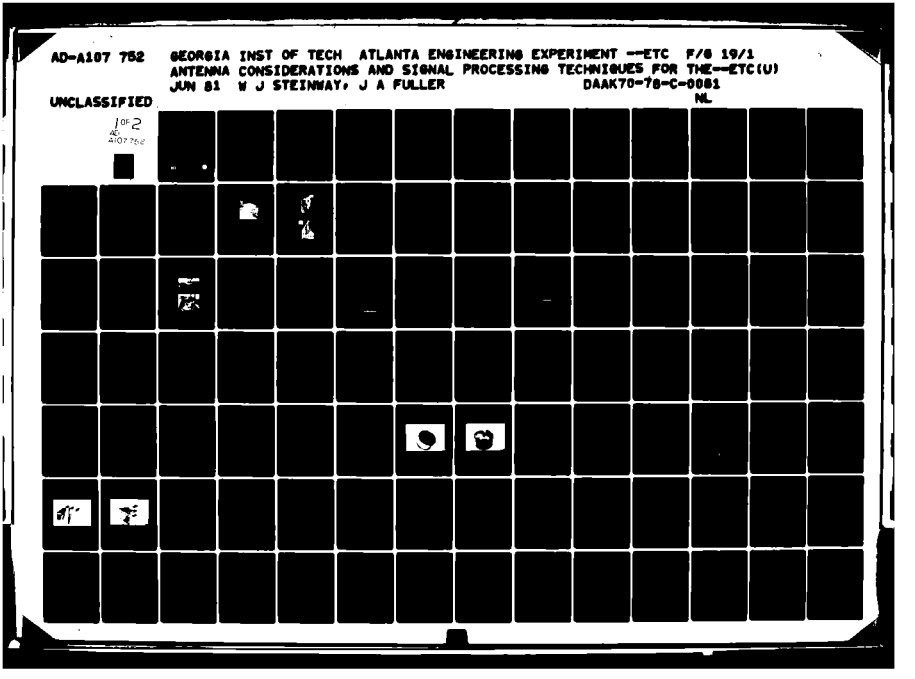

LEVEL II

2

FINAL TECHNICAL REPORT

ANTENNA CONSIDERATIONS AND SIGNAL PROCESSING TECHNIQUES FOR THE IDENTIFICATION OF BURIED NON–METALLIC OBJECTS

By

W. J. Steinway
J. A. Fuller

Prepared for

U.S. ARMY
MOBILITY EQUIPMENT RESEARCH AND DEVELOPMENT COMMAND
FT. BELVOIR, VIRGINIA 22060

Under

Contract DAAK70–78–C–0081

June 1981

GEORGIA INSTITUTE OF TECHNOLOGY
A Unit of the University System of Georgia
Engineering Experiment Station
Atlanta, Georgia 30332

GTEES

1981

FINAL TECHNICAL REPORT

ANTENNA CONSIDERATIONS AND SIGNAL PROCESSING TECHNIQUES FOR THE IDENTIFICATION OF BURIED NON-METALLIC OBJECTS

By

W. J. Steinway,
J. A. Fuller

Prepared for:

U. S. Army
Mobility Equipment Research and Development Command
Ft. Belvoir, Virginia 22060

Under

Contract DAAK70-78-C-0081

June 1981

Georgia Institute of Technology
Engineering Experiment Station
Atlanta, Georgia 30332

PREFACE

The research on this program was conducted by the Radar Analysis Division, Radar and Instrumentation Laboratory, Engineering Experiment Station, at the Georgia Institute of Technology, Atlanta, Georgia, with Dr. W. J. Steinway serving as Project Director, and Dr. J. D. Echard serving as Associate Project Director. The work was conducted for the U. S. Army Mobility Equipment research and Development Command (MERADCOM) under Contract No. DAAK70-78-C-0081, with Messrs. L. Mittleman, Jr., and M. Friedman serving successively as Technical Monitor. For internal control at Georgia Tech, the effort was designated Project A-2185.

This final report summarizes results of the work performed under the contract. Although five tasks were originally planned for this program, only three of these were funded. The work that was completed resolved some serious questions of feasibility and provides a firm basis for recommendations as to how the original objectives of the program may be realized.

This effort was the second phase of a mine detection program, begun at Georgia Tech under Contract No. DAAG53-76-C-0112. During the previous effort, MERADCOM provided to Georgia Tech data and equipment that were retained and used during the current effort. The data were frequency-domain recordings of scattering parameters for various buried objects, which were measured at the National Bureau of Standards, Boulder, Colorado. The equipment was a short pulse radar system, that was developed at Calspan for MERADCOM. We appreciate the contribution made by MERADCOM in providing this assistance. We also acknowledge with appreciation assistance and advice regarding resistively loaded antennas provided by Dr. Motohisa Kanda at the National Bureau of Standards.

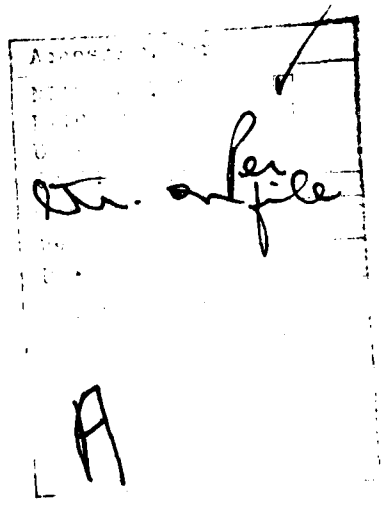

TABLE OF CONTENTS

LIST OF ILLUSTRATIONS

LIST OF ILLUSTRATIONS continued

LIST OF TABLES

SECTION I
INTRODUCTION

The U. S. Army Mobility Equipment Research and Development Command (MERADCOM) has been involved in a program for the development of an off-road mine detection system. In 1978, the Georgia Institute of Technology Engineering Experiment Station (GIT/EES) began a 36 month contract to gather and analyze radar data and investigate antenna designs with the goal of improving the ability to detect, discriminate and classify buried targets. The project included tasks of initial data analysis, antenna design and fabrication, extensive data collection, and algorithm development. The funding for the program was to be incremental in two parts. Due to Army budget reductions, the latter part was not received and, thus, the tasks of extensive data collection and algorithm development were not completed. This final report describes the work accomplished under contract DAAK70-78-C-0081.

Wideband radar data that were available had been collected by personnel of the National Bureau of Standards (NBS) in Boulder, Colorado, using a computer driven automatic analyzer. The equipment was housed in a mobile van and could be driven to any site accessible by vehicle. This equipment included a rubber-tired cart which could be commanded by the computer to advance to any of a set of predetermined positions and to then remain stationary while the data were collected. The measurements made with this equipment utilized a pair of broadband, non-dispersive antennas.

In addition, wideband radar data were collected by GIT/EES personnel using a Goverment Furnished Equipment (GFE) short-pulse radar (SPR) owned by MERADCOM. The MERADCOM radar was mounted on a small cart that could be easily moved by an operator to locations within the GIT/EES laboratory. A broadband, non-dispersive antenna which was adjustable in height was used for measurements. The wideband target signatures obtained using the SPR were compared to the network analyzer measurements to verify equivalency between the two systems. Some additional measurements mines not measured by the NBS personnel were made using the SPR.

GIT/EES personnel analyzed the data to identify characteristics in the temporal and spectral signatures of the targets. This analysis aided in the specification of advanced antenna design concepts. Task II considered many possibly antenna designs

that were suitable in a portable mine detection system. In Task III two of the most promissing antenna candidates were fabricated for testing. The first was a relatively small TEM horn that employed a tapered resistive loading on the (H-plane) walls. The feed design, the introduction of non-contracting partial sidewalls, and the flare geometry were developed at Georgia Tech to minimize the reflection coefficient in the frequency interval of 300 MHz to 1000 MHz. The second design made use of a cavity-backed spiral antenna concept; inherently wideband features of this type of antenna make it particularly applicable. The spira antenna was heavily dielectrically loaded and physically packaged in minimum volume; 12" diameter. Measurements of the reflection coefficient and impedance of both antennas were made to assess their performance characteristics over the frequency range of interest.

As a preliminary part of Task V, algorithm development, GIT/EES developed a discrimination algorithm for spirtral analysis based on the concept of Maximum Entropy Method (MEM). MEM was used to compute the spectral response of the short-data-length return record from the sub-surface target. MEM provides the means of achieving improved resolution in the frequency domain over that of FFT methods. This improved resolution allows a more precise selection of the frequency components in the signal returns and is the key to the success of the discrimination algorithm. Discrimination algorithms applied to the spectra of the returns were designed to separate targets of interest from the sub-surface objects (i.e., roots, rocks, junk, etc.). The results of this technique are illustrated in Section 4.

Section 2 describes the data collection methods used with both the NBS measurement equipment and the MERADCOM short-pulse radar and a preliminary analysis of the data. The objects used in the NBS measurements program included non-metallic mines, a root, a rock, and a metal plate. The objects used for the SPR measurements included a metal plate, two antivehicular non-metallic mines, and two small non-metallic antipersonnel mines. The NBS data were processed "off-line" using Georgia Tech's CYBER 74 computer system to provide plots of time and frequency responses. For the SPR data, time plots were generated using an APPLE II PLUS microprocessor that was directly connected to the radar and could digitize and process data "on-line".

Section 3 deals with the survey of candidate antennas, the design and fabrication of the "best" choices, and the testing of those antennas. Test results for a cavity-backed spiral, and a broadband horn are presented and compared with a dipole antenna.

Section 4 develops the discrimination concept using frequency spectra data and spartial correlation. Both FFT and MEM were used to obtain spectral data for comparison. The results of the discrimination algorithms are given.

SECTION 2
DATA COLLECTION AND ANALYSES

2.1 INTRODUCTION

In the following paragraphs, the two measurement systems used in obtaining the radar data are briefly described, along with the measurements. The objects used in the NBS measurement program were two types of inert non-metallic mines, a root, a rock, and a flat metal plate, all buried in soil. The objects used in the SPR measurements included two catagories of mines and a metal plate. The mines were antipersonnel and anti-vehicular type as opposed to the NBS measurements on anti-vehicular mines only.

Two types of GFE measuring equipment were made available. Initially, a Hewlett-Packard computer-controlled automatic network analyzer, installed in a 19-foot step van and assembled in the S-parameter configuration, was used to obtain reflectivity measurements from various types of objects buried in soil. This equipment was owned by the U.S. Army and operated by the National Bureau of Standards (NBS) in Boulder, Colorado. Later, the Army furnished to Georgia Tech a short-pulse radar (SPR), having a 1 nanosecond pulse length; the SPR was originally developed by the Calspan Corporation. The SPR was used to obtain wideband target signatures for comparison to the NBS measurements and to obtain measurements on additional objects. Each of these equipments is described in more detail in the following paragraphs. Typical data taken from the two measurement systems are presented.

2.2 NBS MEASUREMENTS

The NBS-operated equipment used in collecting the data is discussed and the measurement site is described. The test matrix and some of the data parameters are then explained. This is followed by a discussion of some of the salient features found in the NBS data.

2.2.1 MEASUREMENT SYSTEM

The measurement equipment consisted of a government-furnished Hewlett-Packard computer-controlled automatic network analyzer installed in a 19-foot step

van for mobility. Only its salient features are discussed. The equipment and operation thereof are described in more detail in a manual prepared by NBS personnel [1]. The data were collected by means of an automatic network analyzer whose basic function is to measure the scattering (S) parameter matrix of a two-port network (or device) at a sequence of discrete frequencies. The S-matrix is a set of four complex numbers that describe the network behavior, representing the reflection and coupling coefficients relating incident and reflected waves [2].

Specifically, we may represent incident voltage or electric field waves injected into the two ports by a_1 and a_2, as shown in Figure 1, and waves emerging from these ports by b_1 and b_2. a_1 and a_2 are considered independent quantities applied externally (and simultaneously, if necessary) while b_1 and b_2 represent the resulting response. the reponse involves the S-parameters via the network equations

$$b_1 = S_{11}\, a_1 + S_{12}\, a_2 \tag{1}$$

$$b_2 = S_{21}\, a_1 + S_{22}\, a_2 \tag{2}$$

where S_{11} and S_{22} are the reflection coefficients associated with ports 1 and 2, and S_{12} and S_{21} are port-to-port transmission coefficients. In general, it requires four measurements to determine the four coefficients. For linear passive devices however, $S_{21} = S_{12}$ so only three measurements are needed. In the measurements program, identical antennas were used; hence, it was assumed that S_{22} was essentially the same as S_{11}, and the only two complex quantities measured were S_{11} and S_{21}. All four parameters can be determined by measuring b_1 and b_2 with either a_1 or a_2 set to zero.

Figure 1. Two-port network.

The S-parameters are functions of frequency and the automatic network analyzer could be indexed through discrete frequencies from about 100 MHz through 4 GHz. A minicomputer with 16,000 words of memory was used to control the frequency stepping, as well as to position the antenna cart along a fixed path and to record the measured information on tape. In its factory-delivered configuration, the automatic network analyzer was restricted to a capacity of 53 frequencies due to software stored in core, but NBS personnel were later able to expand this to a total of 128 frequencies.

The device connected to the automatic network analyzer consisted of a pair of non-dispersive, broadband antennas aimed at the ground. The input connector of one antenna became port #1 and that of the other antenna became port #2. Since the electromagnetic fields were not confined within a closed system, the environment surrounding the antennas, including antenna coupling, cable coupling, the ground, and any nearby buried obstacles, were an integral part of the "two-port device." The network analyzer did not know this, of course, and although the physical arrangement of this "network" was complicated, the network analyzer obligingly measured its characteristics.

The antennas were connected to the equipment inside the van by a pair of coaxial cables, each about 50 feet long, and supported by a boom mounted on the van. The system had to be periodically calibrated (every half hour or so, perhaps longer under good conditions) by the substitution of standard devices for the device to be measured. These standard devices (e.g., precision short circuits, matched loads, feed-throughs) were connected at the far end of the cables. The cables themselves changed characteristics with changing temperature, and NBS personnel found that wrapping the cables with metal foil reduced their sensitivity to wind and sunlight.

2.2.2 MEASUREMENT SITE

The NBS data used in this study were derived from measurements conducted on a 35-foot test lane prepared at a site in Boulder, Colorado. Three soil types were represented and, with appropriate test lane flooding, at least three levels of moisture content were achieved. The site was on U. S. Department of Commerce property in the city of Boulder.

The NBS site contained two types of soil, one being a sandy loam trucked in from off the site several years ago to build up a thick layer-- perhaps 4 feet-- of

homogeneous soil. The sandy loam constituted the first 20 feet of the test lane. The remaining 15 feet of the test lane contained soil of essentially the same texture, but interspersed with rocks and pebbles whose exact sizes and distributions were not known with certainty. Near the surface, these rocks were a few centimeters in diameter.

In a previous report by Georgia Tech Engineering Experiment Station [3], NBS data from two sites were available and were edited, plotted and, documented. The two sets of data are sufficiently similar in characteristics that only one set is illustrated in this report if the reader is interested in viewing more data plots are referred to Reference [3].

As shown in the diagram of Figure 2, six targets consisting of both natural and man-made objects were buried 60 inches apart along a straight line. Preliminary background runs were conducted to collect reference data at closely spaced stations along two separate five-foot stretches of the test lanes before the targets were buried. After the measurement program got underway, the cart, provided with electric stepping motors controlled by the minicomputer in the system, was commanded to stop at given positions over or near each target. These positions were -8, -4, 0, 4, and 8 inches from the target, and a sixth position midway between targets (i.e., 30 inches) was included for the purpose of acquiring "background" data. At each position, the frequency was indexed through 123 discrete values at which the S-parameters were measured and recorded automatically on magnetic tape. A boardwalk was laid out and leveled alongside the test lane to provide a smooth runway for the antenna cart. the cart was guided along its path by an aluminum rail pinned to the ground on one side of the boardwalk. The test target positions were carefully located by strings stretched along and across the target centerline track. These and other details of the test lanes can be seen in the photographs of Figures 3 through 5.

The moisture content of the soil was usually, but not always, determined by two different means. The most convenient method used was based on a water-carbide reaction inside a sealed pressure vessel. Known amounts of soil and the carbide reagent were deposited in the container but not allowed to contact each other until the vessel had been sealed. Then the two were mixed by external agitation and the resulting chemical reaction produced acetylene, generating heat and a rise in internal pressure. A pressure gauge calibrated in per cent moisture content converted the pressure reading to moisture content. This "bomb" technique is within a percentage

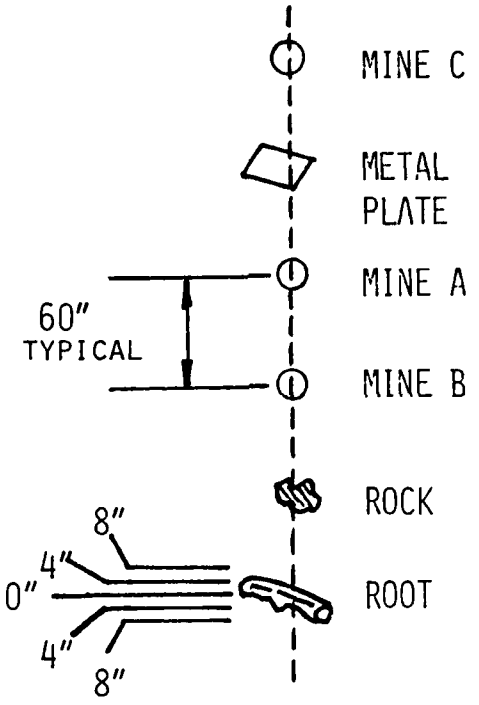

Figure 2. NBS test lane layout.

FIGURE 3. Test site at NBS laboratories in Boulder. Photo was taken during background runs before target burial. Aluminum guide rail can be seen at extreme right just off the edge of the boardwalk. Shed in background shelters an indoor test lane.

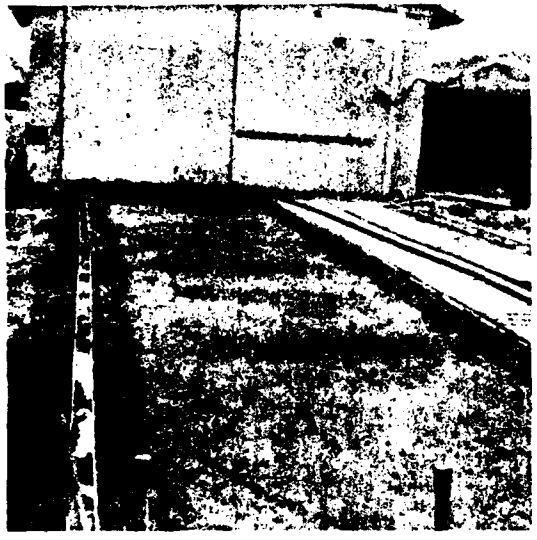

Figure 4. NBS test site prepared for flooding. It required an estimated 2500 to 3000 gallons of water to bring the moisture content up to about 17%.

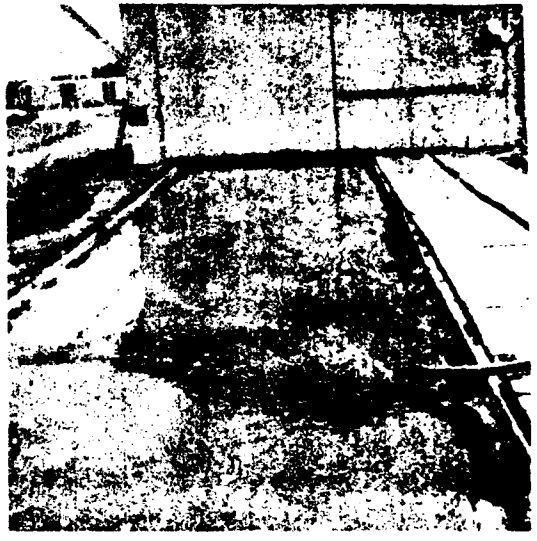

Figure 5. NBS site during flooding.

point in accuracy, it is claimed, and oven-drying techniques tend to support this claim, at least for soils with modest surface area to volume ratios. The oven method which relies on a comparison of sample weight before and after several hours of baking near the boiling point of water was the other method used to determine said moisture content. The oven method is considered more accurate than the bomb technique. Moisture content was not always measured as a function of depth, but in those cases where it was, it tended to be fairly uniform.

2.2.3 NBS DATA

Table 1 shows the matrix of NBS data used for this study. Results of a typical measurement set for a root, a rock, a mine, and a metal plate are presented in Figure 6. At each of 123 frequencies, the real and imaginary parts of the S_{12} parameter (the coupling coefficient from Port 1 to Port 2) were recorded; the magnitude of S_{12} is displayed in Figure 6. The phase angle at each frequency was also calculated from the real and imaginary components and used in the FFT computations. An examination of the plots in Figure 6 shows that the spectra are complicated.

Before the line spectra were transformed to the time domain, the spectral data were weighted with a Chebychev weighting function designed to yield low (-40 dB) time sidelobes. The weighting function is plotted in Figure 7 where it is normalized to the peak amplitude occuring at mid-frequency, f_o. After the spectral data are multiplied by this weighting function, the data are ready for transformation to the time domain. The standard FFT requires that the number of samples be an integral power of 2, and samples were selected for 128 frequencies, including zero frequency (DC). Since the five lowest frequency samples lie below the capability of the equipment and were not measured, zeroes were arbitrarily inserted to represent the unmeasured values.

The FFT algorithm used in the generation of the time domain signals creates an array of 256 data points, 128 of these being the measured data for positive frequencies and the other 128 being their complex conjugates for the corresponding negative frequencies. The total time record length is the reciprocal of the frequency interval, hence, a 24 MHz sampling interval generates a time record 41-2/3 ns long. Virtually all the signals of interest occur in the first half of this record, so only the data for the first 20-5/6 ns are presented.

Table 1

NBS DATA MATRIX

Antenna polarization:	Parallel to direction of travel
Antenna orientation:	Bistatic
Antenna height:	4" nominal
Targets:	Mine types A, B, and C; (1) rock; (1) root, (1) metal plate
Positions:	-8", -4", 0", 4", 8", 30"
Target spacing:	60"
Depths:	3", 6"
Soil types/mosture content:	Loam: 7%, 17%, 18% Bentonite: 12-20%, 13-16%, 26-30%, 30%
Frequencies:	120 MHz to 3048 MHz, 24 MHz steps

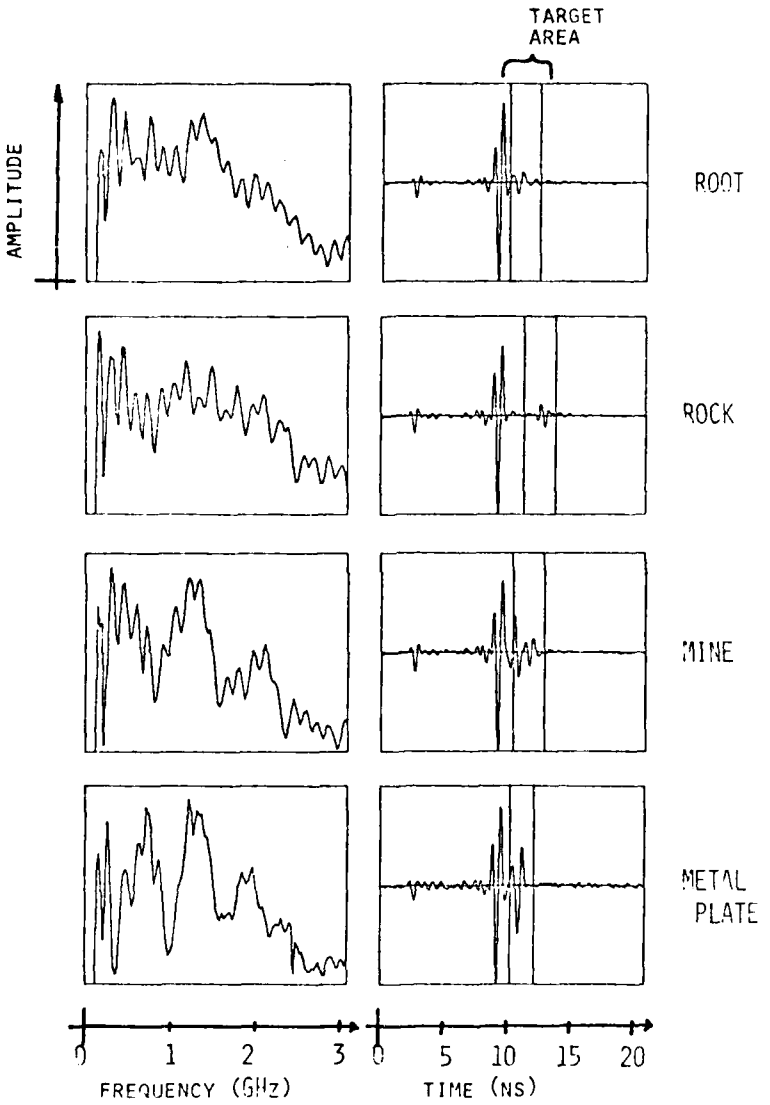

Figure 6. Preliminary processing for NBS data.

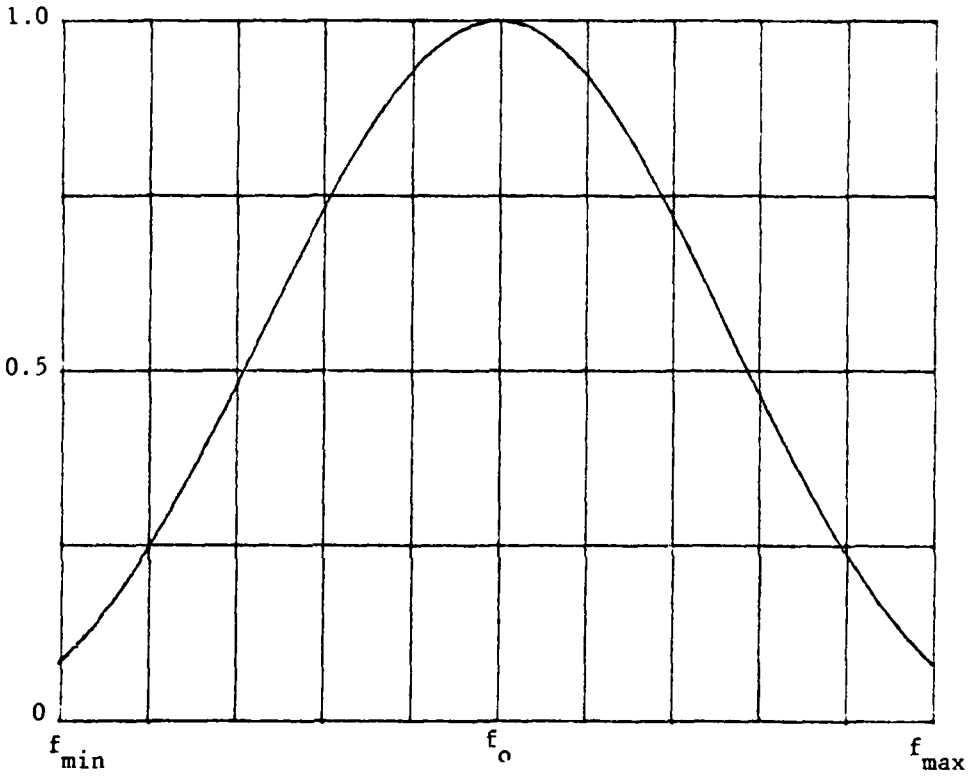

Figure 7. Normalized weighting function, I_1 (x) / x.

Line spectra data such as those in Figure 6 were used to synthesize the performance of a short pulse system by means of the FFT. These figures represent the short pulse response of a metal plate buried three inches deep in relatively damp soil and a Type A mine in relatively dry soil; the amplitude scale of both time histories is normalized with respect to the largest amplitude occuring in the time record.

The first small anomaly near the left side of the time signature is apparently due to a direct leakage of energy between the two antenna connectors which were relatively close to each other. The large return near the center of the diagrams is predominantly the ground return; however, there is an additional contribution due to coupling between the antenna apertures. The target return appears a short time later, after the "ringing" from the ground return has subsided.

Inspection of the returns from different target types indicates that the returns are quite different. In fact, the three-peak characteristic in Figure 6 was recognizable in most of the time histories obtained for the Type A mine. The spectral characteristics of the target alone can be extracted from the time histories by applying a range gate or time "window" that deletes all the returns, except those from the target. Typically, the window need be only a few nanoseconds wide, and the time data can be transformed back to the frequency domain using an inverse FFT or Maximum Entropy Method (MEM). This process generates potentially useful spectral data containing only target characteristics and is discussed in more detail in the discrimination algorithm section.

The metal plate reponse is far more pronounced in the frequency domain than in the time domain. The plate exhibits a single peak (near 700 MHz), but the Type A mine response contains a sequence of peaks and nulls whose frequency separation is remarkably constant (800 MHz per cycle of the pattern). This interference pattern is attributable to two discrete echo sources of comparable magnitude, but going in and out of phase as the frequency is swept. The target is transparent, being made of essentially lossless material, and one reflection occurs at its bottom surface while the other occurs at the top.

Spectra were generated for all seven buried objects and were subjected to analysis in a search for discrimination features.

2.3 SHORT-PULSE RADAR MEASUREMENTS

The short-pulse radar system used for collecting data is briefly described in the following paragraphs. In addition, the condition of the site where the data were taken is reviewed, the test matrix utilized is explained, and some typical data collected are presented.

2.3.1 SPR MEASUREMENT SYSTEM

The radar used to make measurements was an adaptation of the Vehicle-Mounted Mine Detection Radar developed by the Calspan Corporation, Buffalo, New York, [4, 5] for the U.S. Army (MERADCOM, Ft. Belvoir, Virginia). The radar transmited pulses consisting of one cycle at one gigahertz (GHz), i.e., a one nanosecond pulse width. Since one cycle of 1 GHz is a transient type of signal, we needed a bandwidth as much as 2 GHz to prevent distortions of the signal. For our system, this bandwidth was required only in the transmitter, antenna, and sampler. The wide bandwidth was not needed for the video sections because the periodic, real-time return signal was sampled and reconstructed at a much lower frequency. Figure 8 is a block diagram of the system, and the following paragraphs describe the blocks in detail.

2.3.1.1 Timing Generator

The timing for the system was derived from a 15 MHz cystral controlled oscillator. This signal was divided down to produce all gating and trigger waveforms needed in the radar. In particular, the timing generator produced the 5 MHz signal that established the radar pulse repetition frequency (the number of pulses per second transmitted).

2.3.1.2 Transmitter

The transmitter included a short-pulse driver and avalanche pulse generator. The driver was a snap-off, step recovery diode that generated a tranmition across a coaxial pulse forming network, thereby generating a short transition pulse. Amplification was then achieved by a transistor operated in the avalanche mode for high speed switching. This transistor output went directly to the antenna.

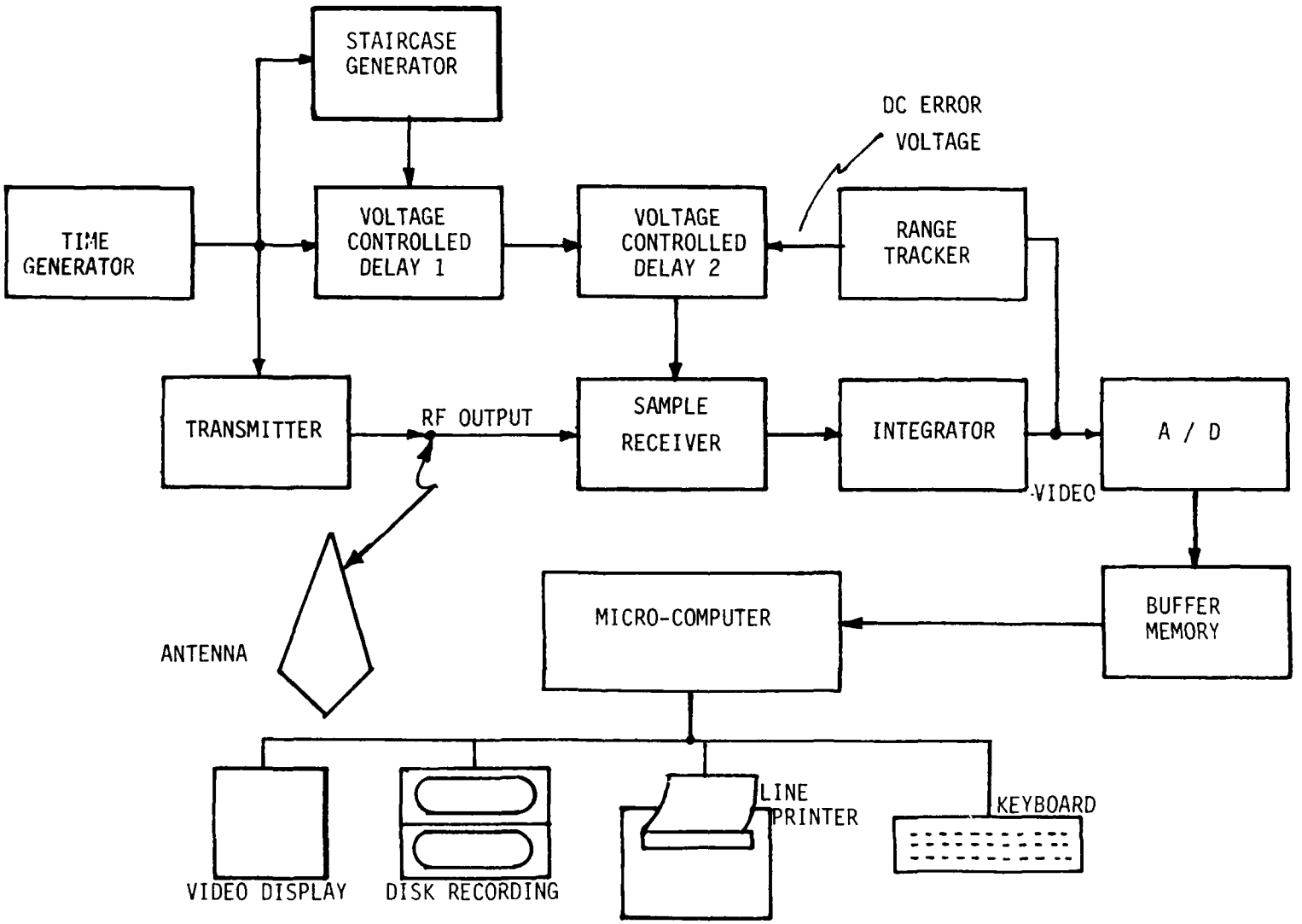

Figure 8. SPR block diagram.

2.3.1.3 Antenna

The antenna was of broadband design, working over the frequency range from 200 MHz to 2 GHz. A TEM (transverse electromagnetic) horn was used to obtain the low frequency response. The plates of the horn were flared and exponentially tapered with resistive card loading on the ends to maintain the required wide bandwidth. Because the antenna had a very low voltage-standing-wave-ratio, most of the energy is transmitted into the medium and there is little reflection of energy from the antenna into the receiver.

2.3.1.4 Sample Receiver

The returning signal was sampled by a Schottky barrier diode that was strobed by a snap off, step-recovery diode at a 5 MHz rate. The periodicity of the received waveform allowed us to take individual samples from pulse to pulse and to reconstruct the waveform over a longer time period as shows in Figure 9, thereby, decreasing the bandwidth requirements on the video and digital subsystems. The 5 MHz signal to the sampler is delayed by voltage controlled delay lines 1 and 2 to enable samples at times differing from the transmit pulse. The control voltage for delay line 1 was a staircase waveform of 200 steps. Each voltage step caused the sample strobe to occur later on the waveform than the previous sample strobe. Because there were 200 steps, we sampled at 200 positions across our real-time waveform. At each of these 200 positions we took 450 samples and then performed intergration to increase the signal-to-noise ratio. Each voltage step moved the sample strobe out 92.5 picoseconds in range. Since there were 200 steps, the width of our sample window was 200 X 92.5 ps = 18.5 nanoseconds. For comparing real-time waveforms to reconstructed waveforms, 18.5 nanoseconds of real time corresponded to 18 milliseconds in reconstructed time. The position of the sample window in range was controlled by delay line 2, via a voltage from the range tracker.

2.3.1.5 Range Tracker

The main function of the range tracker was to establish a fixed time reference position for the surface return. Once this was established, all other video signals are referenced to this time. Video could not be referenced to the transmit pulse; because the antenna height above the ground varied, the position in time of the void return would have varied and made detection difficult. The range tracker locked on the

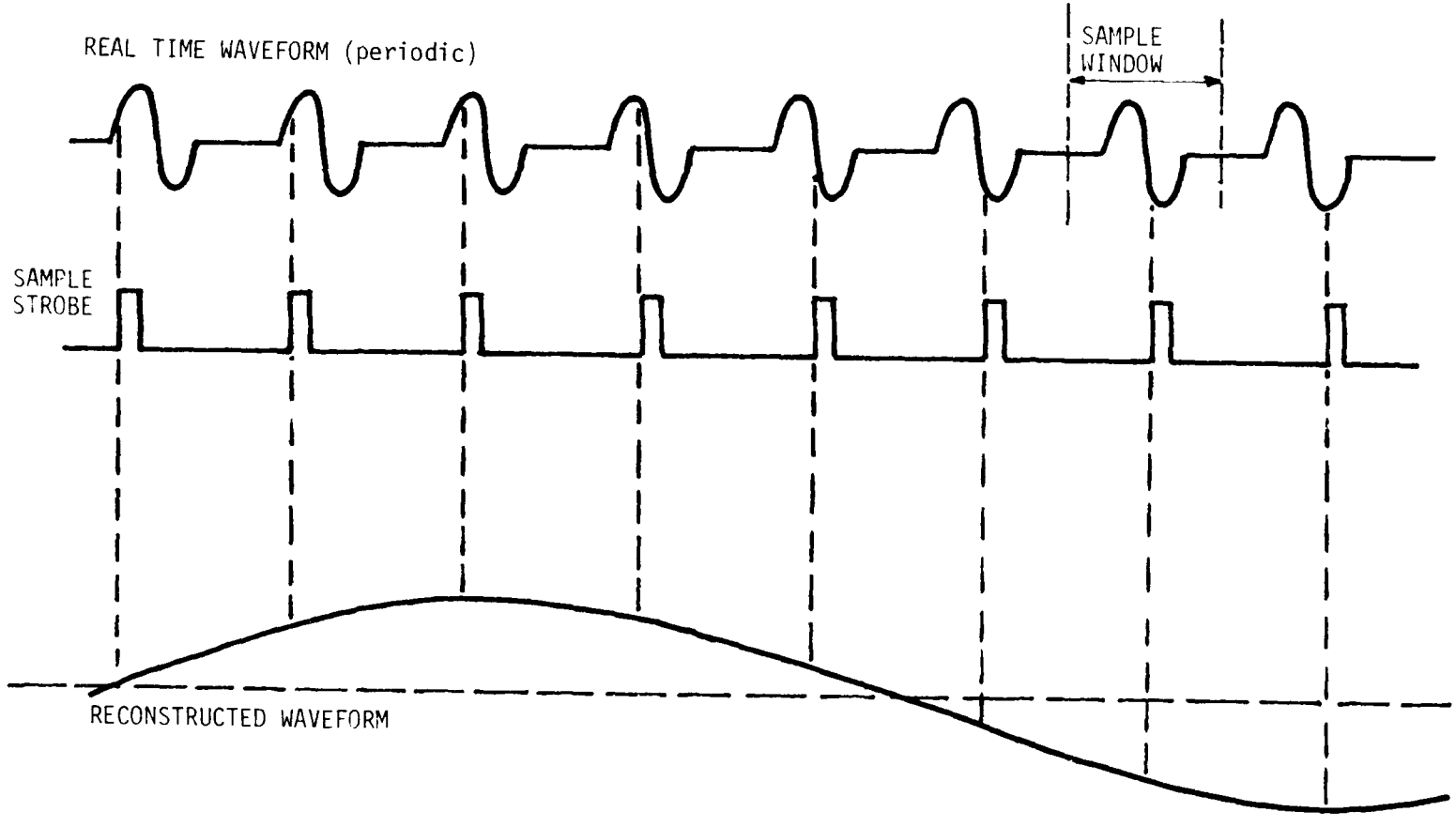

Figure 9. Periodic sampling (single sample position).

surface by applying an error voltage to delay line 2 such that the leading edge of the sample window was locked to a point slightly behind the surface return. The void always remained at the same position within the window, regardless of antenna height.

2.3.1.6 Analog-to-Digital Converter with Buffer Storage

The video information was first converted into a digital format before it was processed by the computer. This was the purpose of the analog-to-digital converter. Figure 10 illustrates the sequential sampling that was used with the converter. The waveform can be represented by samples taken over one cycle of the video waveform. The video was sampled, and, each sample was converted in real time to a digital word and stored in a buffer memory. Both loading and unloading of the buffer were under computer software control.

2.3.1.7 Micro-Computer

The micro-computer chosen for the void detection system was built by APPLE Computer, Inc., Cupertino, California and consisted of the following components.

(1) Main Computer
- 48,000 words of random access memory
- Keyboard interface
- BASIC, PASCAL and, FORTRAN language systems

(2) Video Display
- 9" black and white
- Text and graphics modes of display

(3) Two Mini-Floppy Disk Drives
- 5" floppy diskettes
- 102,000 words of storage each diskette

3 Interface Cards
- Radar interface - digitized radar data
- Communications interface-transfered data to/from the CYBER
- Printer interface - line printer communication

(4) Printer
- Capable of printing out data/program listings or graphics (plots)

Figure 11 is a photograph of the SPR measurement system.

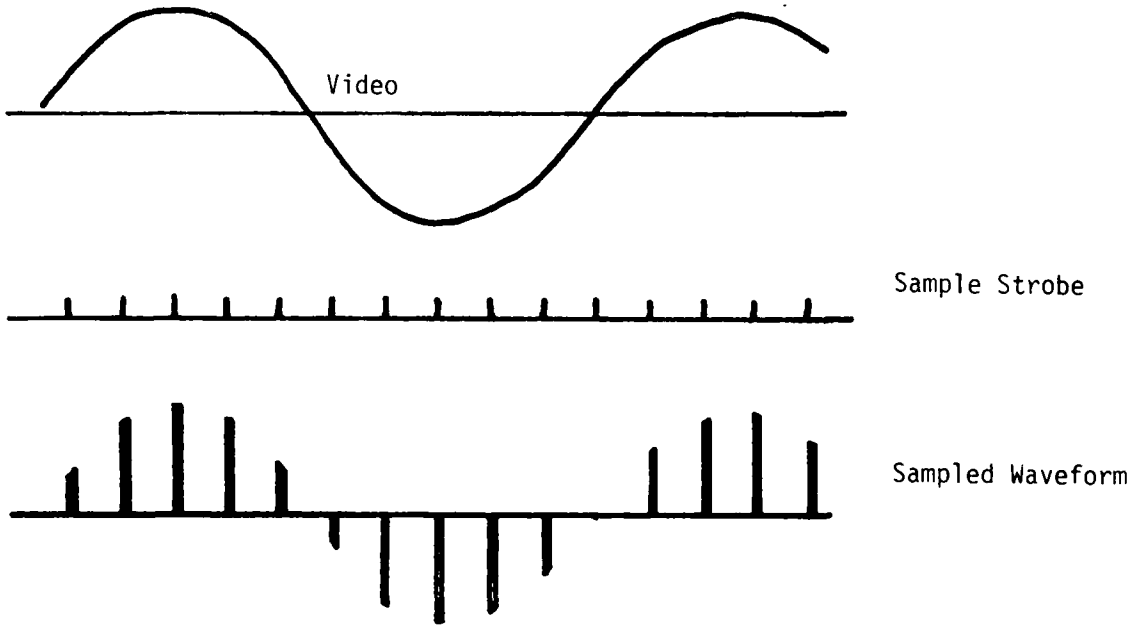

Figure 10. Sequential sampling.

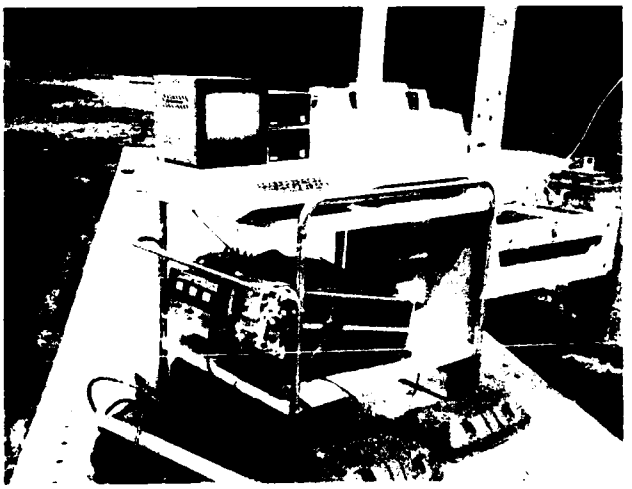

Figure 11. Photograph of measurement system.

2.3.2 SPR DATA

The short-pulse radar measurements were made in a laboratory controlled environment at Georgia Tech's Cobb County Research Facility. The medium in which objects were placed was dry sand with no rocks, pebbles, nor debris present. The radar was used to measure anti-vehicular mines and a metal plate buried at approximately a five inch depth, and small anti-personnel mines and a metal plate on the surface. The antenna was held approximately 10 inches above the surface of the sand.

A listing of measurements made with the SPR is given in Table 2. The major purpose of the short-pulse measurements was to verify that this measurement system yields results which are not significantly different from the results obtained with NBS system. If this is so, then the equivalence between the systems allows discrimination/classification algorithms to be developed and applied to both. Figures 12-16 illustrate the measurements listed in Table 2. The type of plot generated for these measurements is called an Amplitude-Time Sequential Plot, and were printed on the APPLE microcomputer line-printer. The interesting part of each set of signatures and the position of each measurement are indicated on the plots.

2.4 NBS/SPR COMPARISON

Comparison of the NBS and SPR data indicated remarkable similarity in the signal returns from the buried objects. It was also evident that a metal plate on the surface can be seen with significant signal amplitude. As for the two small anti-personnel mines, only small perturbations, if any, were observed, although, the shape of the return signal was as expected.

In the researchers' opinion, the signal returns from the buried objects using either the NBS system or the SPR system yielded equivalent results. The characteristics exhibited were wide bandwidth, or equivalently a short-pulse (1 nanosecond) signal, and a non-dispersirve nature mainly due to the antenna. Thus, any new antenna design must exhibit these characteristics or algorithms developed for this type of data will be invalid.

TABLE 2 SHORT PULSE RADAR MEASUREMENTS

Target	Position	Measurements
METAL PLATE 14"x8"x1/8"	buried 6 inches deep	8 measurements across length 2" increments
MINE A 12" diameter Anti-Vehicular	buried 4 inches deep	8 measurements 2" increments
MINE B 12"x12" Anti-Vehicular	buried 5 inches	7 measurements 3" increments
METAL PLATE 14"x8"x1/8"	on surface	12 measurements 3" increments
MINE C 1-1/2" diameter Anti-Personnel	on surface	2 measurements 1" increment
MINE D 2" diameter Anti-Personnel	on surface	2 measurements 1" increment

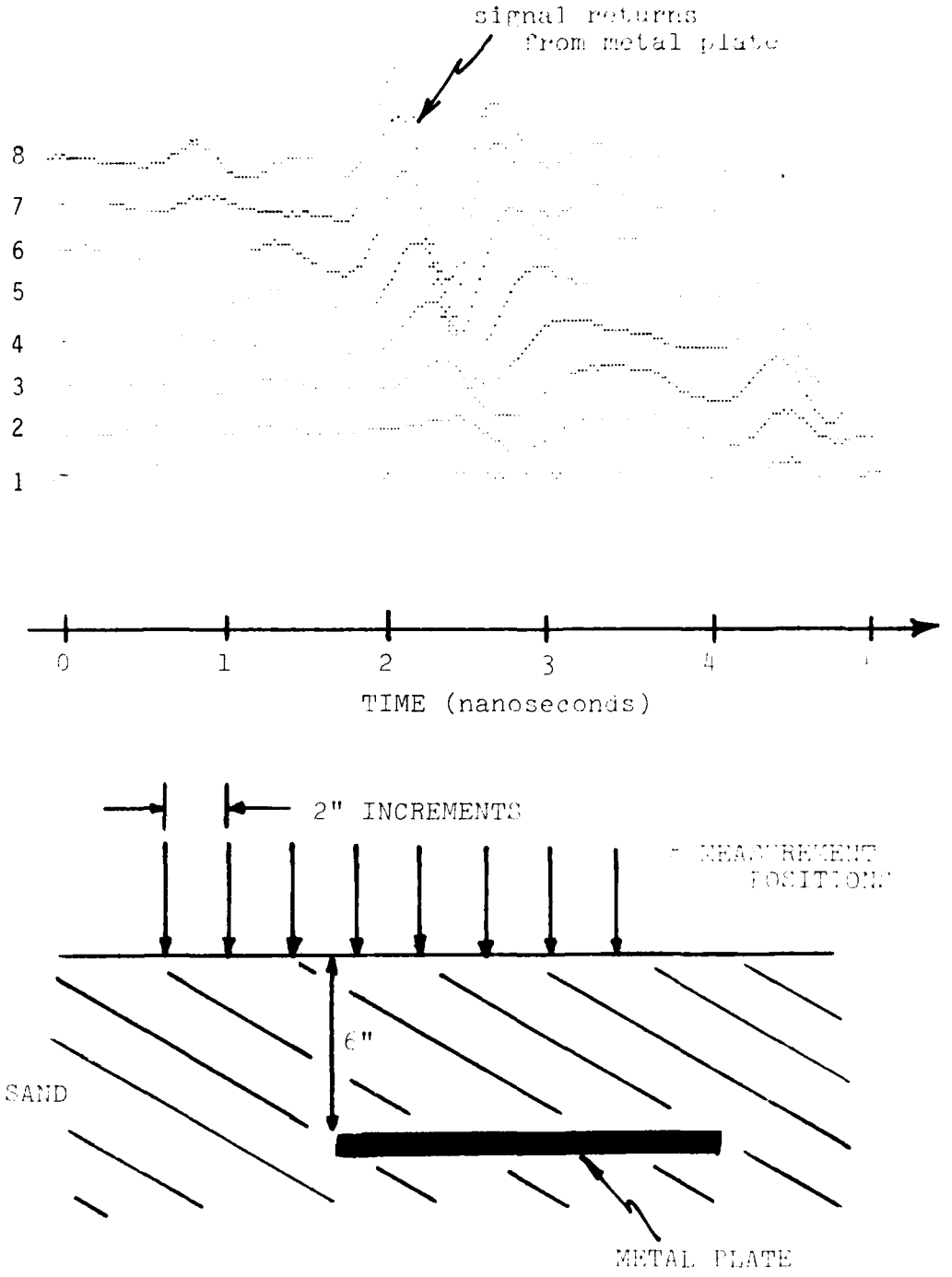

Figure 12. SPR measurements of buried metal plate.

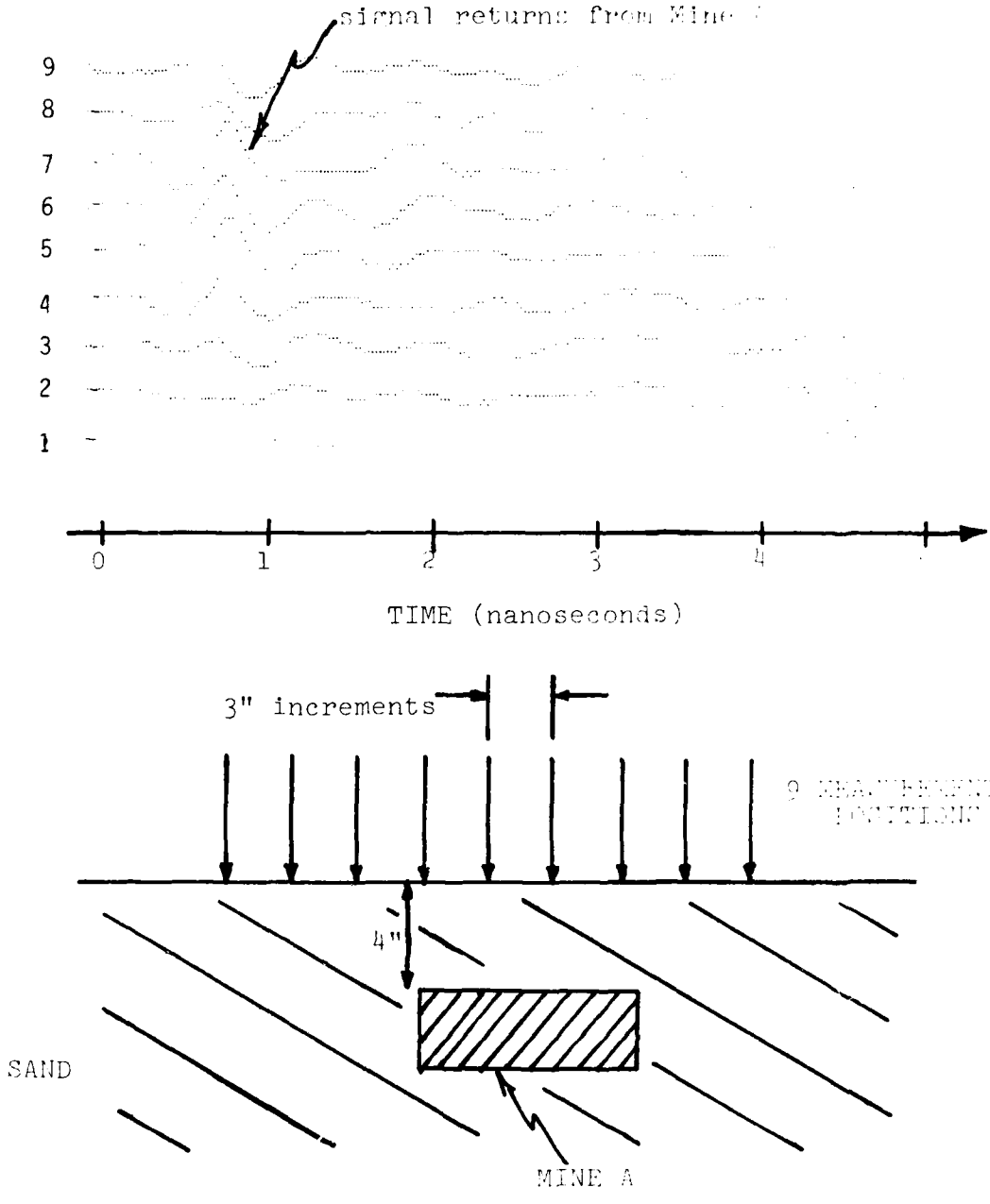

Figure 13. SPR measurements of Mine A.

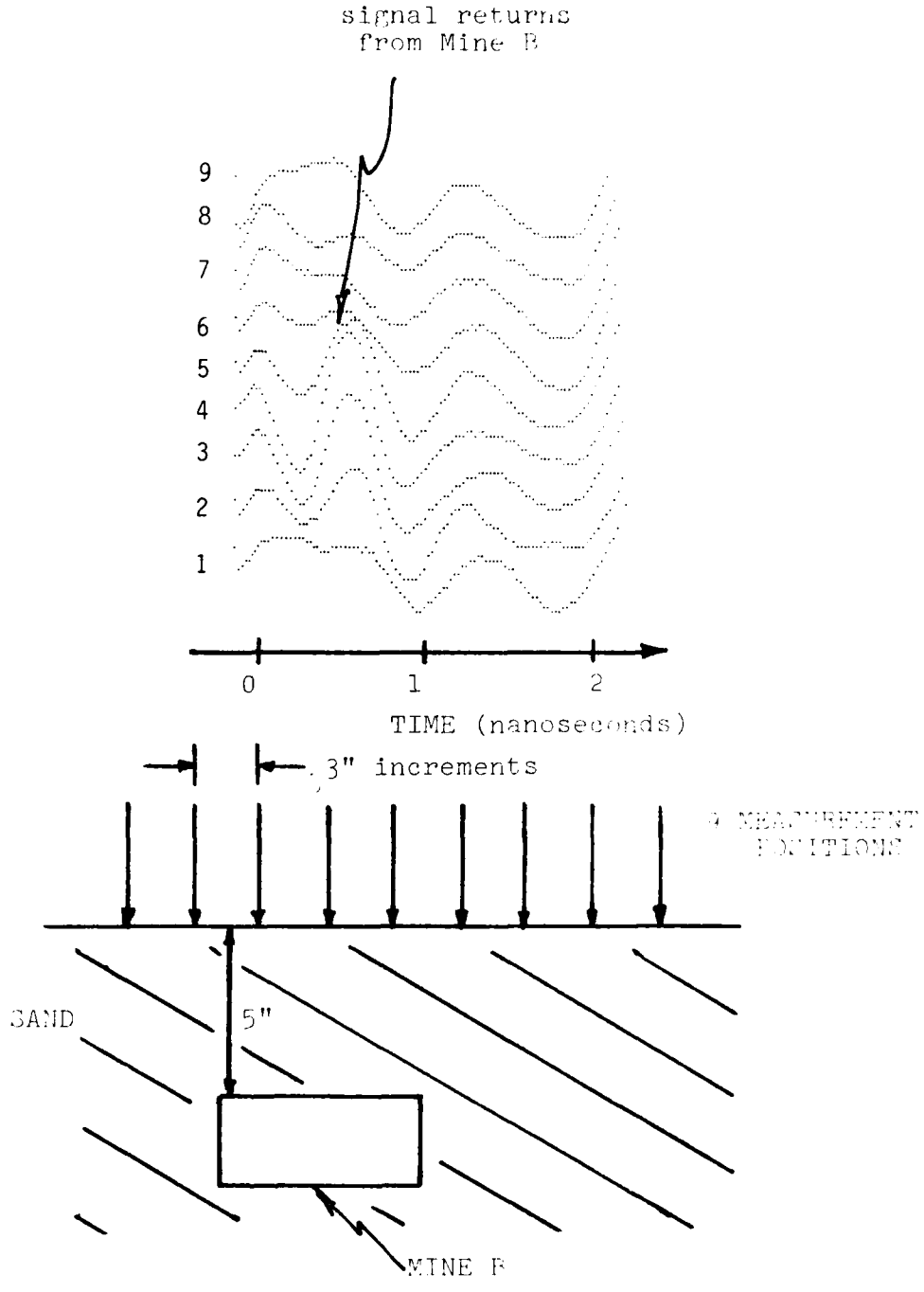

Figure 14. SPR measurements of Mine B.

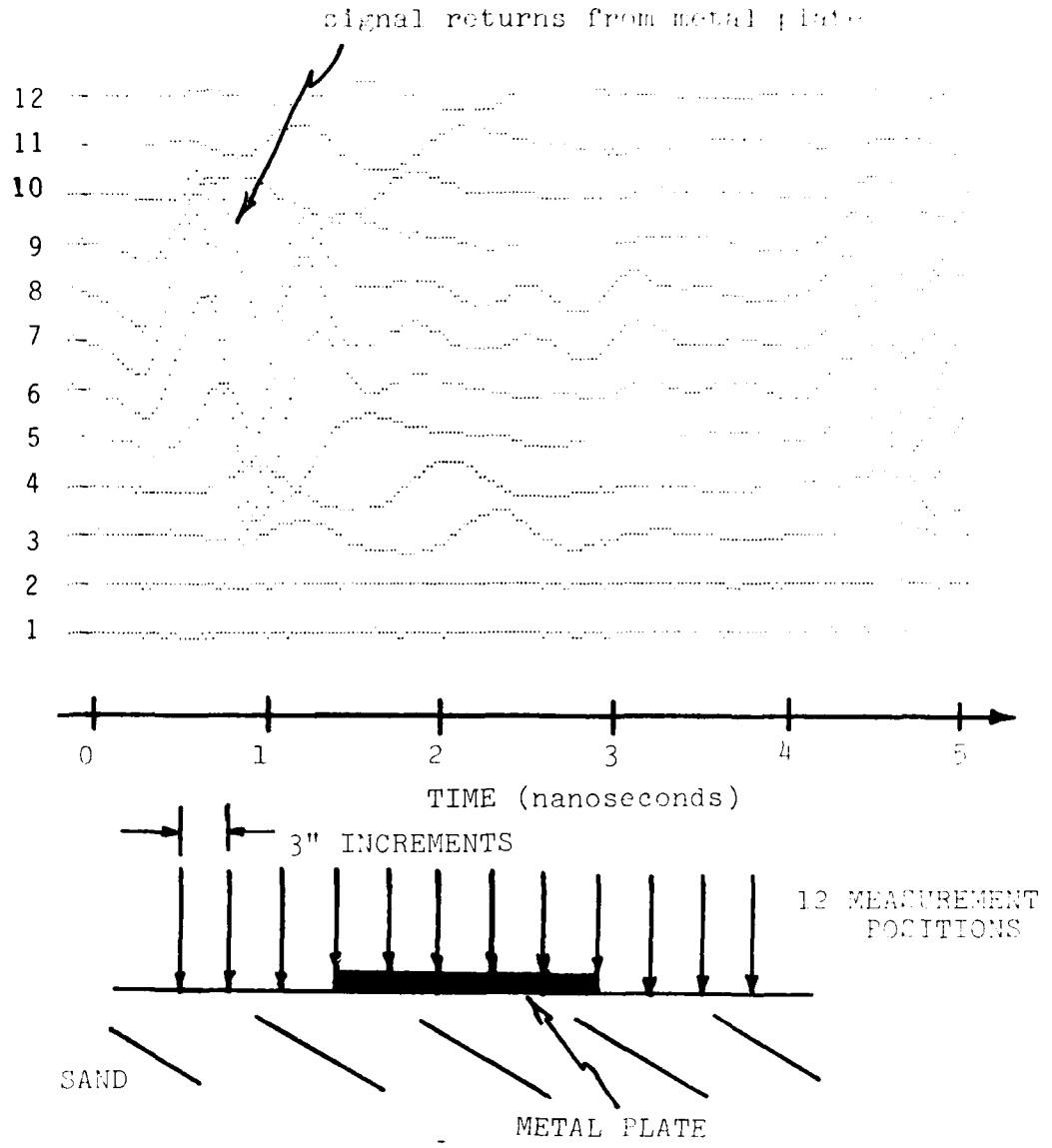

Figure 15. SPR measurements of metal plate on surface.

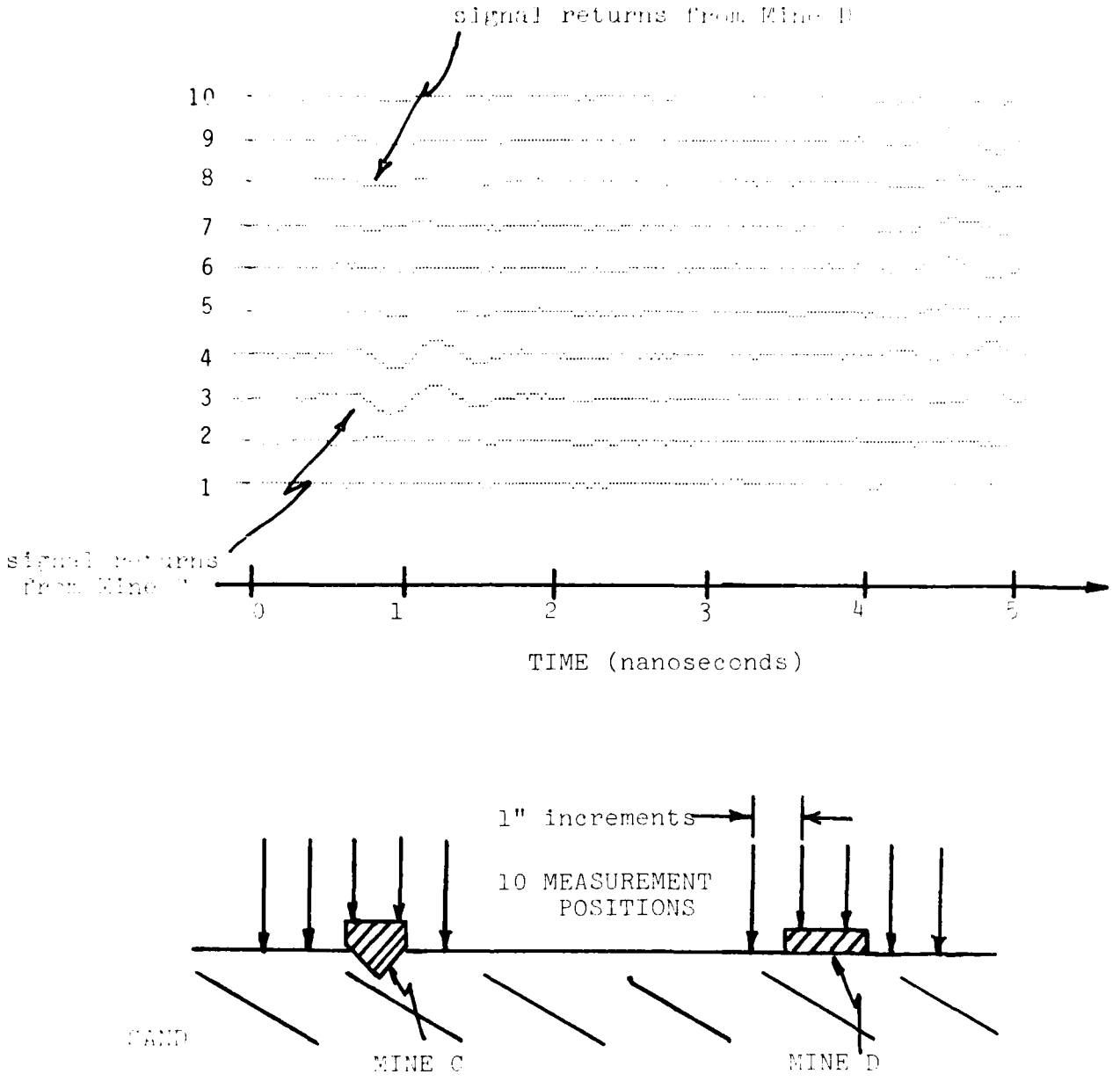

Figure 16. SPR measurements of mines on surface.

SECTION 3
ANTENNA DEVELOPMENT

3.1 ANTENNA REQUIREMENTS

A major goal of this program was to reduce the size of the antenna required for the short-pulse radar system. The Calspan antennas were considered much too unwieldy for use in a man-portable system. An individual Calspan horn is about 45 inches long and has a 9-inch square radiating aperture (exterior dimensions of packaged antenna). The guideline suggested for this work was that the antenna dimensions should not exceed 12 inches. An antenna having the form of a book (or pancake) would be most desirable. All parties recognized that such a form might not be physically possible and that such a small size would at best result in some sacrifice of performance at lower frequencies. Therefore, this program was planned to include signal processing investigations that might decrease reliance on low-frequency signal components and antenna design investigations that might improve the response of electrically small, broadband antennas. Small size was the highest priority constraint imposed on the antenna effort.

On the basis of previous experience in this work [3] and the initial interest in metallic mines, the approach selected was to optimize the antenna for operation in the frequency range of 300 MHz to 1,000 MHz. For comparison, the Calspan antenna was developed for operation over the range 150 MHz to 2,000 MHz which includes the significant spectral content of the radar transmitter pulse [6]. Such a reduction in antenna bandwidth was expected to degrade the pulse fidelity of the radar system; however, frequency-domain signal processing techniques seemed to be more successful than time-domain techniques for this application, and seemed likely that adequate information could be extracted from the reduced band.

The following three performance criteria were identified as being relevant and important to an antenna for the mine detection radar:

(1) Most of the radiated energy should be directed into the ground.

(2) Reflections from the antenna input port should be minimized.

(3) Multiple reflections, or "ringing," within the antenna structure should be effectively eliminated.

The criteria should hold at all frequencies within the operating bandwidth of 300 MHz to 1,000 MHz.

The first criteria was imposed to minimize false alarms caused by returns from objects (e.g., rocks, vegetation) that lie outside the target area. Because the antenna aperture will be placed near the air/earth interface, free-space antenna radiation patterns have little meaning for this application; but it is at least desirable that the spatial distribution of energy have a favorable front-to-back ratio when the antenna is pointed into the earth.

The second criteria was imposed to minimize multiple reflections between the antenna and the radar receiver. The importance of this criteria depends on the impedance mismatch at the receiver. If only the antenna is mismatched, the reflection from the antenna will pass through the receiver before the target return, and the antenna return can be removed by a range gate. If both the receiver and the antenna are mismatched, multiple reflections will cause the transmission line to "ring." The duration of the ring will extend into the period of expected target returns, and the ring cannot be removed by a range gate. Data on the receiver mismatch were not initially available, but the Calspan horn was claimed to have a reflection coefficient below 0.1 for frequencies above 300 MHz [6]. (This corresponds to a reflection level below -20 dB, or to a VSWR lower than 1.23:1.) Such a mismatch was assumed to be acceptable and was taken as a design goal. The acceptability of a worse mismatch would need to be established by demonstration.

The third criteria was imposed to eliminate ringing within the antenna structure, itself. Such ringing might be caused by multiple reflections between the feed point and the radiating aperture, for example, and cannot generally be removed by a range gate.

The electrical design criteria assumed for this work were similar to those placed on the Calspan development, with one exception. Here no a priori assumption was made regarding the dispersive characteristics of the antenna. Because of the initial interest in frequency-domain signal processing, constraints on pulse fidelity were relaxed, with the expectation that processing could compensate for a reasonable amount of dispersion. This allowed consideration of the spiral antenna, which meets the size and form requirements better than any other candidate. The use of measured antenna data to correct antenna-induced errors during signal procesing could require demonstration, but the concept of such error corrections is used routinely in microwave measurements

(e.g., consider the automatic network analyzer [7, 8]).

The antenna work conducted on this program resulted in the fabrication and preliminary testing of good examples of three very interesting types of antennas - a spiral, a TEM horn, and a broadband dipole. The horn and the dipole designs were based on a graded-resistivity metallization process and were derivatives of designs that were developed recently at the National Bureau of Standards [9,10,11,12]. Preliminary tests using frequency-domain methods indicated that the spiral and the horn have significant potential. However, the program was not continued into a planned phase of time-domain testing and optimization, and the capabilities of these antenna have not been conclusively established.

The following sub-sections discuss the types of antennas considered during this program, details of design and fabrication, test results, and conclusions.

3.2 SURVEY OF CANDIDATE ANTENNAS

The selection of an antenna is normally governed by factors such as input impedance and radiation pattern bandwidths, pattern directivity and power gain, polarization, high power capability, and mechanical requirements. These same parameters are relevant to the mine detection radar antenna, but the emphasis is different from that for a conventional radar. For a conventional radar, high gain and low sidelobes are always desired, and bandwidths are normally not greater than ten percent. For the mine detection radar, pattern characteristics are relatively unimportant, but an operating bandwidth of several octaves is required.

Radiation pattern concepts are of questionable importance in this application, first, because the antenna is directed into an electrically dense lossy medium and, second, because the target is not in the far-field zone of the antenna. The main pattern requirement is that radiation backward into the air be minimized, relative to radiation into the ground. This directivity is needed to minimize false alarms and to increase power on the target. Power gain or radiation efficiency are of secondary importance in the mine detection radar system. The ability of the system to recognize targets is limited by the clutter environment, rather than by lack of adequate signal. However, some use of resistive loading in the antenna to achieve good broadband operation with an electrically small antenna must be expected, and radiation efficiencies in such cases will be significantly lower than for the Calspan horn.

There are several basic types of antennas that have an inherent capability

for operation over a frequency range greater than an octave. These include "frequency-independent" antennas such as the spiral and the log-periodic dipole array (LPDA). Conventional horn antennas normally operate over bands of approximately one octave. Multi-octave operation can be achieved by using ridges to suppress higher order modes at the high end of the band and by removing the E-plane side walls to allow TEM mode propagation at the low end of the band. Resonant antennas, such as dipoles, may be modified for broadband operation by using resistive loading to attenuate resonant current distributions.

Investigations of dual polarized systems were not within the scope of this program, but a choice between linear and circular polarization is available. The horn, the dipole, and the LPDA can most easily provide linear polarization, while the spiral provides circular polarization. Circular polarization can be obtained from LPDAs, horns, or dipoles by quadrature excitation of orthogonal linear elements, but the present requirement does not justify these additional complications. It is reasonable to expect that the signal anomaly caused by a mine should be sensitive to polarization, but there is not enough data for the choice to be obvious.

The following paragraphs review the types of antennas that were considered to be practical candidates for this program.

3.2.1 CAVITY-BACKED SPIRAL

From the viewpoint of size reduction, the cavity-backed spiral is the most attractive of all candidates for this application. For an antenna to be an efficient radiator, it must normally have a dimension of at least one-half wavelength. The spiral radiates efficiently when it has an outer circumference of at least one wavelength. This means it needs a maximum diameter of about one-third wavelength. In a transmitting mode, the arms of a spiral are excited by feed point attachments at the center of the spiral. The currents flow outward along the arms until they approach a ring having a circumference of one wavelength. At this point, the energy is radiated into space and the currents disappear. Therefore, the upper frequency limit for efficient spiral radiation is set by the size of the feed point attachments, and the lower frequency limit is set by the outer diameter of the spiral structure. Within these limits, the spiral radiates efficiently in a frequency-independent manner. The input impedance and the radiation patterns will vary little over this frequency range. With any spiral structure that might be used for the mine detection application, an upper frequency of several gigahertz presents no problem. With a 12-inch diameter

spiral, the nominal lower frequency limit is a little below 400 MHz. However, there are several techniques that can be used to extend the lower frequency limit.

One technique to extend the lower frequency limit of a spiral is to place resistive loading at the ends of the spiral arms to attenuate the currents. Although the radiation efficiency of the spiral will suffer from the reduced aperture, broadband operation can be maintained. With no loading, currents that reach the ends of the spiral arms are reflected. The inward traveling reflected currents cause pattern degradation, but worse, they couple out of the antenna through the feed points and appear to the radar as a reflection from the antenna. If the feed point is not well matched, multiple reflections can occur between the ends of the spiral arms and the feed points. These multiple reflections will be sensed by the radar receiver as ringing within the antenna structure. Therefore, special attention must be paid to terminations of the spiral arms to extend the lower frequency limit of operation.

A related technique for a low frequency extension combines the spiral with a helical extension of the arms. The axis of the helix is perpendicular to the plane of the spiral. Qualitatively, it may be argued that the helix increases the radiating aperture by adding length to the antenna. It is still desirable to terminate the helical arms with resistive loading.

A third technique for extending the low frequency limit of operation is to increase the number of arms on the spiral. A spiral or helix with a single arm can be an efficient radiator. However, the antenna characteristics can be improved by using multiple arms to force the current distributions on the antenna to have the desired phase variation. It has been shown that the bandwidth of helices can be made proportional to the number of arms in the antenna [13]. Spirals, which are commonly used in direction finding applications, often have six or eight arms, when only four are nominally adequate to support the desired monopulse modes [14].

Figure 17 shows a schematic drawing of a four-arm cavity-backed spiral with a helix extension on the side-wall of the cavity. The spiral shown and others considered in this work are known as self-complementary, equiangular spirals. The term "self-complementary" means that, the metallized arms and the spaces between arms can exactly cover each other by a simple rotation. The term "equiangular" means that at every point on a spiral contour, the tangent to the spiral makes the same angle with a radial vector drawn from the center of

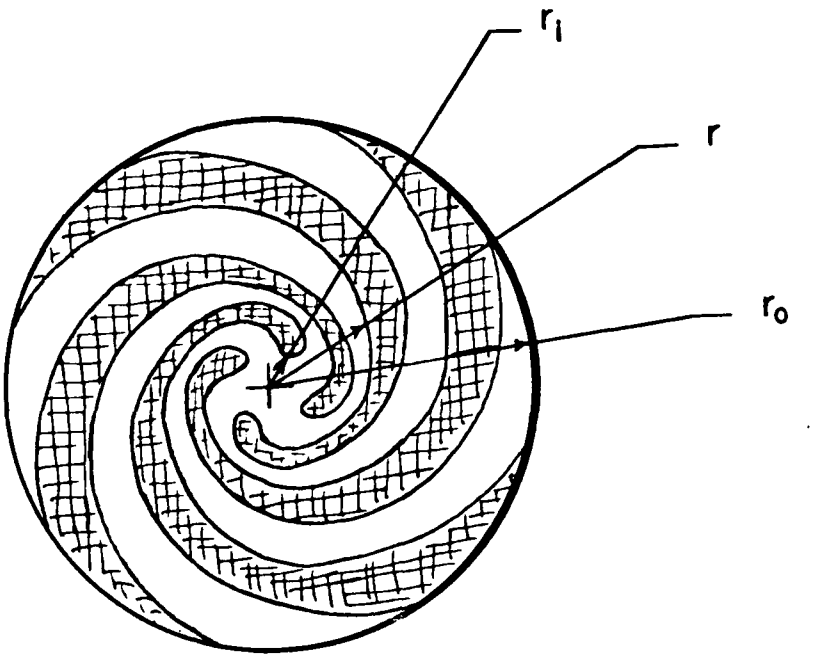

(a) Top View

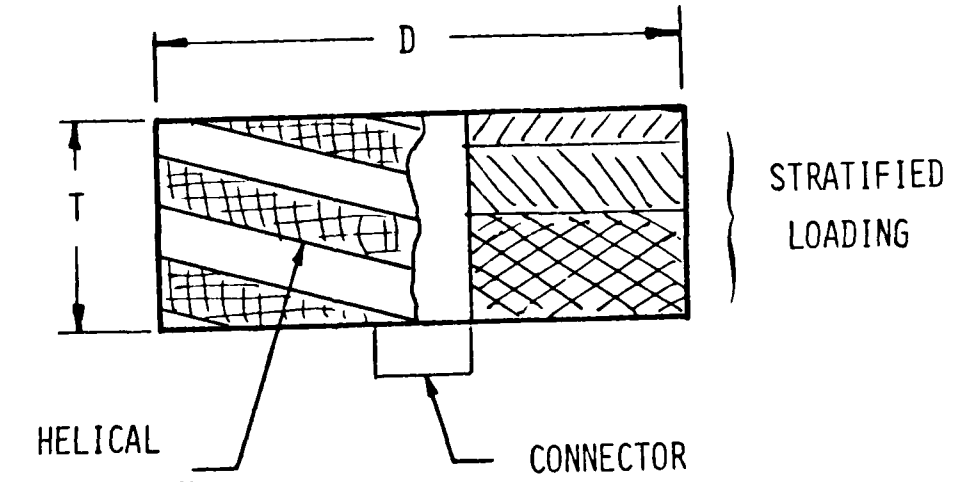

(b) Side View

Figure 17. Schematic drawing of a four-arm cavity-backed spiral with a helical extension to terminate the arms.

the spiral. The spiral contours are described by the equation

$$r_n(\phi) = r_i \exp [\alpha(\phi - \phi_n)]. \qquad (3)$$

where r_n is the radius to the n-th contour at the polar angle ϕ, r_i is the radius to the feed points, ϕ_n is the polar angle at the feed point for the n-th contour, and defines an exponential growth rate for the spiral. (Note that one spiral arm is bounded by two spiral contours.)

The equiangular spiral satisfies the basic conditions for a "frequency-independent" antenna [15,16]. The input impedance of such a structure is ideally real and is determined by the number of feed points, and the impedance and radiation pattern do not vary with frequency. The n-arm spiral may be considered an (n-1)-port antenna that can be excited in (n-1) linearly independent modes [14]. The equiangular spiral is also known as a logarithmic spiral.

Broadband spiral antennas are sometimes made in the form of Archimedian spirals, which are described by the equation

$$r_n(\phi) = r_i [1 + \beta (\phi - \phi_n) \quad , \qquad (4)$$

where β defines a linear growth rate for the spiral. Archimedian spirals sometimes have better radiation pattern characteristics than equiangular spirals, but they do not satisfy theoretical criteria for "frequency-independence," and they were not considered in this work.

Although radiation patterns do not have their usual significance in this work, it is desirable to have the antenna concentrate energy in front of the radiating aperture. Figure 18 illustrates the general shapes of patterns that can be obtained with a multiarm spiral placed in the z = 0 plane. A two-arm spiral with balanced excitation will produce the pattern that has the desired forward concentration of energy as shown for n = 1.

A spiral radiates very pure circular polarization along the boresight axis. The sense of polarization is determined as left-or right-handed, when the thumb points away along the boresight axis and the fingers of the hand follow the direction of spiral growth. If a plane wave with right-hand circular polarization (RHCP) is normally incident on a conducting plane, the reflected wave has left-hand circular polarization (LHCP). In the ideal case, a spiral cannot receive its reflection from a uniform, normally oriented ground plane. However, non-

the spiral. The spiral contours are described by the equation

$$r_n(\phi) = r_i \exp [\alpha(\phi - \phi_n)], \qquad (3)$$

where r_n is the radius to the n-th contour at the polar angle ϕ, r_i is the radius to the feed points, ϕ_n is the polar angle at the feed point for the n-th contour, and α defines an exponential growth rate for the spiral. (Note that one spiral arm is bounded by two spiral contours.)

The equiangular spiral satisfies the basic conditions for a "frequency-independent" antenna [15,16]. The input impedance of such a structure is ideally real and is determined by the number of feed points, and the impedance and radiation pattern do not vary with frequency. The n-arm spiral may be considered an (n-1)-port antenna that can be excited in (n-1) linearly independent modes [14]. The equiangular spiral is also known as a logarithmic spiral.

Broadband spiral antennas are sometimes made in the form of Archimedian spirals, which are described by the equation

$$r_n(\phi) = r_i [1 + \beta (\phi - \phi_n)] \quad , \qquad (4)$$

where β defines a linear growth rate for the spiral. Archimedian spirals sometimes have better radiation pattern characteristics than equiangular spirals, but they do not satisfy theoretical criteria for "frequency-independence," and they were not considered in this work.

Although radiation patterns do not have their usual significance in this work, it is desirable to have the antenna concentrate energy in front of the radiating aperture. Figure 18 illustrates the general shapes of patterns that can be obtained with a multiarm spiral placed in the z = 0 plane. A two-arm spiral with balanced excitation will produce the pattern that has the desired forward concentration of energy as shown for n = 1. .

A spiral radiates very pure circular polarization along the boresight axis. The sense of polarization is determined as left-or right-handed, when the thumb points away along the boresight axis and the fingers of the hand follow the direction of spiral growth. If a plane wave with right-hand circular polarization (RHCP) is normally incident on a conducting plane, the reflected wave has left-hand circular polarization (LHCP). In the ideal case, a spiral cannot receive its reflection from a uniform, normally oriented ground plane. However, non-

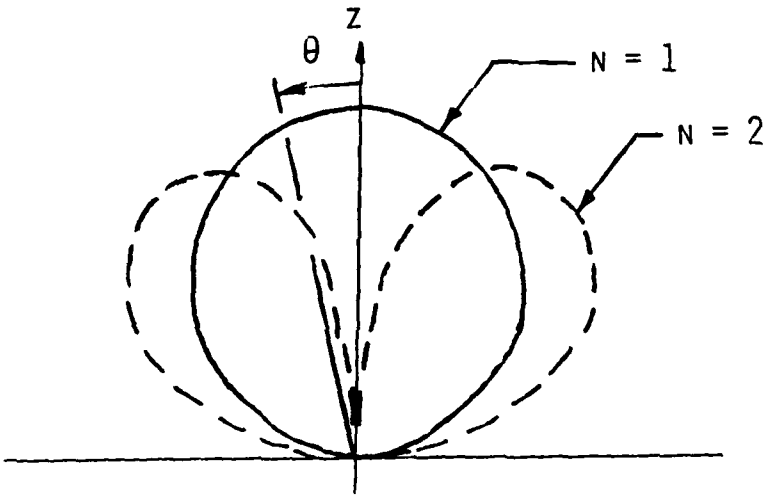

$$E_N(\theta,\phi) = \mathrm{Cos}\theta\ (\mathrm{Sin}\theta)^{N-1}\ \mathrm{Exp}(\mathrm{J}N\phi)$$

Figure 18. Cross-sections of rotationally symmetric radiation patterns for modes 1 and 2 of a multiarm spiral.

uniform localized perturbations, however, will depolarize the reflected wave, so a circularly polarized antenna may provide an inherent capability to remove ground returns from target returns.

For this application, the main question concerning suitability of the spiral is its dispersive signal transfer characteristic. A current pulse excited at a spiral feed point will propagate outward along the spiral arm until all the frequency components are radiated. At one frequency f, radiation occurs near a ring on the spiral where the circumference C is one wavelength ($\lambda = c_o/f$. where c_o is the plane-wave phase velocity). Therefore, the spiral acts like a transmission line that delays low frequencies more than high frequencies. Theoretical calculations of pulse responses have confirmed that a spiral has the effect of radiating an "inverse chirp" pulse [17]. These same calculations have also confirmed that the transmitter pulse can be designed to cancel the antenna dispersion, when high pulse fidelity is required. When such an approach is taken with a monostatic radar, it should be recognized that the transmit and receive responses of an antenna differ by a time-derivative operation on the incident pulse waveform [18,19].

A simple estimate for the dispersive effect of a spiral can be developed by calculating the propagation path length, as a function of frequency, from the feed point to the ring on the spiral at which radiation occurs. The length s of a spiral contour is given by

$$s = r_i \int_o^{\phi_o} \exp(\alpha\phi) d\phi$$

$$= r_1 \alpha^{-1} [\exp(\alpha\phi_o) - 1] \ , \qquad (5)$$

where the contour starts at the feed point, ($r = r_i$; $\phi_n = 0$), and winds outward through the polar angle ϕ_o. At the frequency f, radiation occurs at a radius $r_o = c_o/(2\pi f)$, and at this radius the polar angle is $\phi_o = (1/\alpha)\ln(r_o/r_i)$. Therefore, the propagation path length between the feed point and the radiating region on the spiral is

$$s = \frac{1}{\alpha} \left[\frac{c_o}{2\pi f} - r_i \right] \qquad (6)$$

The time delay associated with this path length is $t_d = s/c_o$, and the phase delay

is $\phi_d = 2\pi s/\lambda$. The feed points are normally located on a circle whose circumference is small compared with the shortest operating wavelength. In such a case, the term r_i/α may be neglected in Equation (6) to obtain the following approximations:

$$s \approx \frac{c_o}{2\pi\alpha f} \quad , \tag{7}$$

$$t_d \approx \frac{1}{2\pi\alpha f} \quad , \text{ and} \tag{8}$$

$$\phi_d \approx \frac{1}{\alpha} \quad . \tag{9}$$

The phase delay is independent of frequency, and the time delay varies inversely with frequency. The magnitude of the delay increases as the spiral is wound more tightly (i.e., the delay varies inversely with the growth rate α).

3.2.2 BROADBAND HORNS

The broadband horn is clearly a practical candidate for this application. The TEM horn developed by Calspan has performed well with the mine detection radar system. The only objection to it is its 45-inch length. The design has been well documented [6], and it will not be discussed in detail. Basically, a TEM horn may be viewed as a derivative of either a parallel plate waveguide or a biconical waveguide. An infinite structure of either form can support a TEM mode which is nondispersive. The Calspan horn is formed form a pair of flat copper sheets that are cut into a tear-drop shape. The sheets are 40 inches long and are flared from the feed point to the radiating aperture at an angle of 11.6°. The flare angle was derived from a constraint on the allowable dispersion for the horn, and the shape of the sheets was derived from a constraint on the reflection coefficient. According to the theoretical model used, the 40-inch length of the horn was necessary to keep the reflections below -40 dB. The horn was excited through a self-balancing coaxial connector attached at the broad end of the sheets. At the radiating end of the horn, resistance cards were attached to the narrow ends of the copper sheets to terminate residual currents. Measurements made at the National Bureau of Standards (NBS) show that reflections from the Calspan horn were below -22 dB at frequencies between 300 and 1,000 MHz

and were below -14 dB at frequencies between 200 and 2,000 MHz [11]. Time-domain measurements obtained by Calspan indicated that before the fiberglass package was added, the reflection levels were below -40 dB [6]. The Calspan horn is a carefully optimized example of a TEM horn, and it is not reasonable to expect that similar performance may be obtained with a much shorter version of the horn.

A horn antenna may be viewed as an impedance transformer that guides a propagating wave from a constrained region in the throat of the horn, through a radiating aperture, into free space. Conventional microwave horns have closed, pyramidal, or conical sidewalls, and they will not propagate energy at frequencies below the cut-off frequency for the lowest waveguide mode that can exist in the hollow structure. Pyramidal and conical horns are normally limited to bandwidths of less than one octave. The useful operating range can be extended to over two octaves by the use of ridges inside the horn. Figure 19 illustrates the basic concept of a broadband horn. A space between a pair of conducting ridges is excited by a coaxial probe, and the ridges are flared into a radiating aperture. Metallic sidewalls surrounding the ridges are illustrated by the dashed lines. If the walls are in place, the horn cannot propagate energy below the cut-off frequency of its dominant mode. At lower frequencies, the walls of the horn will effectively short-circuit the coaxial connector. If the walls are removed, a TEM mode can be excited at any frequency. For the TEM mode to radiate efficiently, the horn must provide an effective impedance transformation between the coaxial connector and the radiating aperture to free space. The length L and the aperture width D must normally be at least one-half wavelength at the lowest operating frequency to achieve a reasonable impedance transformation. Unless the aperture dimension is several wavelengths, the radiation pattern will have very little directivity. Therefore, it can be expected that dimensions of at least 20 inches should be required to achieve reasonable performance at 300 MHz. The Calspan horn, which is 40 inches long and operates down to 150 MHz, fits this guideline, but a 20-inch dimension is not acceptable for this application.

It is fairly clear that resistive loading must be incorporated to achieve a low reflection coefficient with a small horn. With excessive resistive loading, a horn can obviously be turned into a well-matched coaxial termination. The design challenge, then, is to use resistive loading to achieve a satisfactory impedance transformation while maintaining a reasonable radiation efficiency.

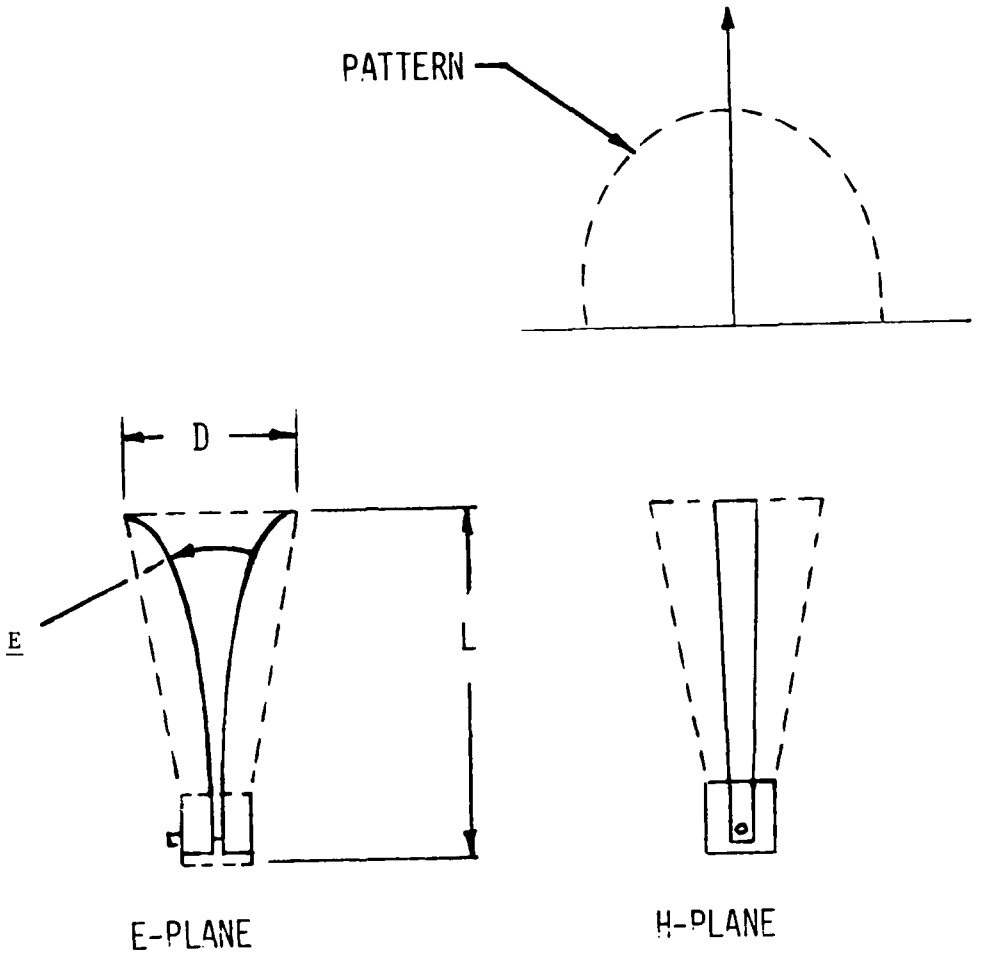

Figure 19. Schematic illustration of a rudimentary horn.

Substantial progress in this direction has been made by Dr. M. Kanda at NBS [11]. He has developed a broadband TEM horn that has walls with graded resistivity. The walls are formed by depositing a metal alloy (nickel/chrome) on plastic (polycarbonate) sheets. The metallization is dense near the feed point and very thin near the radiating aperture. Therefore, the resistivity is low near the feed point and high near the radiating aperture. The metallized sheets are used to form H-plane walls of a TEM horn in a manner similar to the Calspan structure. Reflections for the NBS horn are reported to be below -20 dB between 600 and 2,000 MHz. Below 600 MHz, reflections for the NBS horn are similar to but higher than, reflections for the Calspan horn. Above 2,000 MHz and up to 6,000 MHz, reflections from the NBS horn are below -15 dB. For a horn that is only about 14 inches long, these results are encouraging. If the low frequency behavior can be improved and the radiation efficiency is satisfactory, a similar horn may be suitable for this application.

3.2.3 BROADBAND DIPOLE

A conventional dipole antenna is not a practical candidate for this application. The dipole is highly resonant, because it must be nearly one-half wavelength to support the desired sinusoidal current distribution. Also, energy is radiated in an omni directional pattern about the dipole cylinder axis, so the desired unidirectional concentration of energy in the near-zone cannot be achieved. However, recent developments with non-resonant, resistively loaded dipoles indicate that very good pulse fidelity may be achieved [9,10]. While there is no expectation that satisfactory energy concentration can be achieved, the resistively loaded dipole may be of interest as a reference antenna for comparing the pulse responses of more suitable antennas.

Figure 20 illustrates the concept of resistively loaded dipoles,in terms of resistively loaded monopoles that are imaged in a conducting ground plane. The resistive bow tie and the resistive dipole both attempt to establish a current distribution along the structure that has a traveling wave nature, rather than a resonant nature. The resistive bow tie may be viewed as a perturbation of a biconical antenna in which the resistive loading is used to relieve the effect of terminating the structure at a finite length. The resistive card spreads the current and decreases the current density at the end of the antenna.

The resistively loaded dipole is based on a theoretically determined resistive profile that forces the current to have a traveling wave nature [20,21]. A practical realization of this antenna has been developed recently at the

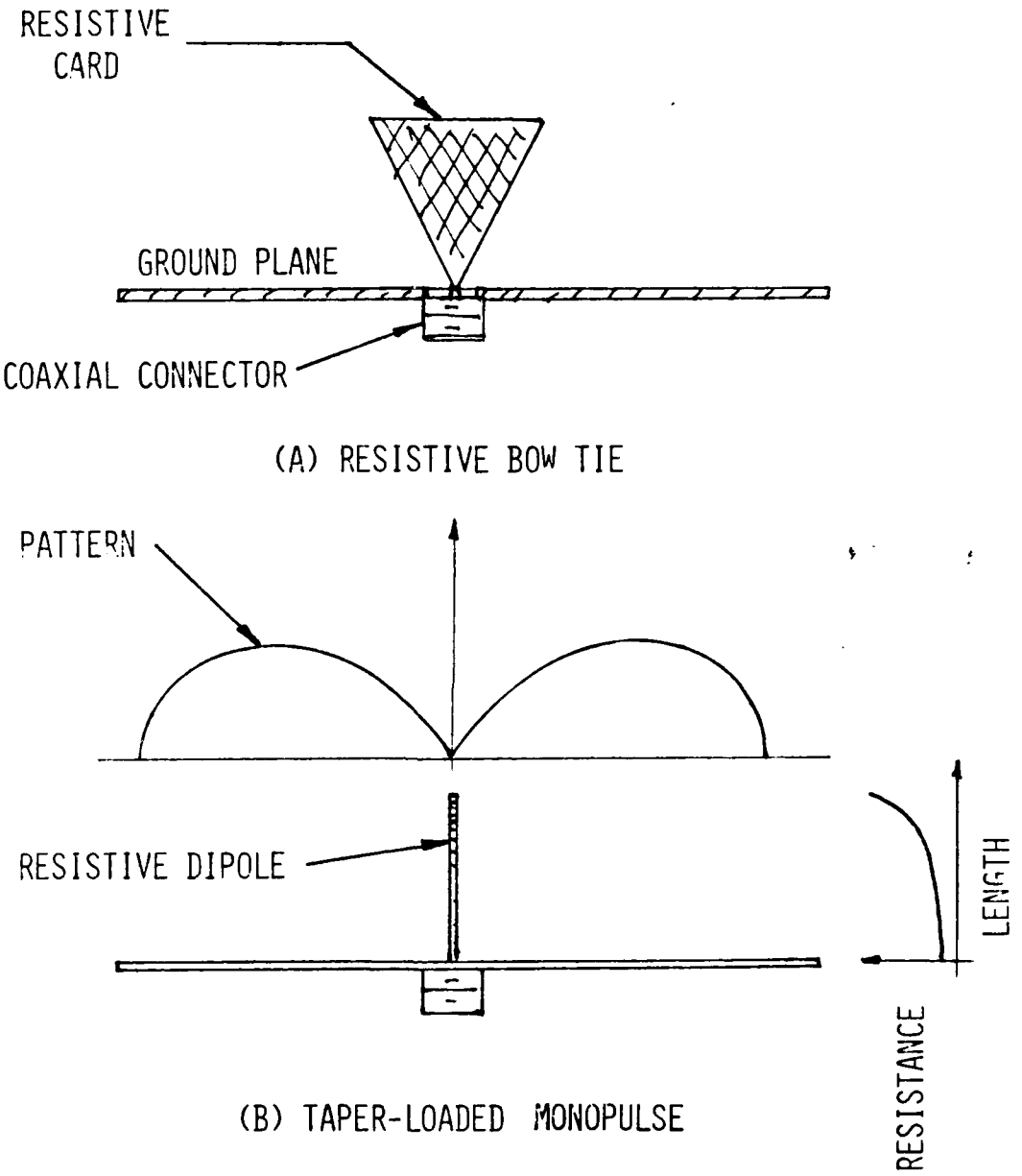

Figure 20. Schematic illustration of broadband monopoles incorporating resistive loading.

National Bureau of Standards [9,10]. The desired resistive profile is obtained by sputtering a metal alloy on a glass rod. The reported experimental results for this antenna agree well with theoretical calculations, and very good pulse responses have been obtained. Qualitatively, the broadband nature of the resistively loaded dipole may be explained by noting that the increasing resistivity near the ends of the dipole causes the element to appear shorter in length at higher frequencies. The input impedance of the antenna is not frequency independent. In the range from 300 MHz to 1,000 MHz, the resistance is nearly constant at about 50 ohms. However, the reactance varies from 300 ohms to 100 ohms over that same range. Therefore, the impedance mismatch between such a dipole and the mine detection radar will be large, and multiple reflections may prevent satisfactory operation. However, this newly developed antenna deserves further investigation.

3.2.4 LOG-PERIODIC DIPOLE ARRAY

The log-periodic dipole array (LPDA) is not a frequency-independent antenna in the strict sense, but it can have almost unlimited operating bandwidth. The antenna is a traveling wave structure formed by a linear array of dipoles that have increasing lengths. Figure 21 illustrates the general structure of the LPDA. A traveling wave is excited at the feed end and propagates along the structure towards the connector end. The length of the shortest dipole at the feed end must be somewhat less than one-half wavelength at the highest operating frequency, and the length of the longest dipole at the connector end must be at least one-half wavelength at the lowest operating frequency. The lengths of any pair of successive dipoles have a fixed ratio τ, which is typically between 0.9 and 0.99. The spacing between pairs of adjacent dipoles is also fixed by the ratio τ. A traveling wave excited at the feed propagates along the structure to a region where the dipole length is about one-half wavelength at the operating frequency. Within that region, the energy in the traveling wave is coupled through the dipoles and radiated forward into space. The phasing of the dipole elements in the radiating region is such that the energy is radiated forward in the direction opposite to the direction of traveling wave propagation.

While there are many variations of LPDA structures[21,22], the antenna cannot be made to operate efficiently when the length, L, and the width ,W, are much less than one-half wavelength at the lowest operating frequency. Small LPDA structures typically have a reflection coefficient greater than -10 dB,

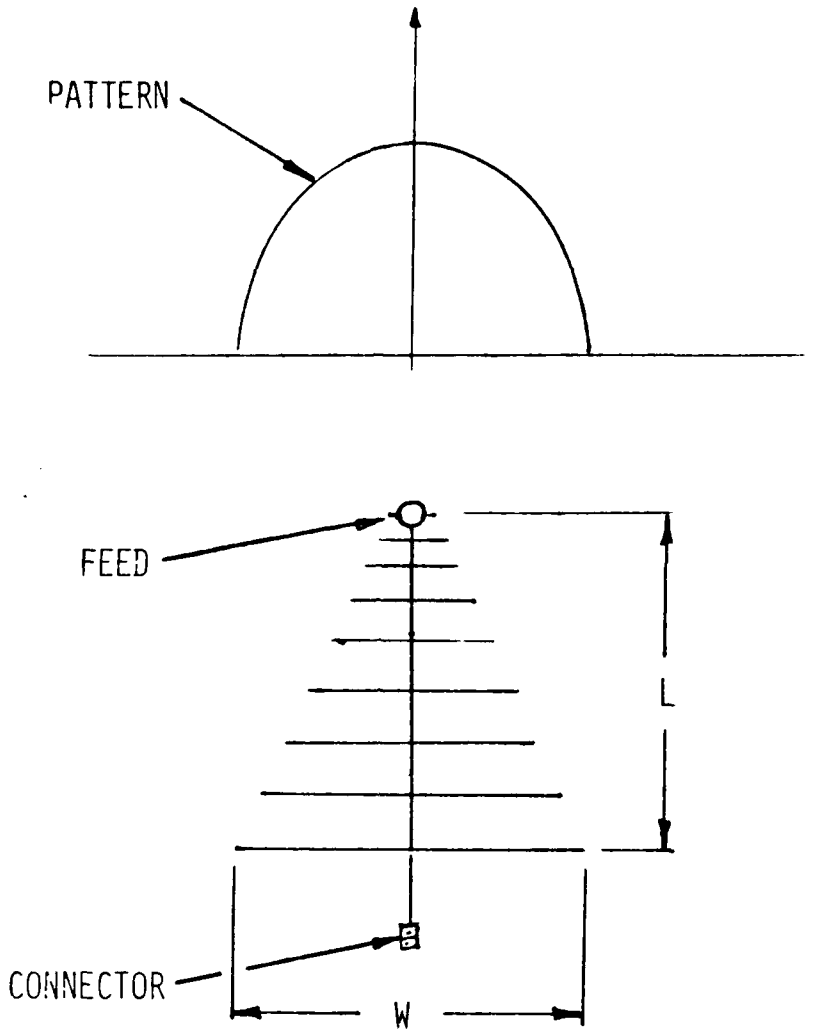

Figure 21. Schematic illustration of a log-periodic dipole array.

and they have substantial backlobe radiation. The LPDA is dispersive because the phase center of radiation moves away from the feed point as the frequency decreases and the dipoles present discrete rather than continuous, loads to the traveling wave structure. Therefore, the LPDA does not seem to have the characteristics required for the mine detection radar application.

3.2.5 ANTENNA SELECTIONS

Table 3 presents a qualitative comparison of the candidate antennas. The spiral antenna offers the most attractive packaging potential. It could possibly be packaged as a disk having a diameter of 12 inches and a height of 2 to 4 inches. It provides efficient broadband concentration of energy in front of the radiating aperture and makes the most efficient use of the available aperture for low frequency radiation. The primary concern with the spiral is whether the dispersive characteristics can be overcome by signal processing techniques. The Calspan horn is known to perform satisfactorily with the mine detection radar, but there is good reason to expect that the same concept will not give acceptable performance if the length is decreased substantially. Also, tests conducted as part of this work indicate that the low frequency energy is not well concentrated near the radiating aperture. The use of resistive walls in a horn may permit a reduction in length with some sacrifice in efficiency. The resistive dipole is the smallest known candidate antenna that provides good pulse response. However, the expected impedance mismatch of a dipole makes it unacceptable for use in the monostatic radar that uses the same antenna for transmit and receive. The log-periodic dipole array is a popular broadband antenna, but it does not seem to have any of the important characteristics needed for the mine detection antenna system.

Initially, the spiral was selected as the antenna to receive primary attention on this work. Two spirals were fabricated and developed through preliminary frequency domain testing. Later in the program, Dr. Motohisa Kanda, of the National Bureau of Standards (Boulder, Colorado), made available one of his resistive dipoles, and he indicated that metallized walls for the resistive TEM horn could be procured. (A small production run was recently completed at Vac-Tec Systems, Boulder, Colorado.) As a result, a pair of walls were obtained, and a TEM horn with resistive walls was developed. The fabrication of these antennas is discussed in the following subsection.

TABLE 3. QUALITATIVE SUMMARY OF ANTENNA CHARACTERISTICS

Antenna	Pulse Response	Energy Concentration	Size, Shape
Spiral	Dispersive	Good	Good
Horn	Good	Fair	Poor
Dipole	Mismatched	Poor	Good
LPDA	Poor	Poor	Poor

3.3 ANTENNA FABRICATION

Three generic types of antennas were fabricated as part of this work. Two 12-inch diameter cavity-backed spirals were fabricated. One spiral had a cavity depth of four inches; the other had a cavity depth of six inches. A broadband TEM horn was fabricated using graded resistivity H-plane walls. The horn had an overall length of 14 inches and aperture dimensions of 10 inches. A broadband dipole obtained from NBS required only the attachment of feed connections. The length of the dipole was 6.5 inches. Fabrication details are discussed in the following paragraphs.

3.3.1 CAVITY-BACKED SPIRAL

The cavity-backed spirals were packaged in plexiglas housing. The spirals were photo-etched on 1/16-inch, G-10 printed-circuit-board material, and feed connections were made through female SMA connectors and semirigid coaxial cable. Figure 22 shows a drawing of the final spiral antenna assembly. Two antenna housings were fabricated. One had a cavity depth of four inches; the other had a cavity depth of six inches. Two units were fabricated to investigate performance sensitivity to the depth of the cavity. The cavity must be loaded with microwave absorber to insure that the spiral radiates only in the forward direction. The arrangement of the absorber in the cavity has a great effect on the impedance of the antenna; in other applications, adjustment of the absorber loading is important in controlling the radiation characteristics of the antenna. Tests conducted during the development of these antennas indicated that the six-inch cavity gave better performance, but that similar performance could be achieved with a four-inch cavity with additional optimization.

The major effort required in the experimental development of these antennas was the optimization of the cavity loading material. In general, the cavity load consists of layers of microwave absorber and foam dielectric as indicated in Figure 22. All of the materials used in this work were manufactured by Emerson and Cumming, Inc. Approximately 70 arrangements of absorber were evaluated in terms of their effect on the antenna reflection coefficient. The final configurations selected for the six-inch spiral consisted of 1/4-inch of Eccofoam FS placed against the spiral surface, followed by a 4.5-inch layer of Eccosorb AN-79, with a final layer of 3/4-inch Eccosorb LS-26 placed at the rear of the cavity.

Two types of feed attachments were investigated. For the better feed illustrated in Figure 22, the two arms of the spiral were connected through a pair

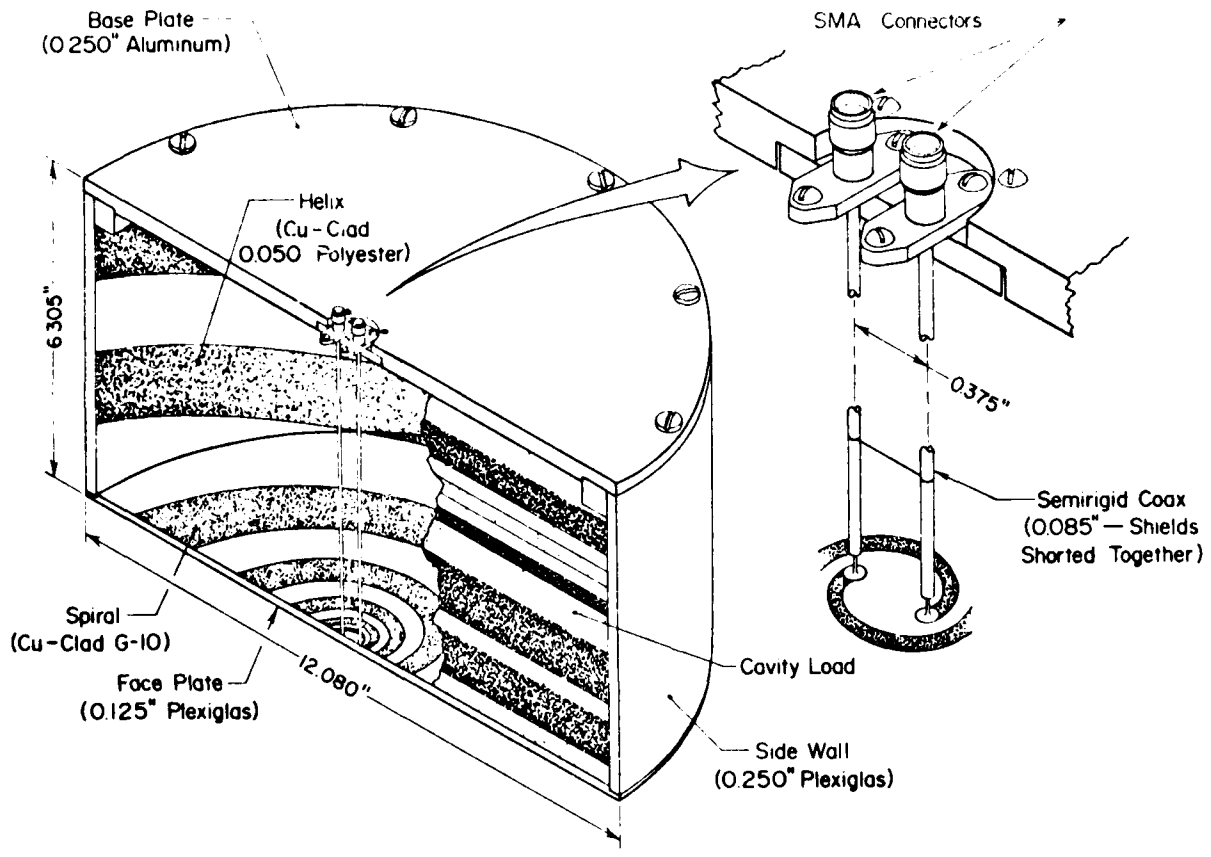

Figure 22. Drawing of the six-inch spiral antenna assembly.

of coaxial lines to an externally mounted 180° hybrid that served as served as a balun. The hybrid was an Anzac H-9. For the second feed that was considered, a single coaxial cable was connected to the two spiral arms through a small pulse transformer that functioned as a balun. The pulse transformer has dimensions less than 0.5 inch and was attached directly to the spiral arms. Two transformers were considered. One, an Anzac TP-101, transformed 50 ohms unbalanced to 50 ohms balanced. The other, an Anzac TP-103, transformed 50 ohms unbalanced to 200 ohms balanced. Neither pulse transformer provided reflection coefficients as low as the H-9 hybrid. However, the hybrid separates even and odd returns from the balanced spiral structure, and the even returns are terminated in a matched load in this application. Additional tests with the radar will be needed to determine conclusively that the hybrid is better than the smaller and much cheaper pulse transformer balun.

Spiral structures with three different growth rates were etched for investigating the effect of spiral dispersion on the radar performance. The relative appearance of the three spirals is illustrated in Figure 23 which shows reduced copies of the three negatives used to etch the spirals. The exponential growth rate, α, is defined in Equation (3). The factor F is defined as $F = \exp(2\pi\alpha)$. The factor F is the ratio of two radii, after a 360° rotation around the spiral. Therefore, F = 3 indicates that the radius grows by a factor of three each time a point is moved 360° around the spiral. As part of this work, a computer program was developed to produce Calcomp plots of the spiral contours. Oversized spirals were drawn on paper and colored in by hand. Film negatives with the desired 11.5-inch outer diameter were obtained by photographic reduction.

Figure 24 illustrates the dispersive characteristics of the three spirals that were fabricated. The time delay and the phase delay, as defined in Equations (8) and (9), are plotted as functions of frequency. Spiral B is the one used in the final assembly. In terms of the antenna reflection, there was little difference in the three spirals, and additional tests with the pulsed radar will be needed to determine whether any one of the spirals is to be preferred.

The antenna performance was significantly improved at low frequencies when the spiral arms were terminated by a helix placed against the sidewall of the cavity. The helix was formed by two copper strips etched on a thin flexible teflon-glass substrate (K-6098-10, 3M Corporation). The strip width was 1.5 inches and the pitch angle of the helix measured from the face of the spiral was 10°.

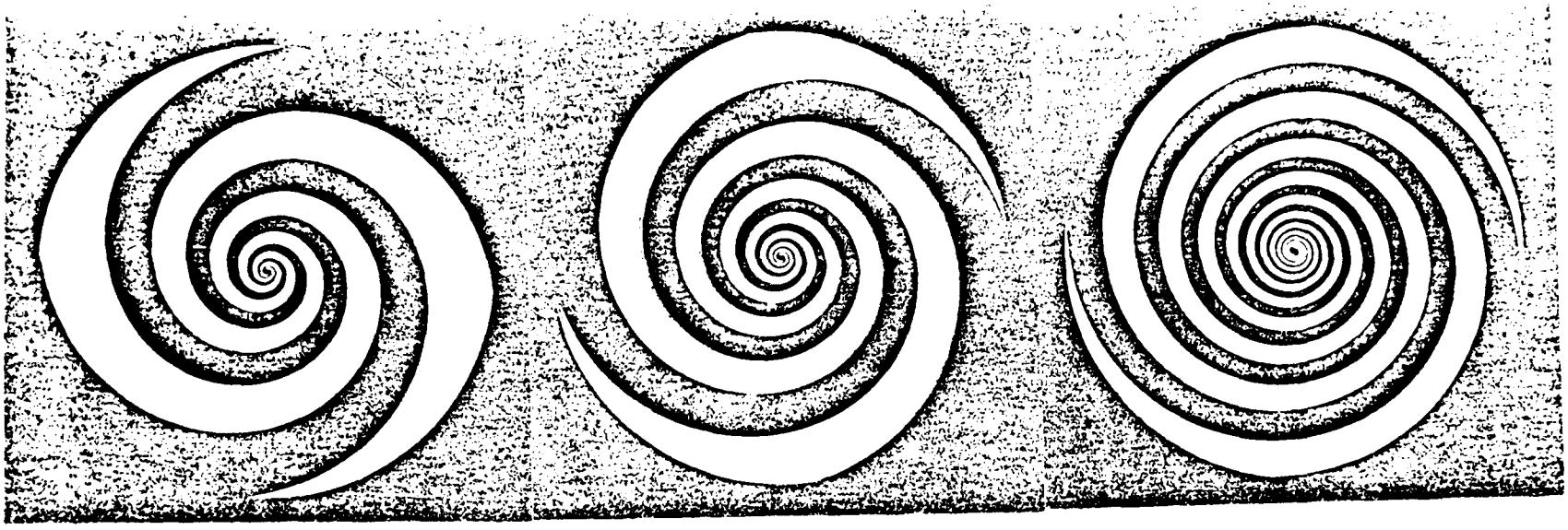

Spiral A:
(a) $\alpha = 0.221$
$F = 4$

Spiral B:
(b) $\alpha = 0.175$
$F = 3$

Spiral C:
(c) $\alpha = 0.110$
$F = 2$

Figure 23. Reduced copies of the three negatives used to etch spirals.

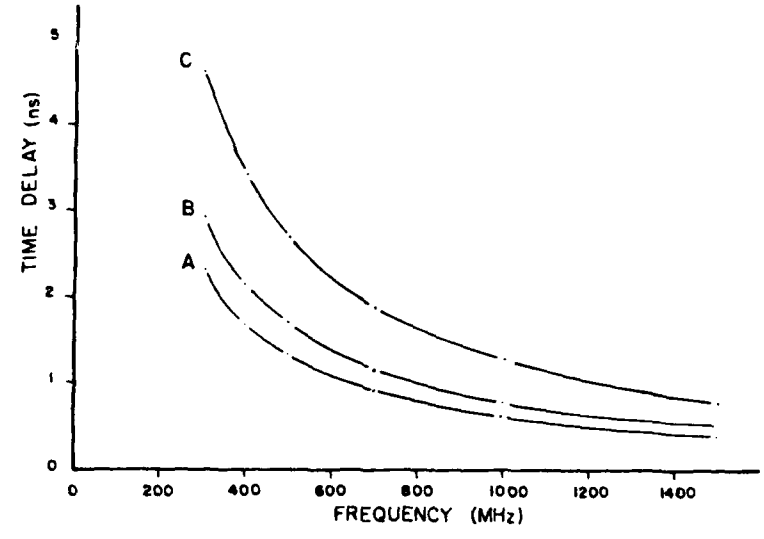

(a) Time Delay

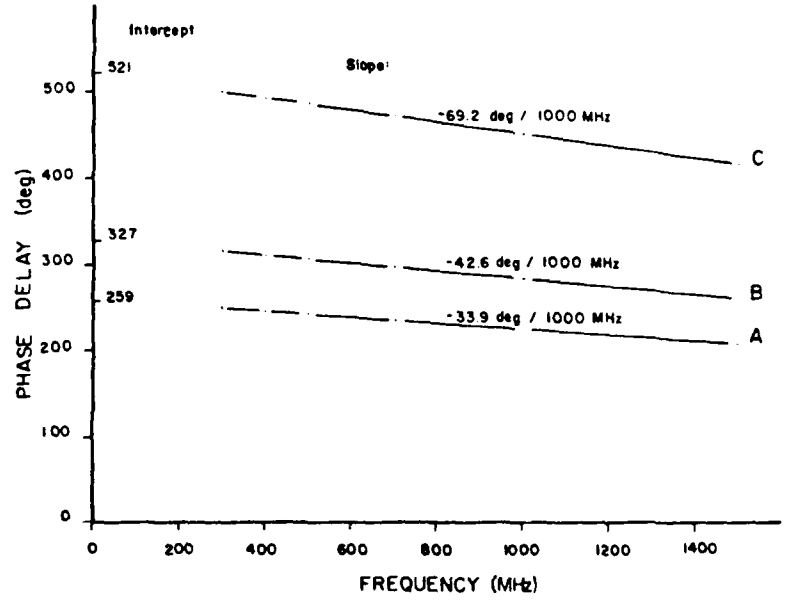

(b) Phase Delay

Figure 24. Dispersive characteristics of the three spiral structures A, B, and C.

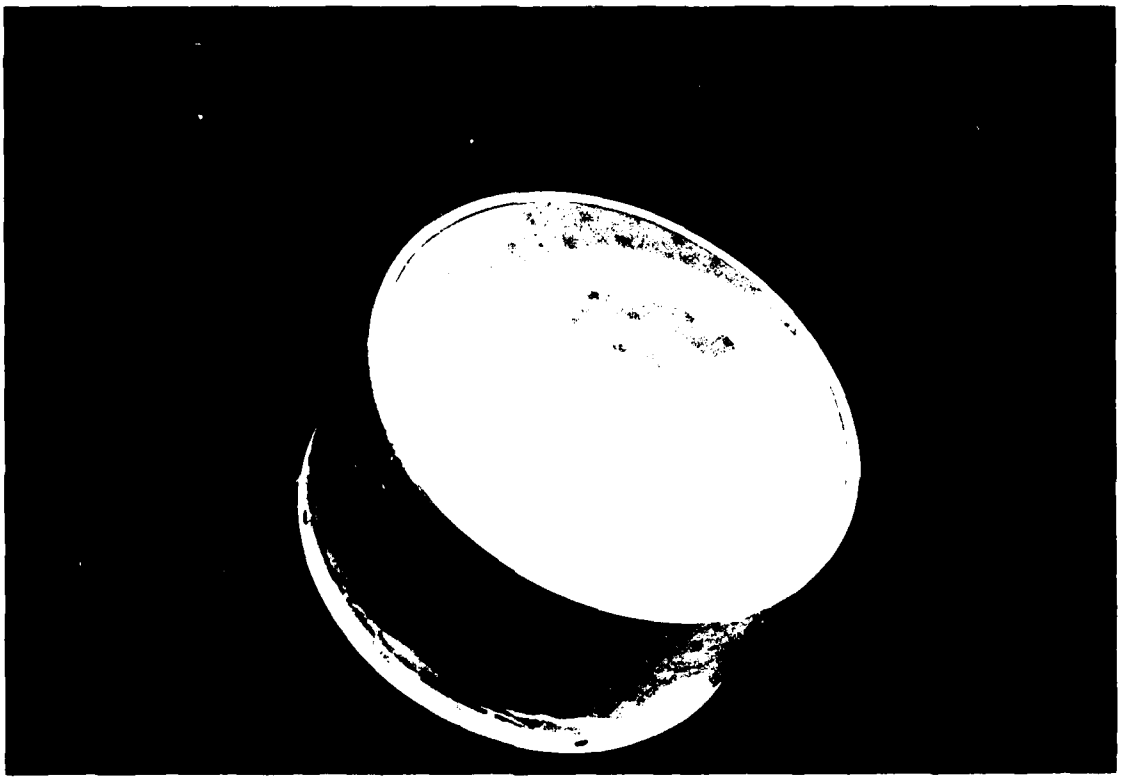

Figure 25. Photograph of the six-inch spiral antenna (face view).

Figure 26. Photograph of the six-inch spiral antenna (rear view).

Figures 25 and 26 show photographs of the front and rear sides of the six-inch spiral antenna. The rear view in Figure 26 also shows the Anzac H-9 hybrid mounted on the base plate. The primary concerns in the design of this package were structural integrity, potential for weatherproofing, and suitability for repeated assembly and disassembly. The antenna could be repackaged in a very lightweight fiberglass case with no change in performance.

3.3.2 BROADBAND HORN

The broadband TEM horn developed on this program was derived from the NBS model [11]. The H-plane walls, which have the graded resistivity metallization, were procured from Vac-Tec Systems in Boulder, Colorado. These were initially packaged with a 16^{0} flare angle as seen in the E-plane, but subsequent efforts to improve the impedance match at low frequencies resulted in a substantially different arrangement. A drawing of the final assembly is shown in Figure 27. Changes in the design were primarily to introduce an exponential flare in the E-plane and to add non-contacting metallic walls in the E-plane. It was necessary to prevent electrical contact between the H-plane walls and the E-plane walls to achieve propagation through the throat of the horn at low frequencies. A hollow waveguide formed by a single conductor cannot support TEM propagation and cannot support higher order modes at low frequencies. While the field in this resistive horn is not a TEM mode in the strictest sense, it can be reasonably interpreted as a perturbation of a TEM mode in a perfectly conducting structure.

The horn is excited through a self-balancing coaxial feed connection. A drawing of the feed is shown in Figure 28. A short piece of 0.085 inch semirigid coaxial cable joins an SMA connector to the apex of the horn. At the open end of the coax, the shield of the coax is joined to the metallization on the upper H-plane wall, and the center conductor is joined to the metallization on the lower H-plane wall. As the details in Figure 28 illustrate, the effect is to excite the horn by a voltage applied across a small circumferential gap in a copper tube that joins the H-plane walls. This feed structure has sufficient electrical symmetry in the operating frequency range that it functions very well as an unbalanced-to-balanced transition. Impedance matching is achieved by adjusting the shape and spacing of the walls of the horn.

The dimensions of the purchased H-plane walls are shown in Figure 29. The metallization is applied by vacuum deposition on 0.062 inch polycarbonate sheets. The polycarbonate is very flexible and can easily be deformed into an exponential curve.

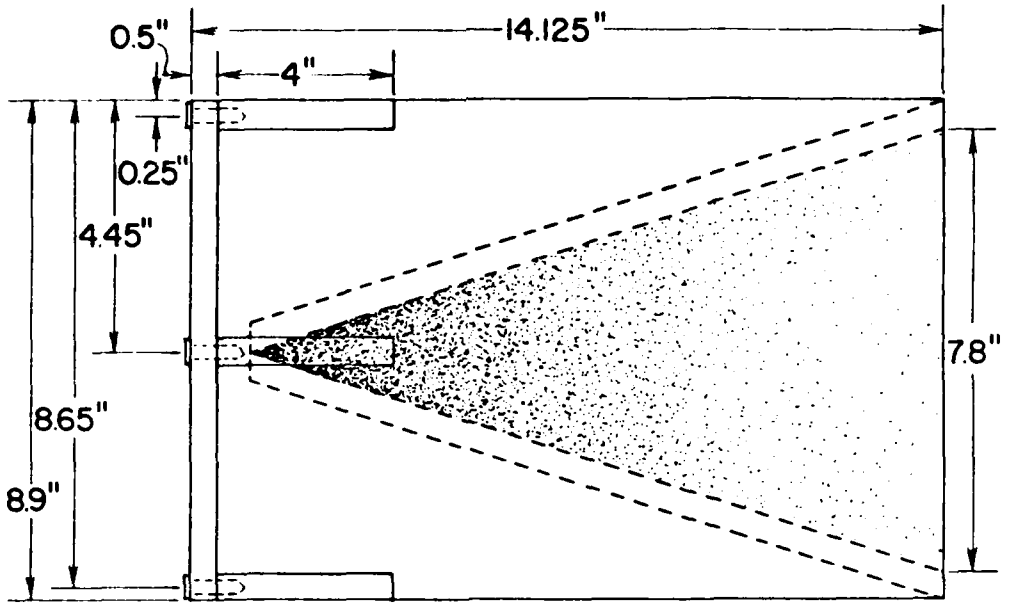

(a) H-Plane View

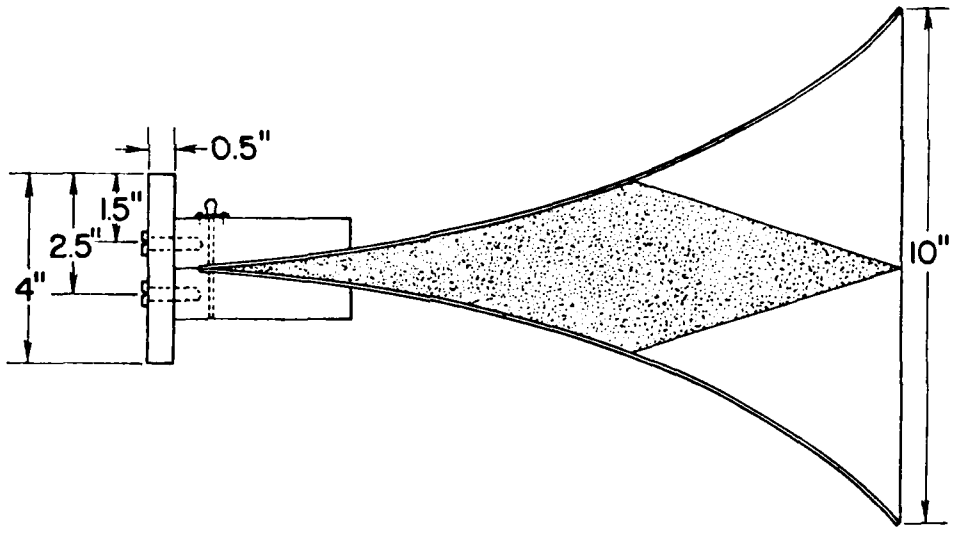

(b) E-Plane View

Figure 27. Drawing of GIT/EES horn assembly.

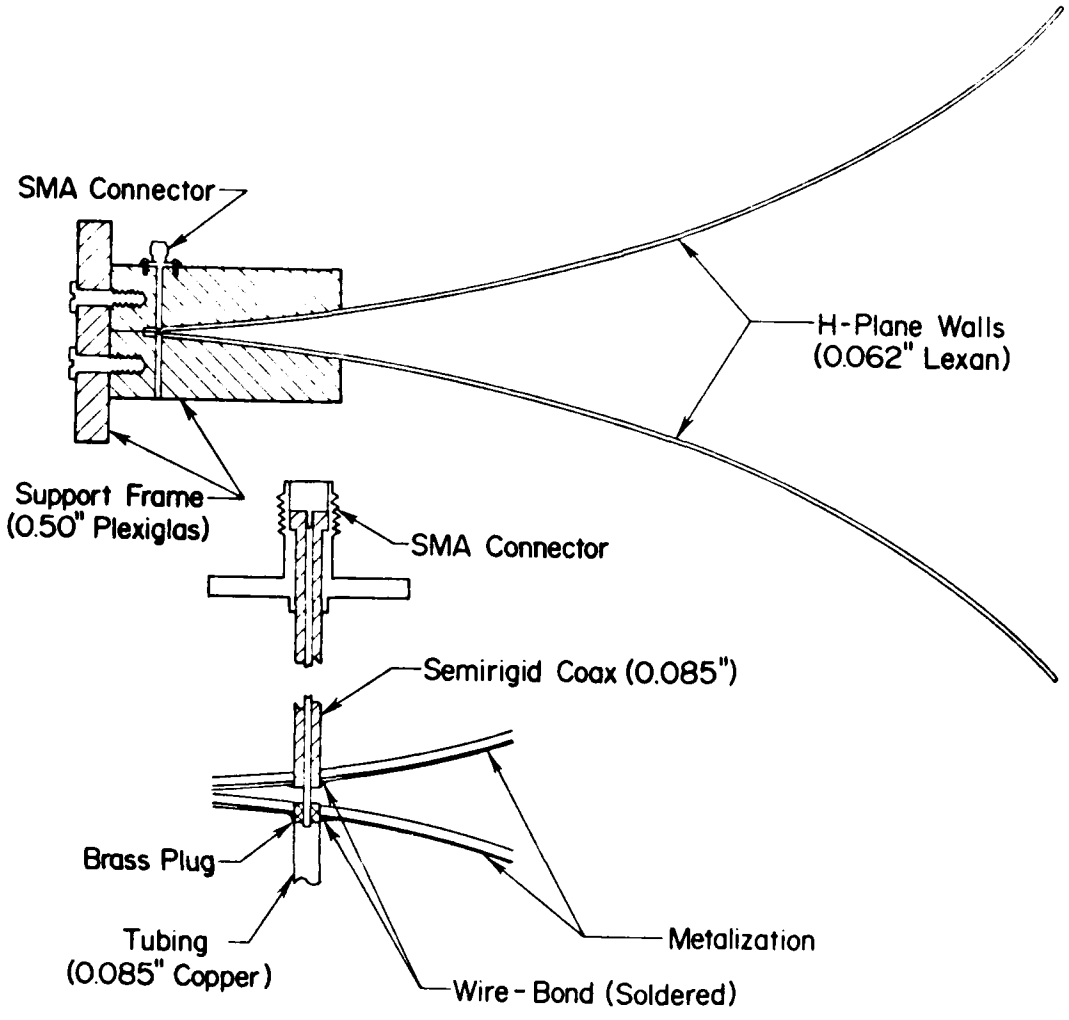

Figure 28. Drawing of feed connections for GIT/EES horn.

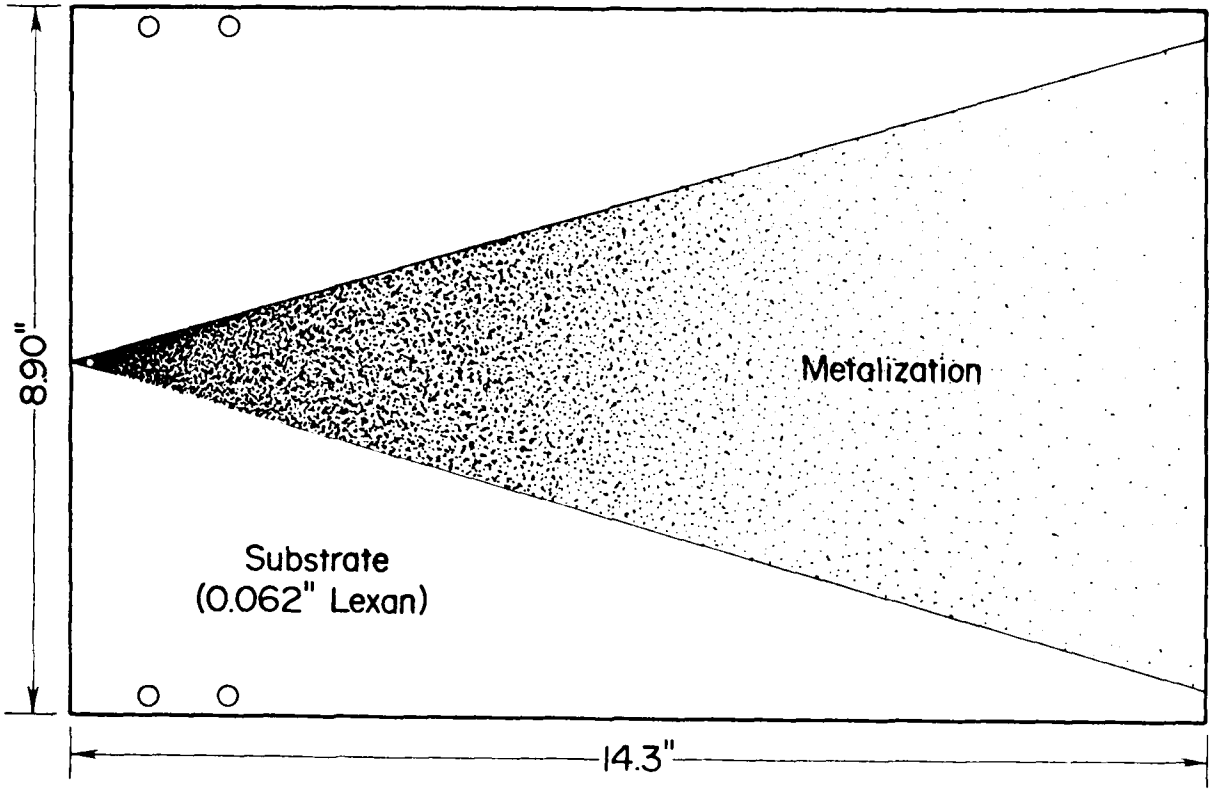

Figure 29. Drawing of graded-resistivity H-plane wall for GIT/EES horn.

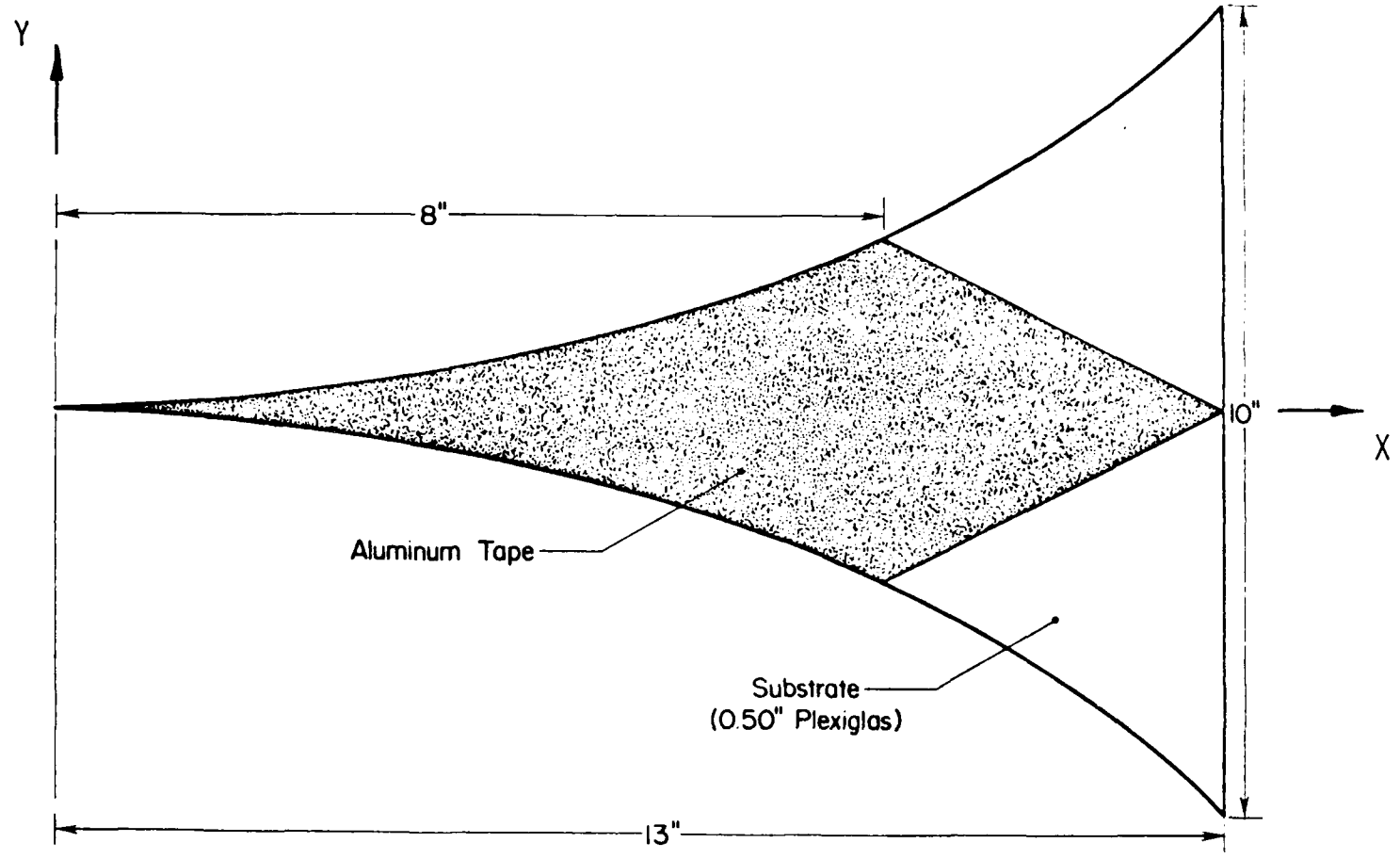

Figure 30. Drawing of E-plane wall for GIT/EES horn.

The H-plane wall is shown in Figure 30. This wall is formed by aluminum tape applied to 0.5-inch thick plexiglas. The tape is trimmed slightly away from the curved edges to insure that there is no electrical contact between the E- and H-plane walls. The tape is trimmed to a point at the aperture end of the wall to improve the impedance match of the antenna. The shape of the curved edges is based on an experimental minimization of the antenna reflection coefficient. The curve used in the final antenna is described by the following equation:

$$y = 0.060 + 0.4\,[-1 + \exp(0.22x)\,],\ x \leq 8.9"$$

$$y = 0.611x - 2.943,\ x \geq 8.9" \,. \qquad (10)$$

The E-plane walls are placed between the H-plane walls along the edges of the metallized area, and the flexible H-plane walls are screwed to the edges of the thick plexiglass walls. Photographs of the asembled horn are shown in Figures 31 and 32.

3.3.3 BROADBAND DIPOLE

A resistive dipole was obtained for use on this program through the courtesy of Dr. Motohisa Kanda of the National Bureau of Standards in Boulder, Colorado. The dipole is described in other publications [9,11]. An alloy, primarily nickel and chrome, is deposited on a glass tube. The diameter of the tube is 0.25 inches and the length is 6.45 inches. A pair of gold bands are provided at the center of the dipole for feed attachments, and the density of metallization decreases from the center to the ends of the tube.

Feed attachment was the only fabrication required for this antenna. It was suggested that a pulse transformer (Anzac TP-103) could be used as a balun between coaxial cable and the dipole. A drawing of the assembled antenna is shown in Figure 33. Reflections from this antenna were found to be very high, and there seemed to be no parameters that can be conveniently adjusted to reduce the reflections.

3.4 TEST RESULTS

All of the test results discussed in this section are based on measurements of antenna reflections as a function of frequency. These measurements were made with a microwave network analyzer. Where continuous, analog recordings of reflection are shown, the analyzer was operated in a manual mode with no special calibration or error correction. Where results are shown at discrete

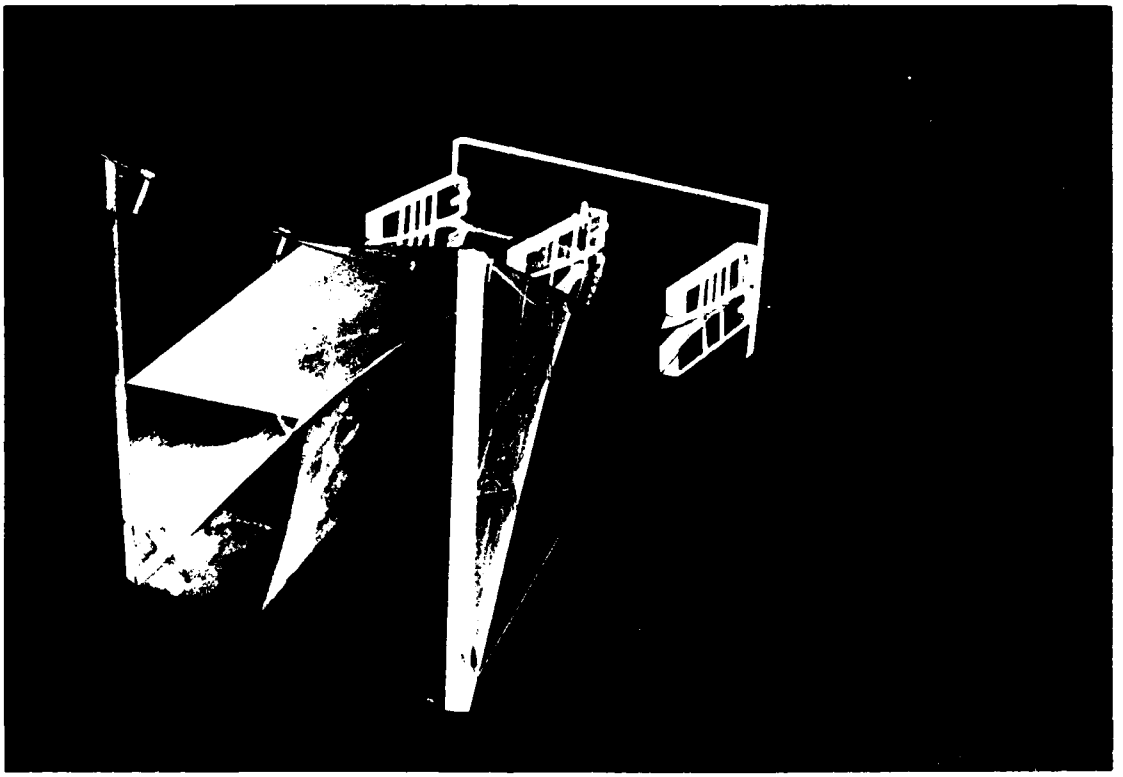

Figure 31. Photograph of the GIT/EES horn (E-plane vertical).

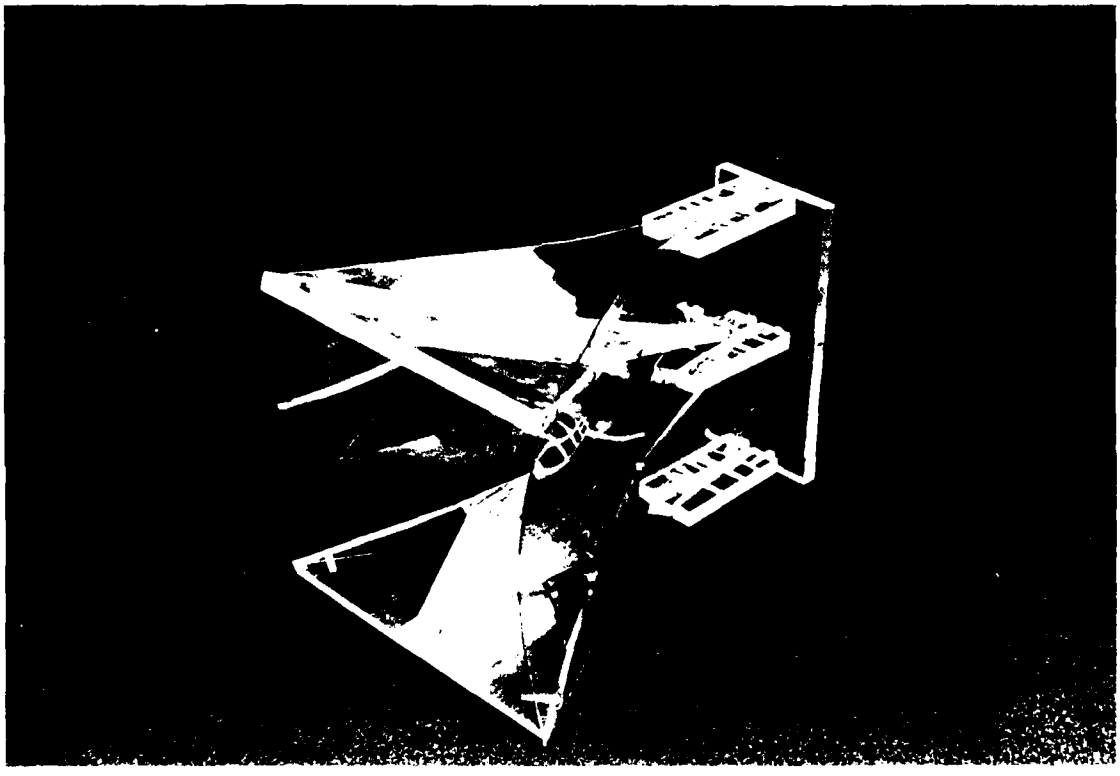

Figure 32. Photograph of the GIT/EES horn (H-plane vertical)

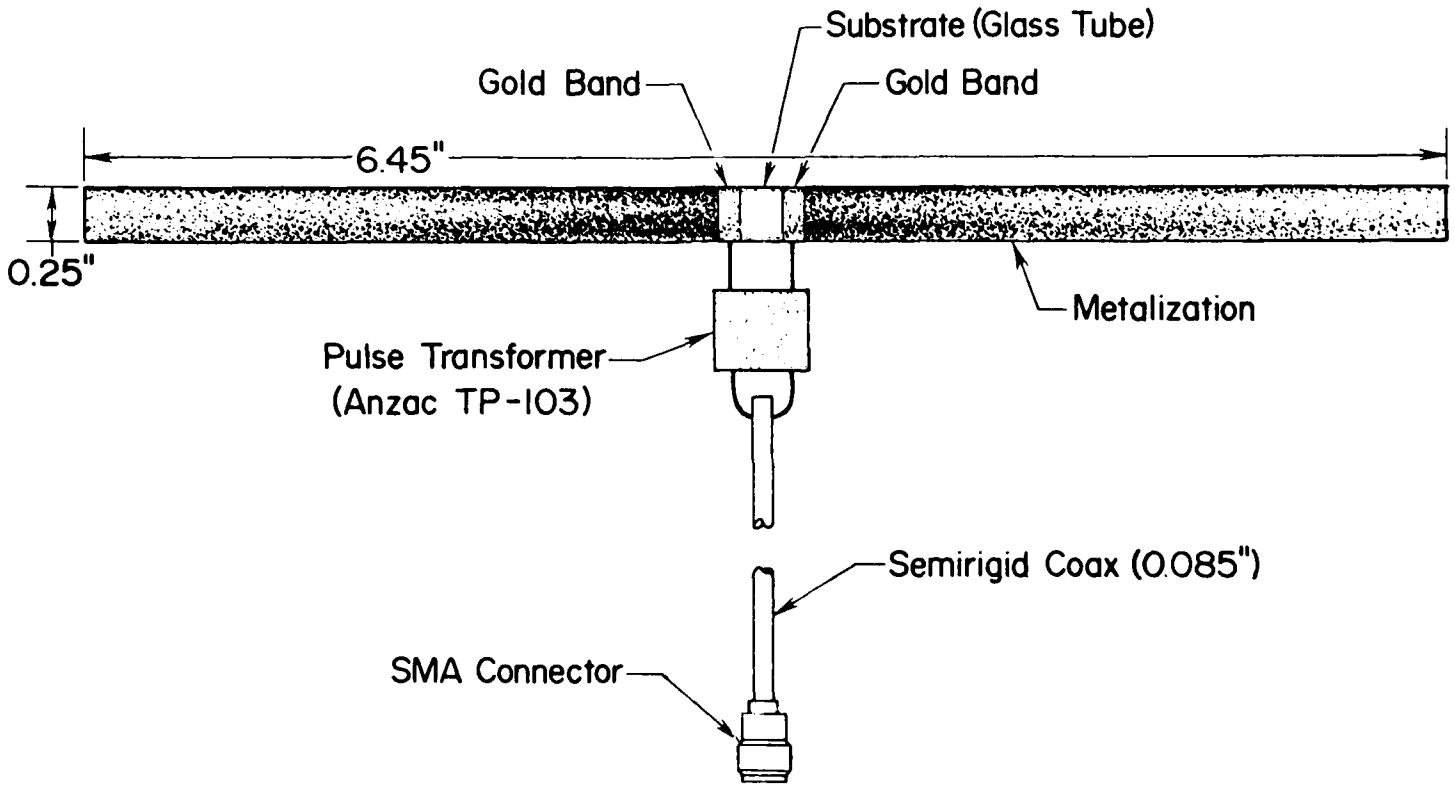

Figure 33. Drawing of NBS broadband dipole.

frequencies, the measurements were recorded using an automatic network analyzer (ANA) which operates under computer control and includes calibration and error correction [7,8] .

A few measurements of reflections from simulated targets placed near the antennas under test have been obtained. For these tests, the ANA was used to separate the target return from the combined return of antenna-plus-target. This was accomplished by first measuring the phasor reflection coefficient of the antenna alone, and then subtracting the antenna reflection coefficient from the phasor reflection coefficient for the combined antenna and target configuration. This subtraction measurement in the frequency domain corresponds to removing the antenna return by a range gate in the time domain, provided that the antenna does not cause severe pulse spreading. However, the frequency domain subtraction is effective whether or not there is dispersion in the antenna system. Therefore, this measurement indicates the effectiveness with which the antenna return can be removed by signal processing techniques.

The following paragraphs present frequency domain data obtained for the cavity-backed spiral, the broadband horn, and the broadband dipole.

3.4.1 CAVITY-BACKED SPIRAL

Figure 34 shows an analog recording of return loss measured for the six-inch cavity-backed spiral with a hybrid balun, a helix termination, and with no absorber loading in the cavity. (Return loss is the power reflection coefficient, expressed in negative decibels; i.e., RL = -20 log R, where R is the magnitude of the reflection coefficient.) Figure 35 shows the return loss for the same antenna when an optimized absorber load is placed in the cavity. A comparison of Figures 34 and 35 shows that the absorber dramatically reduces reflections from the antenna. It is likely that the reflections can be reduced even more, but additional effort is not warranted until test can be conducted with the mine detection radar to verify that the dispersive effects of the antenna can be compensated. Figures 36 and 37 show analog plots of return loss for the 4-inch spiral with Anzac TP-101 and TP-103 transformers, respectively. These data were recorded with the cavity loaded, but without a helical termination. Considerable experimentation with the absorber loading did not yield any significant improvements over the reflections shown in the figures. The hybrid provided a better balun than the pulse transformers.

Figure 38 shows the return loss for the six-inch spiral over the extended frequency range from 200 to 2,000 MHz. These data were recorded using the

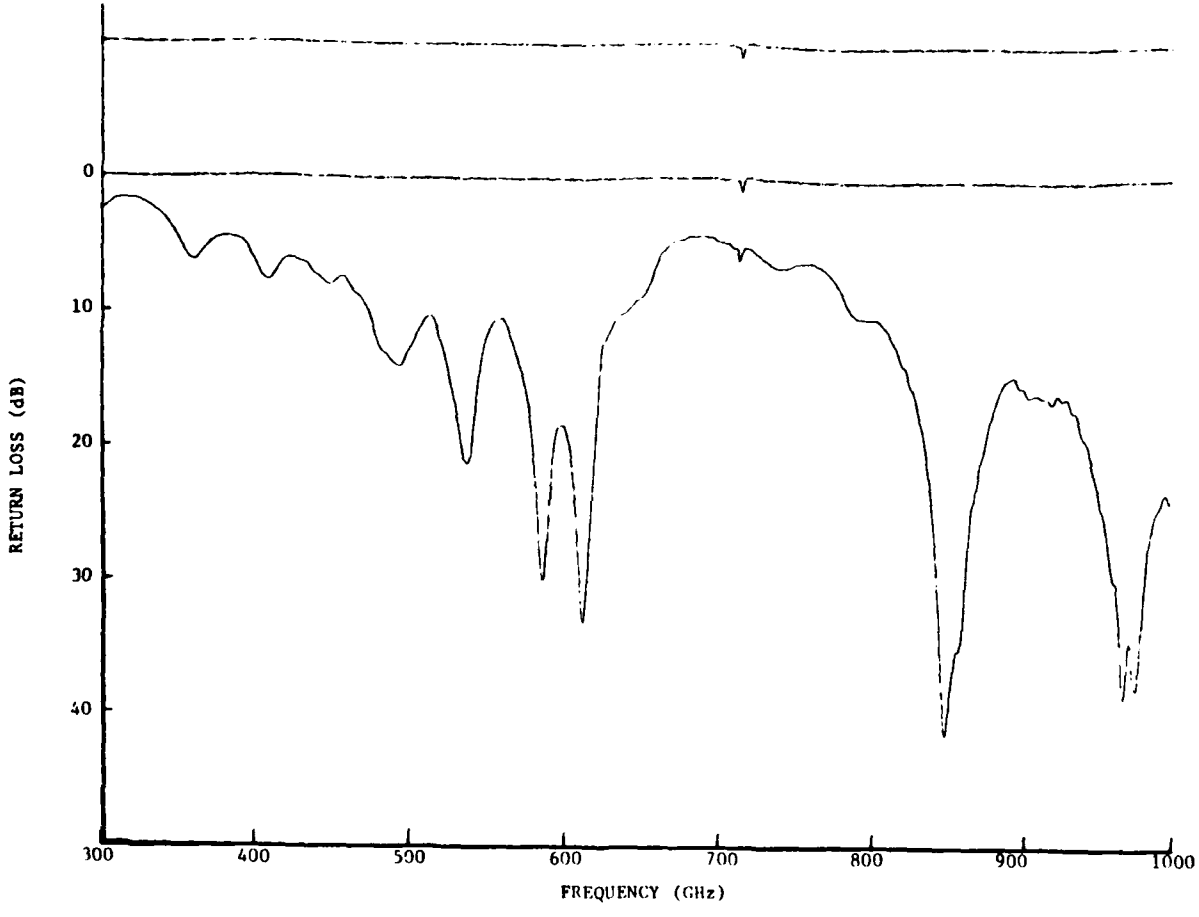

Figure 34. Swept-frequency recording of reflections from the six-inch spiral, measured at input to Anzac H-9 hybrid balun. Cavity absorber removed.

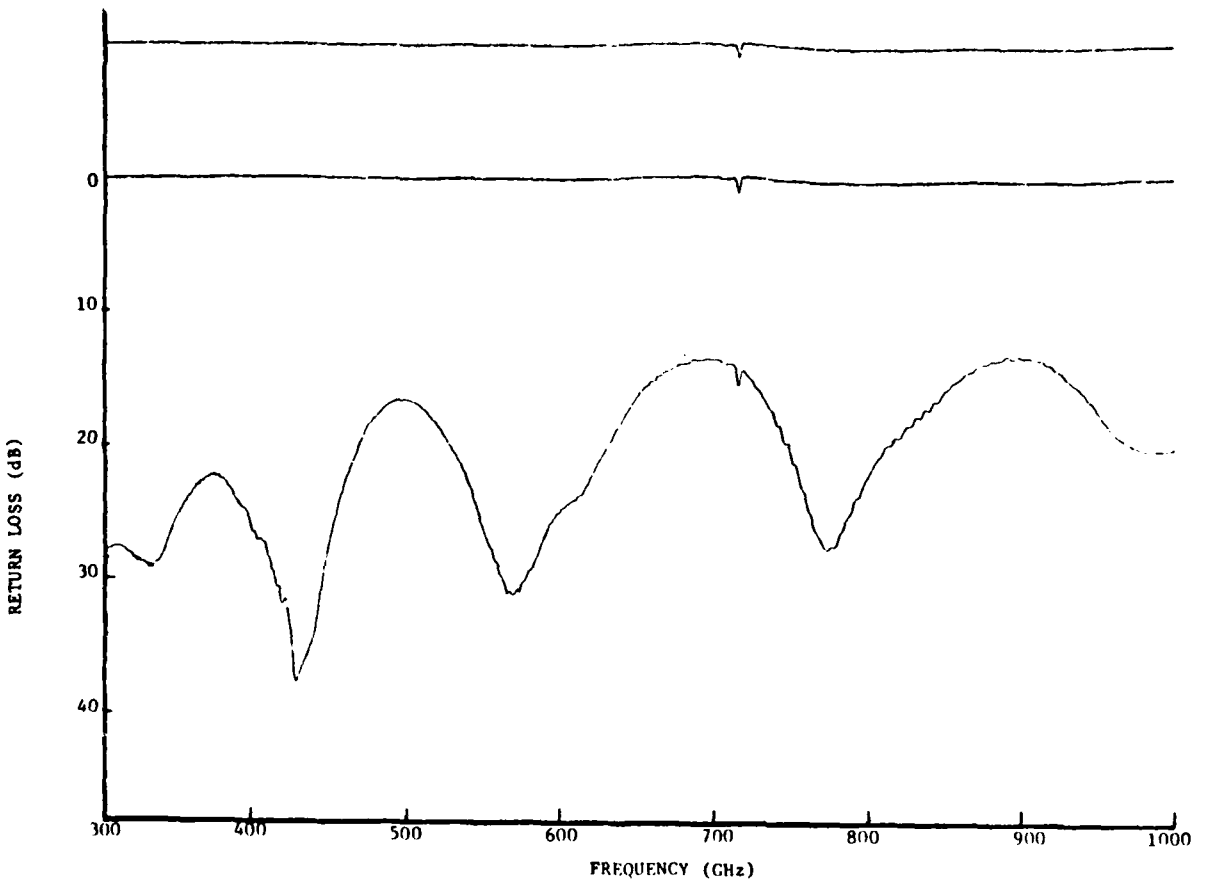

Figure 35. Swept-frequency recording of reflections from the six-inch spiral, measured at input to Anzac H-9 hybrid balun. Cavity absorber in place.

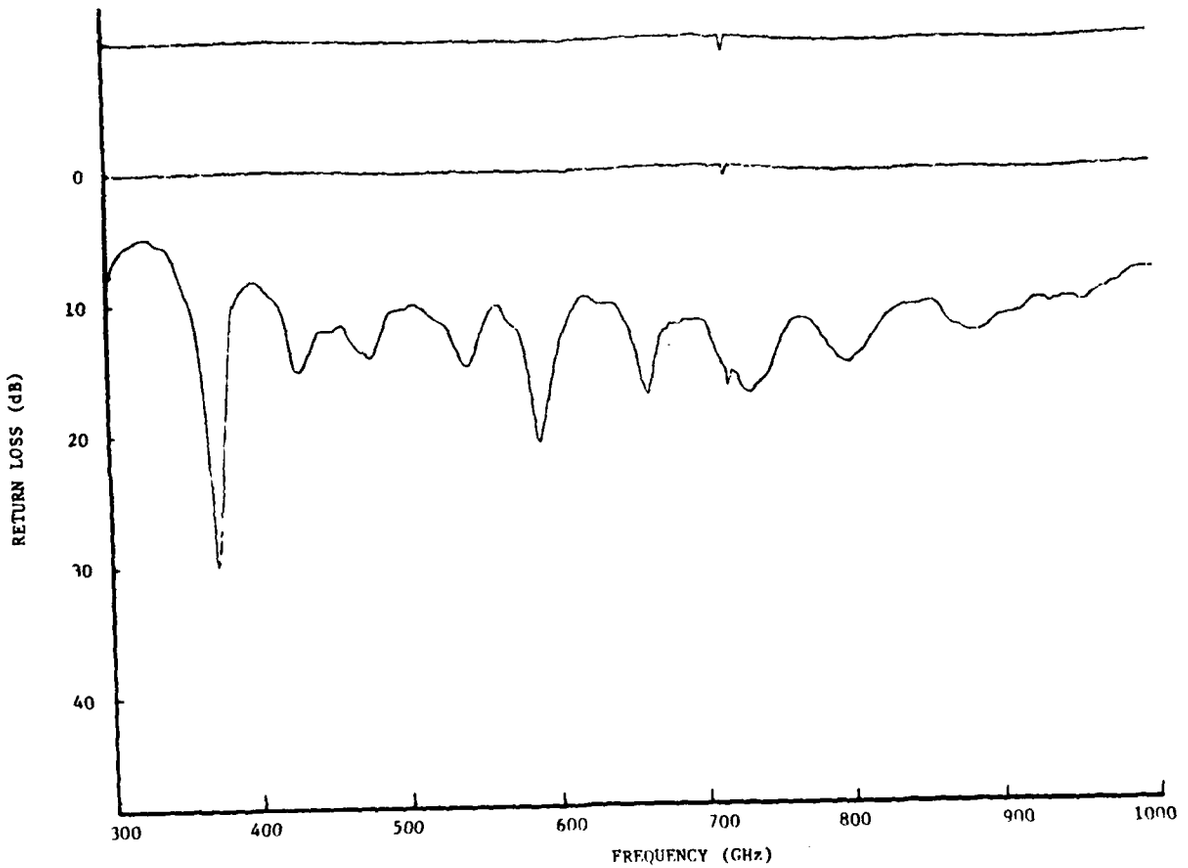

Figure 36. Swept-frequency recording of reflections from the four-inch spiral, with an Anzac TP-101 transformer balun (50Ω to 50Ω).

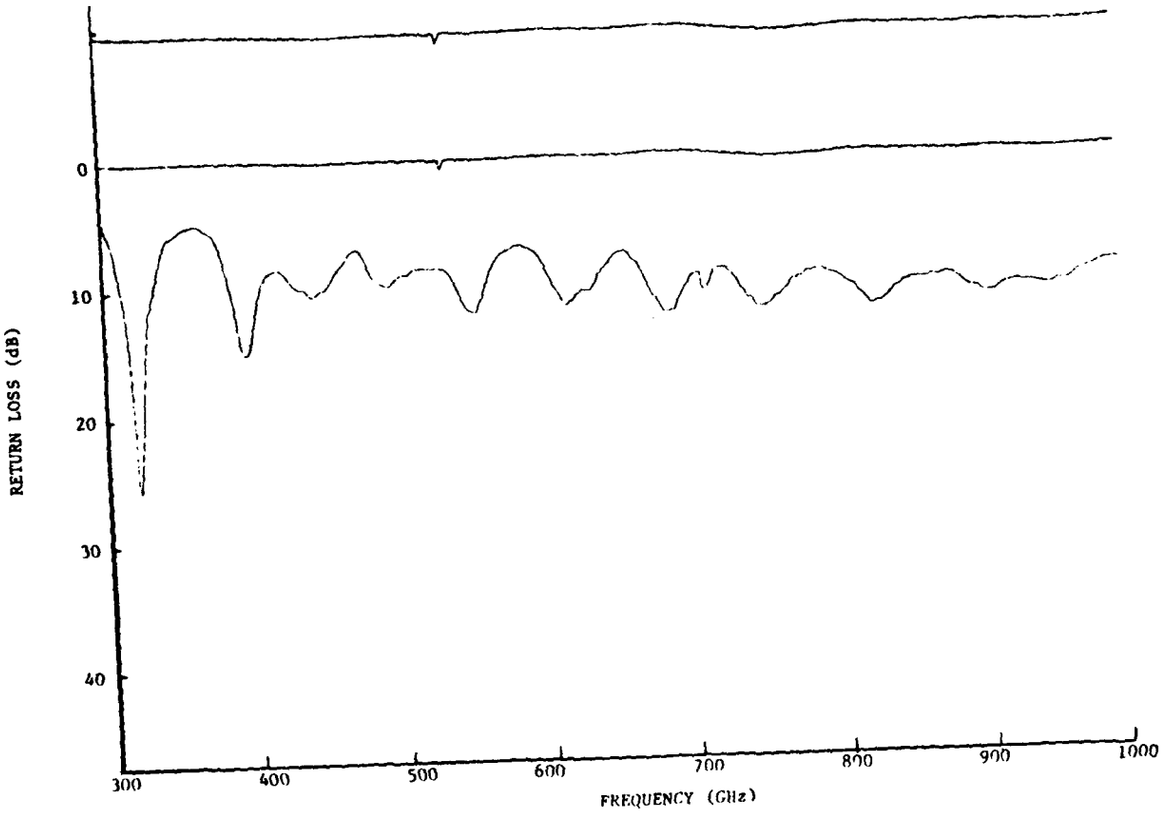

Figure 37. Swept-frequency recording of reflections from the four-inch spiral, with an Anzac TP-103 transformer balun (50Ω to 200Ω).

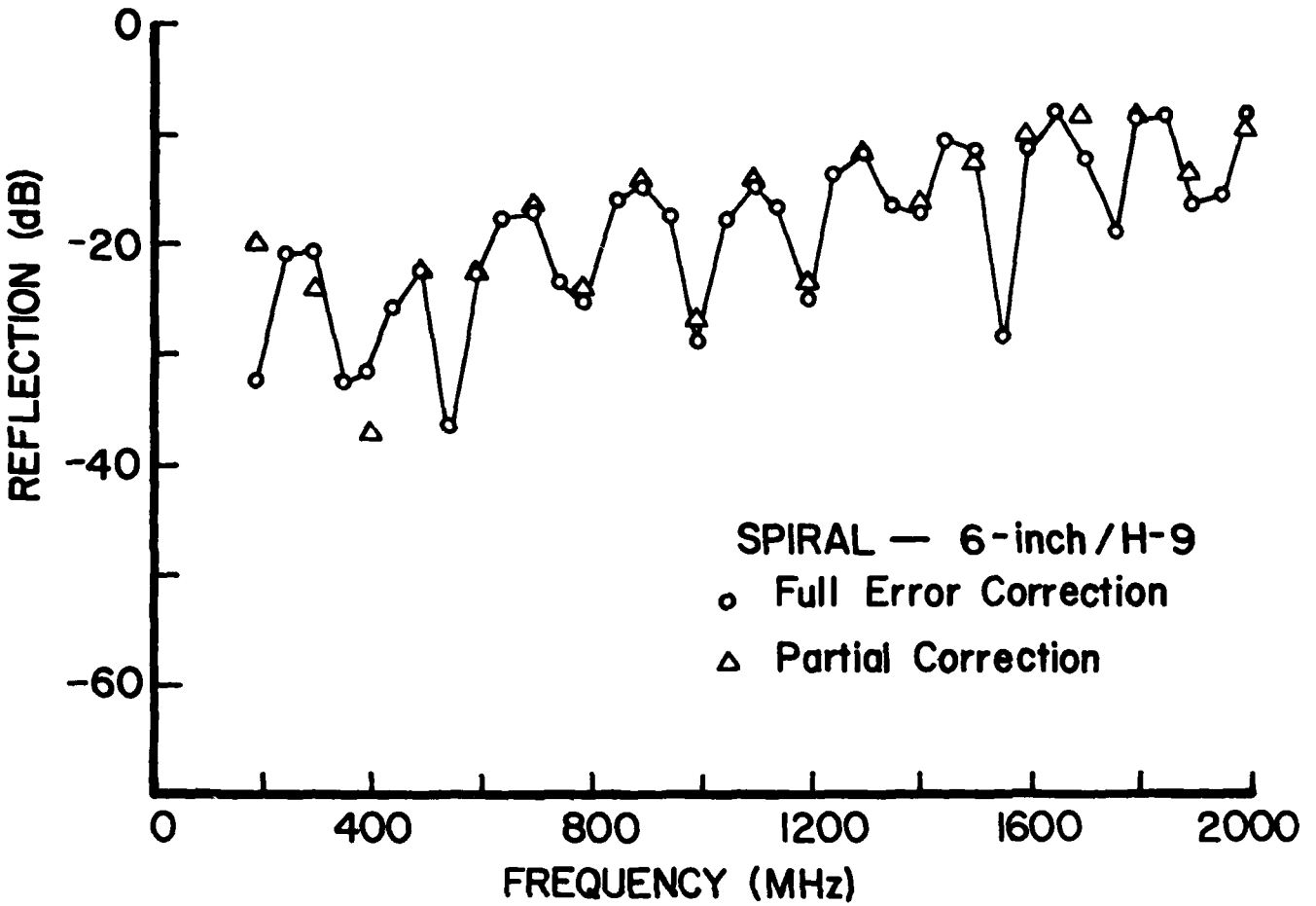

Figure 38. ANA recording of reflections from the 6-inch spiral, as it radiates into free space.

automatic network analyzer (ANA). The points obtained with full error correction resulted from a calibration to correct for source mismatch, tracking errors, and imperfect directivity of the network analyzer [8]. The points obtained with partial error correction include only a calibration to correct for tracking errors; in this case, the differences are insignificant.

Figures 39 and 40 show "target returns" measured for the six-inch spiral, using the ANA to remove the antenna reflection. For these tests, data were recorded from 100 to 1,000 MHz. For Figure 39, the target was a six-inch square aluminum plate, placed four inches from and parallel with the face of the spiral. The plate was centered on the axis of the antenna for one measurement, and was offset toward the edge of the spiral for the other measurement. The higher return for the offset case indicates that the spiral is more sensitive to asymmetrical targets, and this is expected with the circular polarization characteristic of the antenna. Figure 40 shows the "target return" for a large flat layer of microwave absorber and for a length of X-band waveguide placed behind the absorber. The 30-inch section of waveguide was one-half wavelength long at 196 MHz, and the target return shows a deep null at 200 MHz. This is a case of extremely near-zone scattering, and it is not obvious what result should be expected, but it is clear that this antenna system is sensitive to a target resonance. Also, it is clear that the waveguide can be detected and perhaps characterized by a measurement through two inches of absorber. The return from the absorber alone has a null near 850 MHz. This reflection null could be associated with a half-wave resonance of the layer, but dielectric constant and loss properties for this material are not available to verify such an hypothesis. An effective dielectric constant of about 12 could produce such a null, and this value is not unreasonable for a lossy material.

The measured data presented here show that the relatively small spiral antenna couples energy efficiently with a fairly low reflection coefficient over a frequency band exceeding 1,000 MHz. These data do not directly indicate how the spiral will distort a short pulse, but distortion is inevitable. However, these data do indicate that target characteristics can be identified in broadband frequency-domain data, and it is very reasonable to think that signal processing techniques may be developed to extract information from time-domain data. If minimizing antenna size is of primary importance, the spiral should prove to be the most effective of the candidates for concentrating broadband energy on the target.

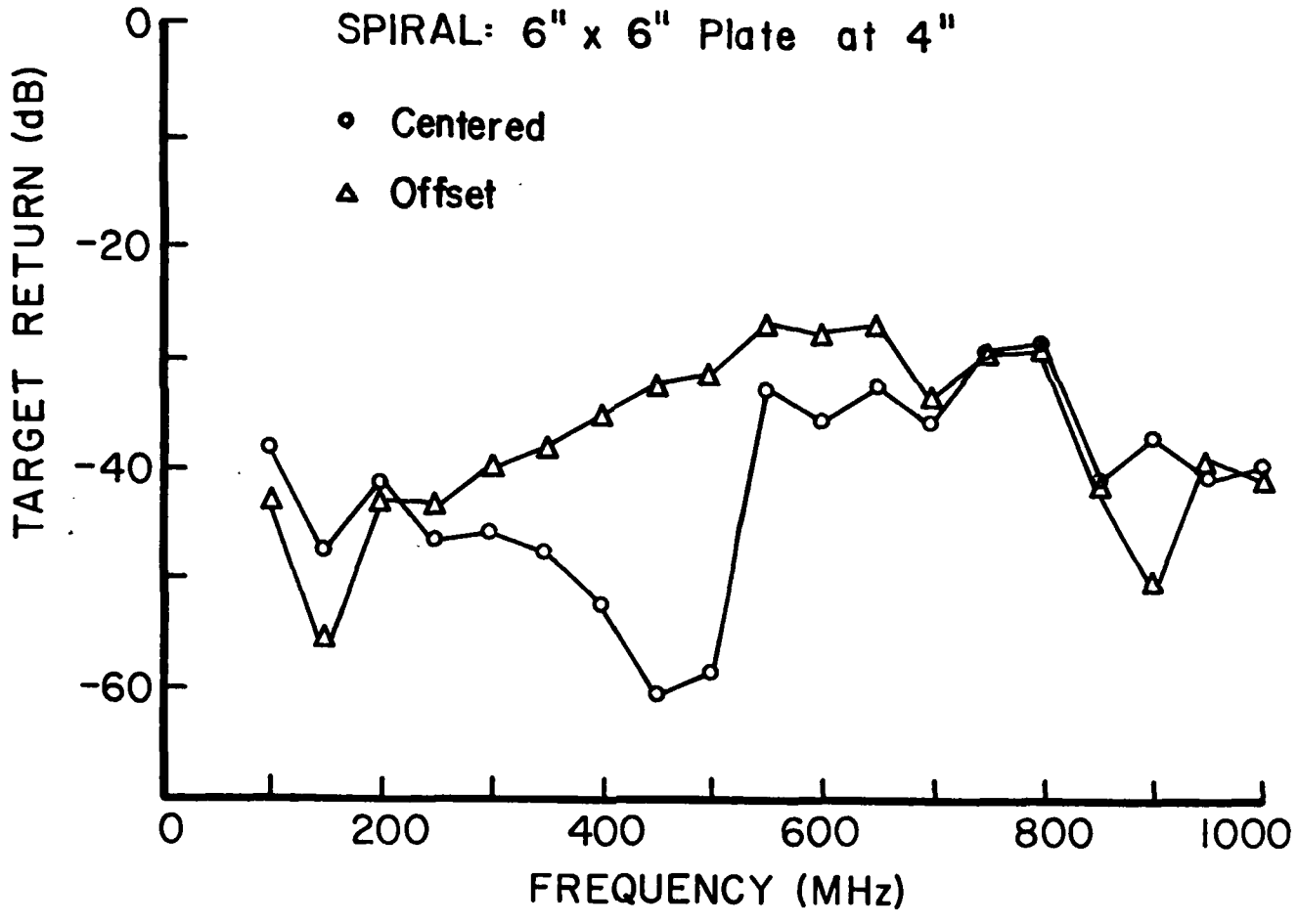

Figure 39. ANA recording of "Target Return" from a square 6"x6" metal plate, as measured with the six-inch spiral at a distance of four inches. (Plate parallel with face of spiral.)

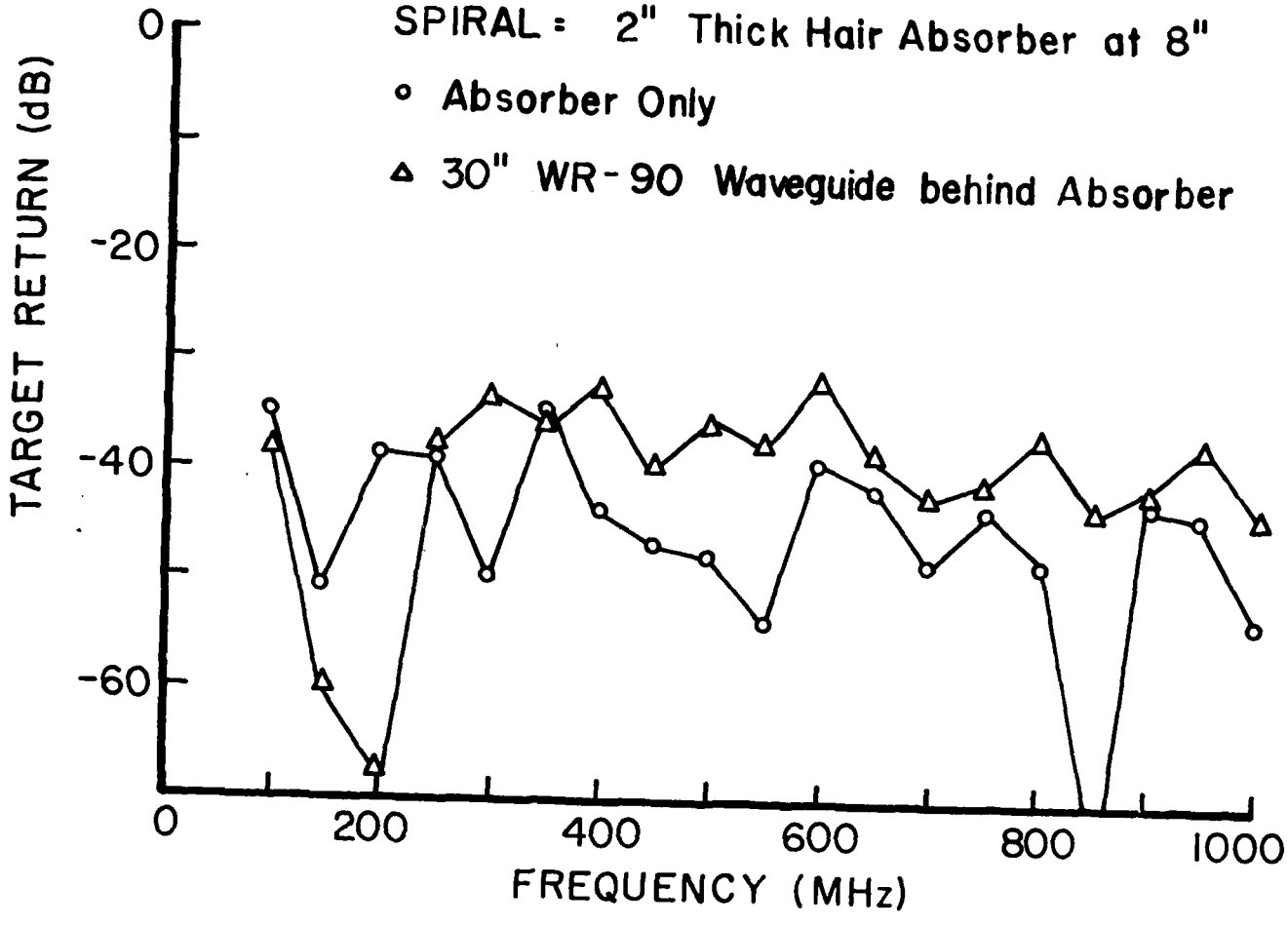

Figure 40. ANA recording of "Target Return" from a section of copper WR-90 waveguide (X-band: 1/2" x 1" x 30") placed behind a layer of microwave absorber (Eccosorb MF-2), as measured with the six-inch spiral at a distance of eight inches. (Waveguide and absorber layer parallel with face of spiral.)

3.4.2 BROADBAND HORN

Reflection data for the Calspan horn were recorded to establish an acceptable level of performance for frequency-domain data. Results are shown in Figures 41 through 43. Analog recordings of return loss for frequencies from 200 to 2,000 MHz were made. For frequencies between 400 and 1,900 MHz, the return loss is greater than 25 dB. Between 200 and 400 MHz, the return loss increases from 15 to about 25 dB. These results are in reasonable agreement with data recorded by NBS [11]. The results of two experiments to determine the sensitivity of the Calspan horn to targets are shown in Figures 42 and 43. For these experiments, the frequency was swept very slowly while a target was moved back and forth near the antenna. The target was a stainless steel pan with a diameter of about 12 inches. The pan was moved over a distance of about two feet along the boresight direction in front of the horn to obtain the data in Figure 42. A schematic illustration of the motion is included on the figure. As the pan is moved, the reflection from the pan and the reflection from the antenna itself may combine in-phase or out-of-phase so that the recorded total reflection cycles between maximum and minimum levels as the pan is moved. In addition to amplitude variations caused by relative phasing, the recorded reflections will vary inversely with the distance between the radiating aperture and the pan. Therefore, at any fixed frequency, the sensitivity of the antenna to the target may be qualitatively evaluated by observing variations in the reflected signal as the pan is moved. When the frequency is varied slowly, compared with the rate at which the pan is moved, the sensitivity of the antenna to the target is indicated by the envelope of recorded isolations in return loss. Figure 42 indicates that the antenna is sensitive to targets placed in front of the radiating aperture for frequencies between 400 and 2,000 MHz. Figure 43 was recorded while the pan was moved back and forth near the open side of the horn. This recording indicates that the antenna is sensitive over the entire frequency band to objects placed near the open side. Figures 42 and 43 together suggest that, while the antenna is well matched over the entire band, the low frequency energy radiated by the antenna may not be well concentrated in front of the radiating aperture. It appears that when this antenna is used with the mine detection radar, relatively little use is made of energy transmitted in the 200-400 MHz band.

Figure 44 shows an analog recording of return loss for the broadband horn developed as part of this work. The antenna reflections are not as low as for the

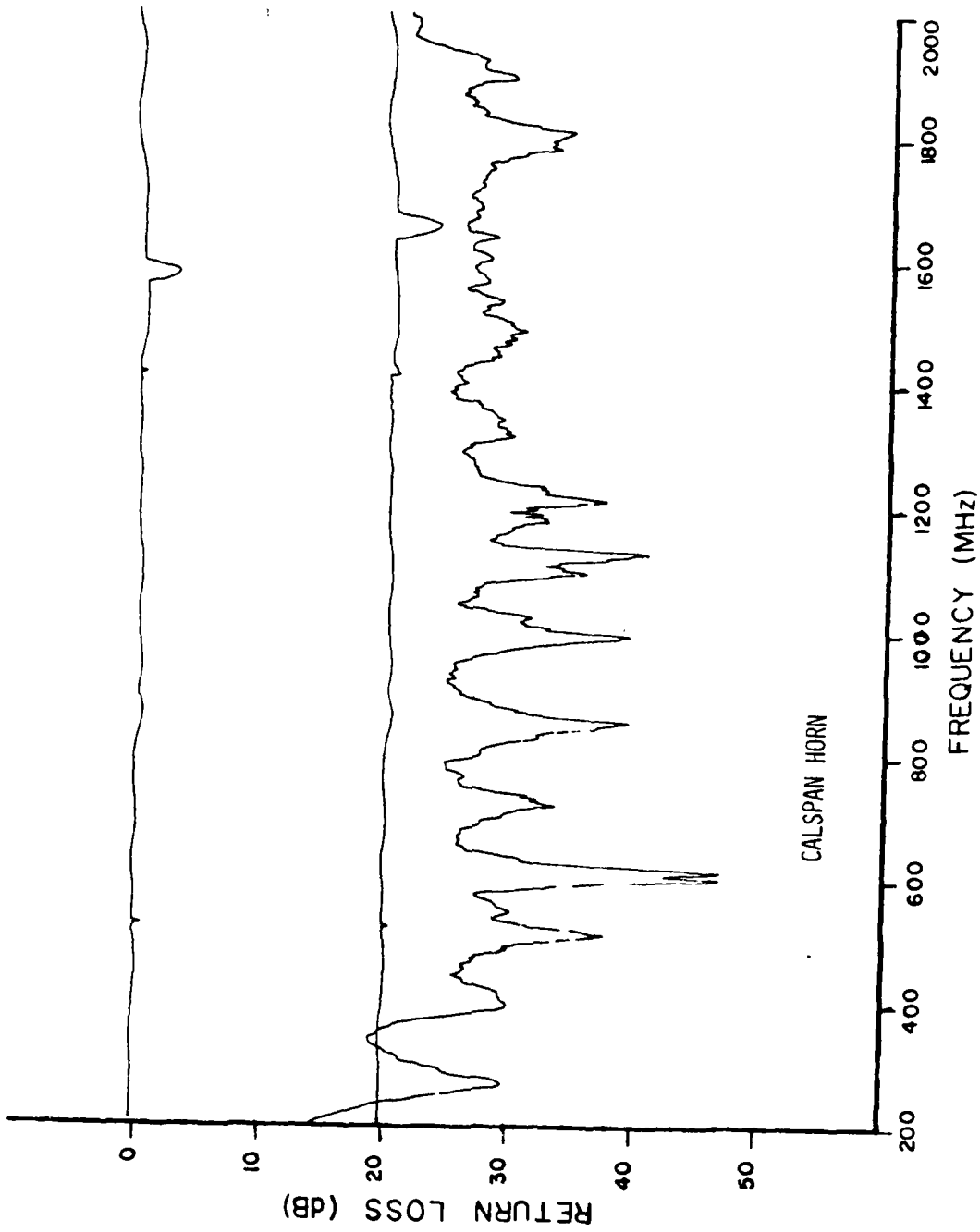

Figure 41. Swept-frequency recording of reflections from the CALSPAN horn, as it radiates into free space.

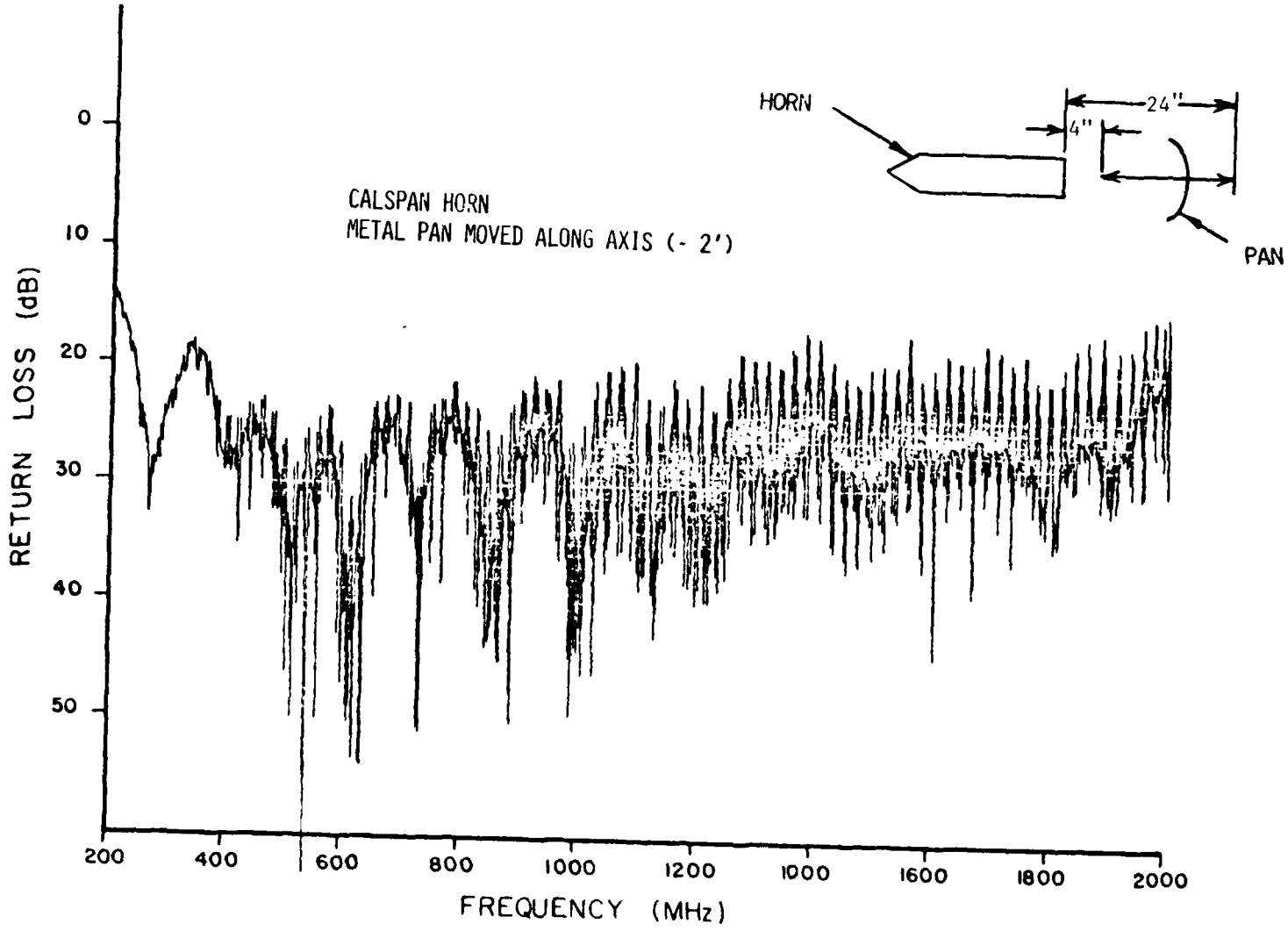

Figure 42. Swept-frequency recording of reflections from the CALSPAN horn, as a 12-inch metal pan is moved axially.

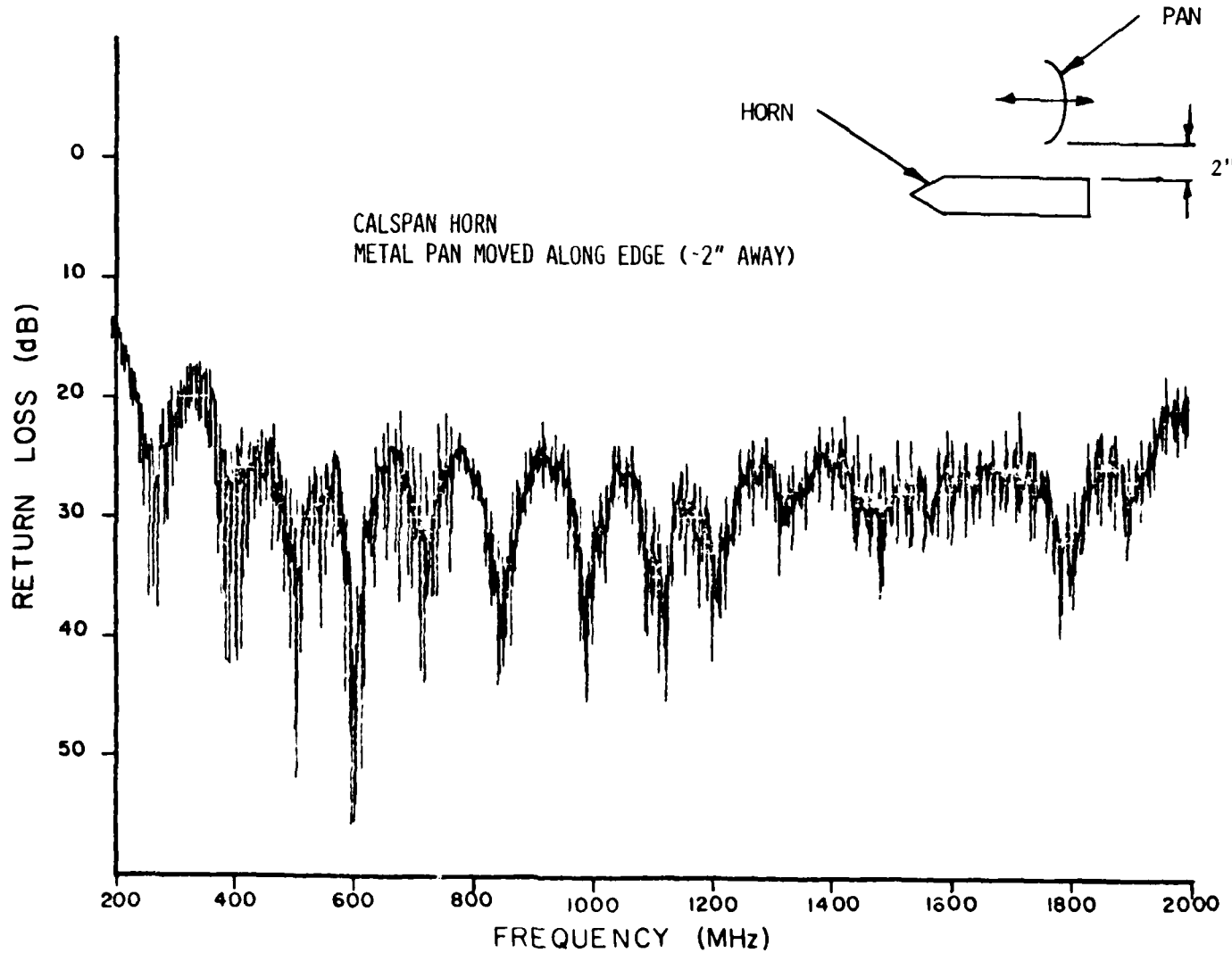

Figure 43. Swept-frequency recording of reflections from the CALSPAN horn, as a 12-inch metal pan is moved along a side.

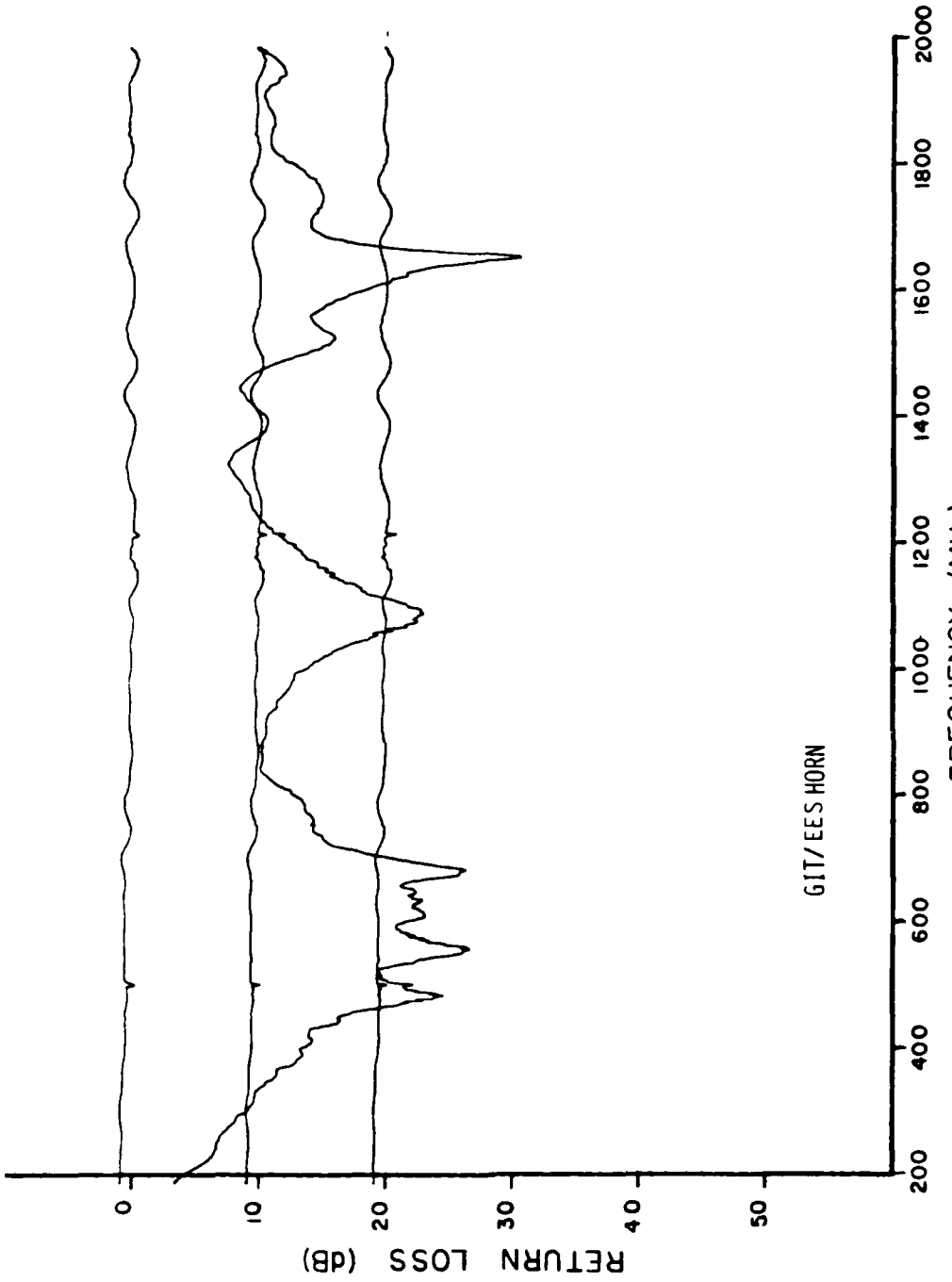

Figure 44. Swept-frequency recording of reflections from the GIT/EES horn, as it radiates into free space.

Calspan horn or for the spiral. The experimental effort concentrated on minimizing reflections in the frequency range between 300 and 1,000 MHz. This work, indicates that reflections in the frequency range below 700 MHz cannot be greatly reduced for a horn of this type and size. However, by careful attention to the construction of the feed point, the reflections in the range from 700 to 2,000 MHz can probably be kept below -20 dB. The horn used in this work was assembled and disassembled a number of times; in the process, the metallized surfaces on the polycarbonate sheets were significantly degraded. New H-plane walls would need to be procured to improve performance of this design. It is interesting to note that the length of the horn is about one-half wavelength at 500 MHz, where the horn becomes reasonably well matched.

The sensitivity of the GIT/EES horn was evaluated using a moving target in the same manner as for the Calspan horn. The data shown in Figure 45 clearly indicate that the horn has reasonable sensitivity to a target placed in front of the aperture over the frequency range from 400 to 1,200 MHz. Between 300 and 400 MHz, this horn may be more sensitive than the Calspan horn.

Figure 46 shows ANA recordings of reflections for the Calspan horn and for the GIT/EES horn over the frequency range from 200 to 2,000 MHz. These data are included to verify by a more accurate measurement process the analog reflection recordings presented in previous figures.

Figures 47 and 48 show "target returns" recorded with the GIT/EES horn using the ANA. The complex reflection coefficient of the horn alone was subtracted from the measured reflection when a target was placed in front of the horn to obtain these data. Figure 47 shows the return for a six-inch square aluminum plate placed in front of the horn at distances of 8 inches and 17 inches. It may be significant to note that there is a null in the target return at 900 MHz, where one-half wavelength is 6.6 inches. The data plotted for "target return" with no target present indicates a noise floor for this type of measurement. The rise in the noise floor above 1,800 MHz was probably caused by drift of equipment between the time of calibration and the time of data collection. Figure 48 shows target returns for the GIT/EES horn measured over the frequency range from 100 to 1,000 MHz. The targets were a six-inch square aluminum plate and a large, 18-inch by 28-inch aluminum sheet. Again, the return from the six-inch target shows a dip near 900 MHz, and the return from the large sheet is substantially higher than the return from the small plate. Therefore, this antenna has reasonable sensitivity to target characteristics.

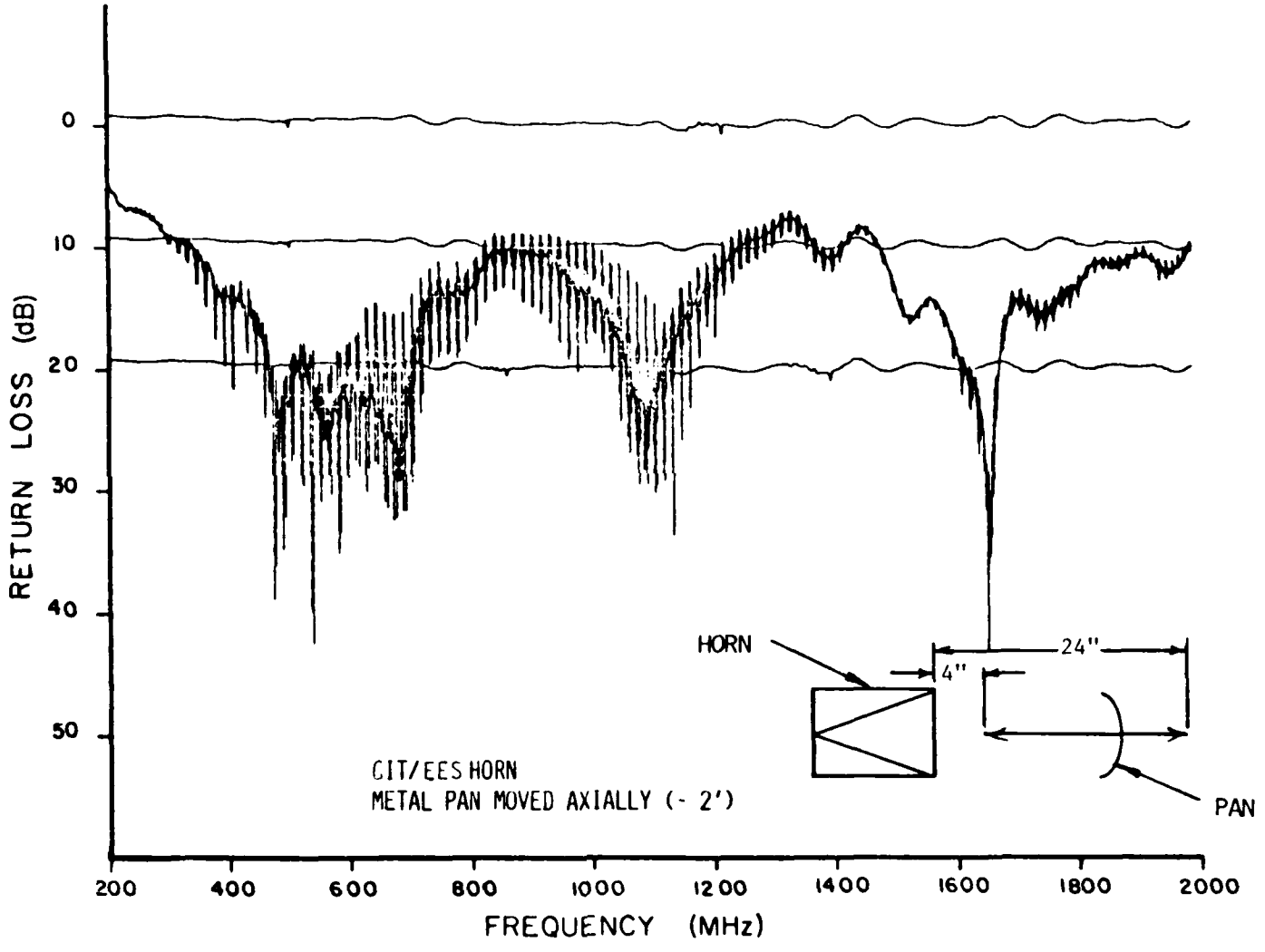

Figure 45. Swept-frequency recording of reflections from the GIT/EES horn, as a 12-inch metal pan is moved axially.

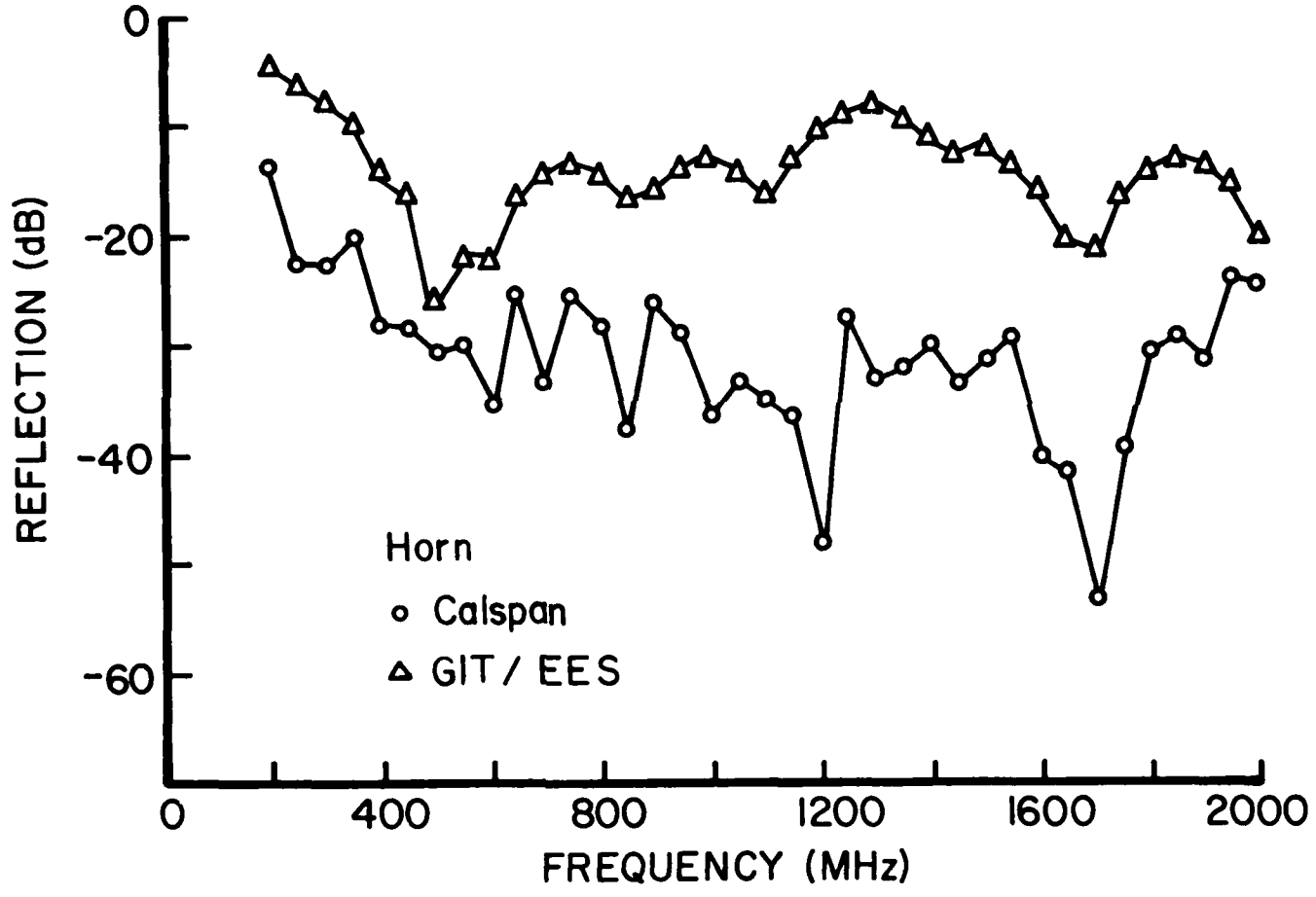

Figure 46. ANA recording of reflections from TEM horns radiating into free space.

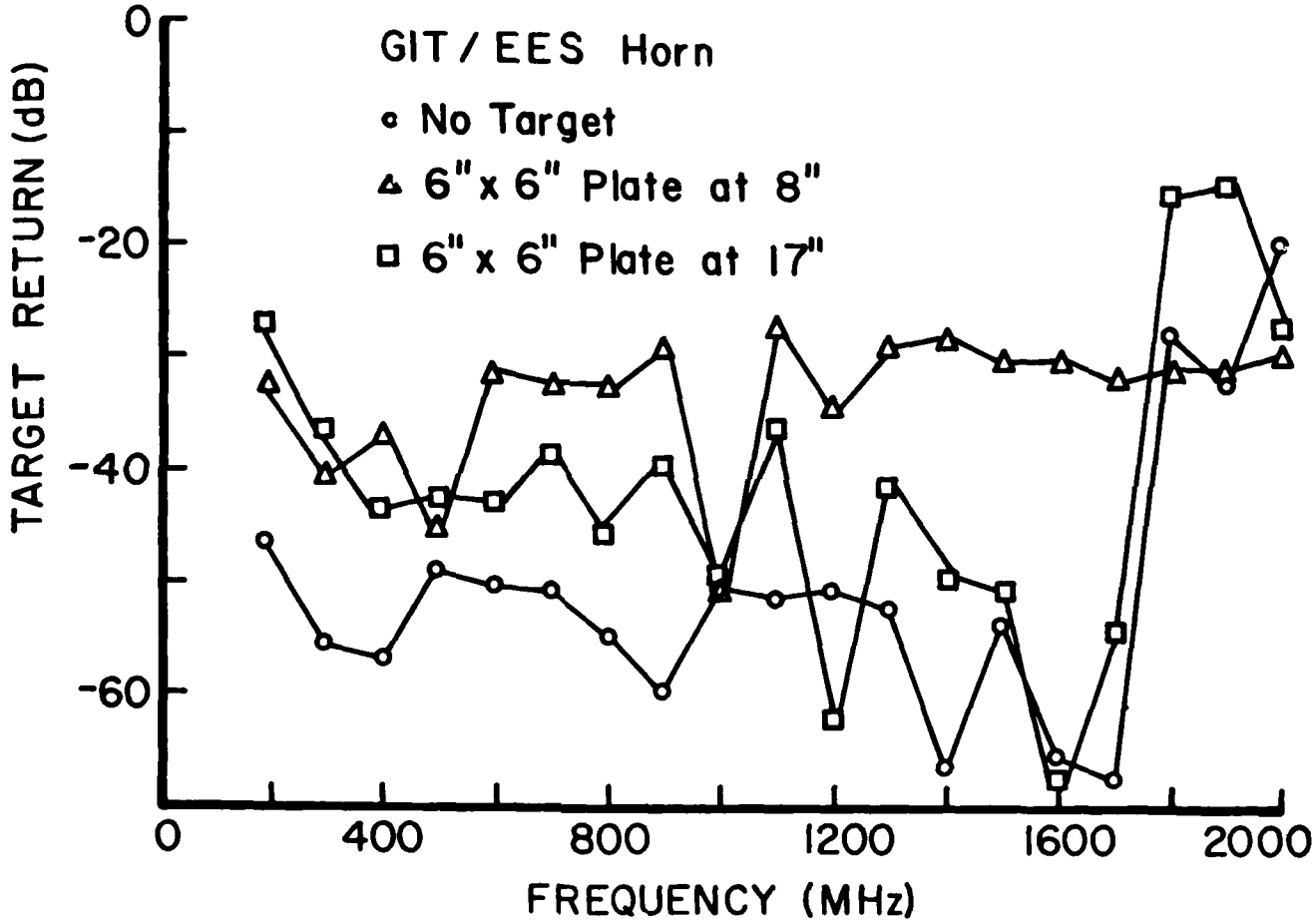

Figure 47. ANA recordings of "Target Returns" from a square 6" x 6" metal plate, as measured with the GIT/EES horn at distances of 8 and 17 inches. (Plate parallel with horn aperture.)

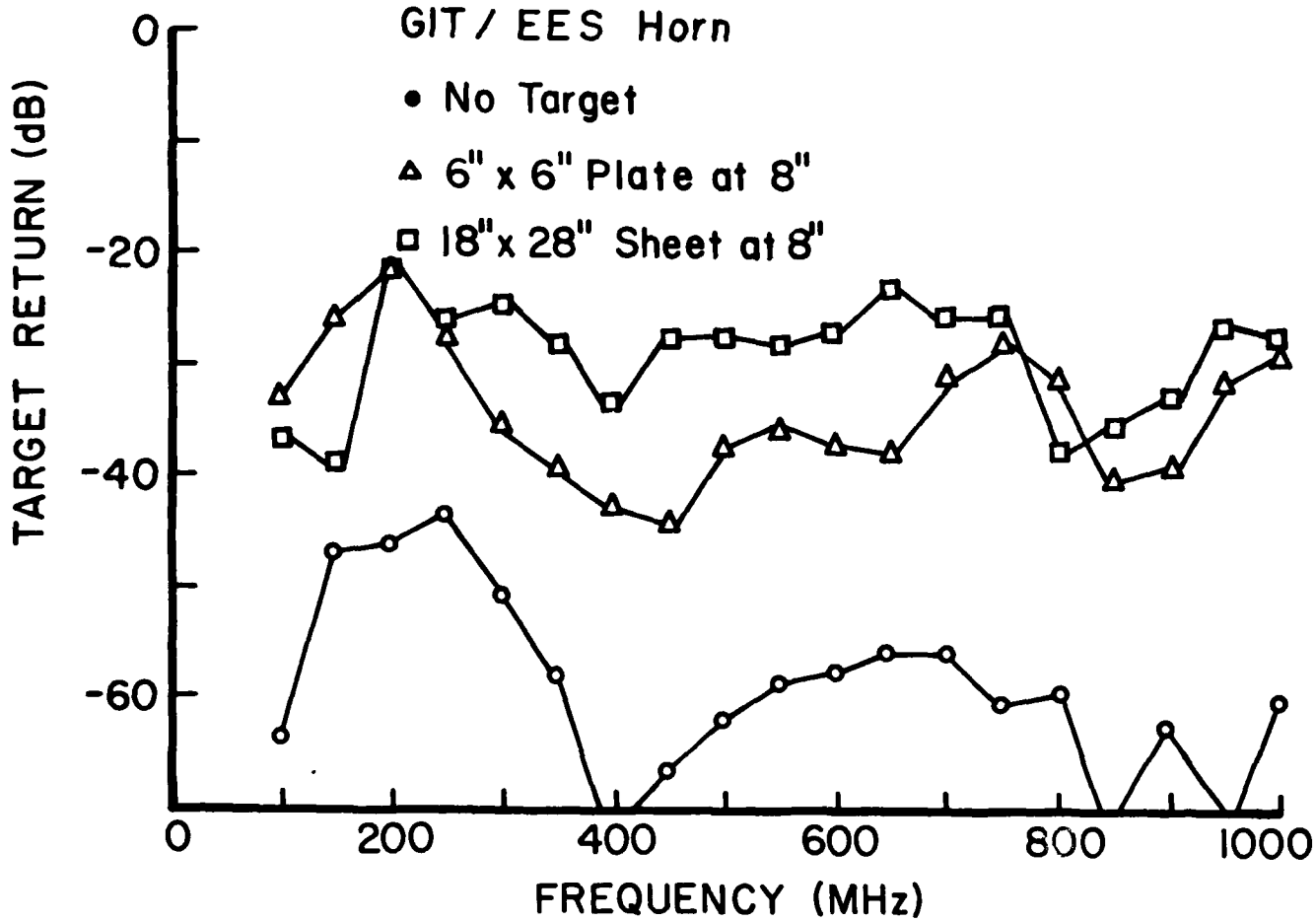

Figure 48. ANA recordings of "Target Returns" from a 6" x 6" metal plate and a 18" x 28" metal sheet, as measured with the GIT/EES horn at a distance of eight inches. (Targets parallel with horn aperture.)

Although the data presented in the previous figures shows only the amplitude of antenna reflections, the ANA provides accurate measurements of amplitude and phase. The phase data can be useful in estimating where on a traveling wave structure reflections occur. If the reflections are caused primarily by a single localized discontinuity, the phase of the reflection coefficient can usually be made to vary slowly with frequency by selecting the phase reference plane at the coordinate of the discontinuity. Using this approach, it has been determined that reflections in the Calspan horn do not occur at a localized discontinuity, but reflections in the GIT/EES horn occur primarily at the feed point. This suggests that, except near the low end of the band, the performance of the antenna may be substantially improved by improving the feed point connection. Tables 4 and 5 show reflection data for the Calspan horn and the GIT/EES horn, respectively. These tables show the amplitude and phase of reflection coefficients in decibels and degrees as a function of frequency. The real and imaginary parts of the load impedance are tabulated for reference. The phase reference plane for the reflection coefficient can be moved along the transmission line, using software in the ANA controller computer. The reference planes for the tabulated data are placed precisely at the feed point of the horns. The reflection phase for the Calspan horn oscillates slowly, while the reflection phase for the GIT/EES horn is nearly constant over large portions of the band. Moving the reference plane out through the horn had little effect on the reflection phase for the Calspan horn, but such a change greatly increased the phase variation for the GIT/EES horn. Therefore, the primary reflection in the GIT/EES horn originates at a feed point.

For reference, Table 6 shows reflection data measured with the first horn that was assembled at GIT/EES using the metallized polycarbonate sheets. This horn was an attempt to duplicate the model developed at NBS. The results obtained were not nearly as good as reported by NBS, nor were they as good as were obtained in the final version of the GIT/EES horn. The feed construction in a horn such as this critically affects the impedance. Minor mechanical variations can cause major electrical variations, and it is expected that differences in feed construction could explain why the NBS results were not reproduced.

3.4.3 BROADBAND DIPOLE

The reflection data obtained for the broadband dipole are presented in Table 7. These data were measured with ANA. The transition from coaxial

TABLE 4. ANA REFLECTION DATA FOR THE CALSPAN HORN

CORRECTED REFLECTION COEFFICIENTS AND IMPEDANCES

REFERENCE PLANE OFFSET (INCHES TOWARD LOAD) 0.000

MHZ	DB	DEG	Z-REAL	Z-IMAG
200.000	-13.832	149.43	.689	.149
250.000	-22.654	63.25	1.059	.140
300.000	-22.657	-168.13	.865	-.026
350.000	-20.438	90.24	.981	.188
400.000	-28.180	-31.08	1.068	-.043
450.000	-28.488	161.75	.931	.022
500.000	-30.664	-9.86	1.059	-.011
550.000	-30.909	-136.00	.959	-.038
600.000	-35.765	-52.75	1.020	-.026
650.000	-25.518	-115.94	.950	-.091
700.000	-33.700	-162.56	.961	-.012
750.000	-25.986	-124.19	.942	-.078
800.000	-28.500	168.11	.929	.014
850.000	-37.976	-119.80	.987	-.022
900.000	-26.694	154.66	.919	.036
950.000	-29.171	68.53	1.024	.066
1000.000	-36.498	-121.57	.984	-.025
1050.000	-33.741	93.22	.997	.041
1100.000	-35.027	-76.42	1.008	-.035
1150.000	-36.592	155.48	.973	.012
1200.000	-48.258	27.87	1.007	.004
1250.000	-27.984	-125.73	.953	-.062
1300.000	-33.282	168.07	.958	.009
1350.000	-32.414	-129.28	.969	-.036
1400.000	-29.019	-163.79	.934	-.018
1450.000	-33.551	-174.88	.959	-.004
1500.000	-31.358	-165.07	.949	-.013
1550.000	-29.321	158.48	.938	.024
1600.000	-40.220	110.87	.993	.018
1650.000	-41.760	127.40	.990	.013
1700.000	-53.138	-141.78	.997	-.003
1750.000	-39.959	-80.06	1.003	-.020
1800.000	-30.816	-98.30	.990	-.056
1850.000	-29.507	-154.17	.941	-.027
1900.000	-31.534	-120.18	.973	-.045
1950.000	-24.010	-148.40	.896	-.059
2000.000	-24.404	166.43	.889	.025

TABLE 5. ANA REFLECTION DATA FOR THE GIT/EES HORN

CORRECTED REFLECTION COEFFICIENTS AND IMPEDANCES

REFERENCE PLANE OFFSET (INCHES TOWARD LOAD) 0.000

MHZ	DB	DEG	Z-REAL	Z-IMAG
200.000	-4.427	-166.17	.253	-.114
250.000	-6.941	136.81	.429	.331
300.000	-8.079	72.75	.916	.818
350.000	-10.062	16.46	1.816	.359
400.000	-14.655	-19.94	1.407	-.184
450.000	-16.681	-82.73	.994	-.295
500.000	-26.031	-178.51	.905	-.002
550.000	-29.086	138.41	.948	.044
600.000	-26.561	100.96	.978	.090
650.000	-22.758	114.20	.934	.125
700.000	-22.645	122.52	.917	.115
750.000	-16.915	123.08	.833	.203
800.000	-14.608	102.40	.866	.326
850.000	-13.595	73.93	1.031	.433
900.000	-14.792	37.05	1.302	.296
950.000	-16.783	-16.30	1.318	-.109
1000.000	-16.014	-161.14	.736	-.077
1050.000	-14.607	118.65	.796	.269
1100.000	-16.551	121.75	.830	.215
1150.000	-13.727	114.66	.789	.308
1200.000	-10.619	99.22	.773	.492
1250.000	-9.045	78.29	.892	.704
1300.000	-8.611	54.17	1.226	.856
1350.000	-9.913	35.51	1.543	.638
1400.000	-11.004	25.72	1.610	.428
1450.000	-12.500	16.77	1.567	.227
1500.000	-12.696	6.80	1.595	.093
1550.000	-13.930	-2.24	1.503	-.025
1600.000	-16.426	-10.96	1.345	-.079
1650.000	-20.811	-9.12	1.197	-.035
1700.000	-21.859	34.05	1.138	.104
1750.000	-16.919	47.70	1.183	.255
1800.000	-14.620	39.58	1.290	.316
1850.000	-13.844	25.82	1.419	.262
1900.000	-14.101	14.45	1.463	.150
1950.000	-15.893	4.14	1.381	.033
2000.000	-20.753	18.89	1.188	.071

TABLE 6. ANA REFLECTION DATA FOR THE GIT/EES HORN

CORRECTED REFLECTION COEFFICIENTS AND IMPEDANCES

REFERENCE PLANE OFFSET (INCHES TOWARD LOAD) 0.000

MHZ	DB	DEG	Z-REAL	Z-IMAG
200.000	-6.212	153.12	.360	.209
250.000	-5.048	54.27	1.042	1.377
300.000	-3.533	5.29	4.743	1.047
350.000	-2.868	-26.41	2.110	-2.791
400.000	-3.085	-52.52	.797	-1.743
450.000	-3.839	-77.59	.516	-1.104
500.000	-5.555	-104.69	.467	-.660
550.000	-9.444	-139.23	.546	-.271
600.000	-29.871	120.44	.967	.054
650.000	-12.210	-18.47	1.580	-.261
700.000	-8.030	-47.24	1.362	-.942
750.000	-6.517	-72.16	.832	-.963
800.000	-5.990	-90.65	.592	-.794
850.000	-6.384	-116.33	.465	-.519
900.000	-9.129	-139.84	.530	-.272
950.000	-14.700	-150.09	.714	-.136
1000.000	-17.676	-111.32	.884	-.219
1050.000	-12.705	-86.11	.926	-.452
1100.000	-9.178	-104.24	.681	-.522
1150.000	-8.408	-119.82	.562	-.433
1200.000	-8.200	-142.51	.480	-.268
1250.000	-9.101	-157.69	.495	-.150
1300.000	-11.106	-177.38	.565	-.016
1350.000	-14.254	176.62	.676	.016
1400.000	-20.201	-174.05	.823	-.017
1450.000	-17.561	-136.46	.812	-.151
1500.000	-14.623	-134.94	.744	-.203
1550.000	-11.702	-147.88	.618	-.183
1600.000	-11.473	-163.86	.586	-.094
1650.000	-11.208	-179.06	.568	-.006
1700.000	-12.198	172.51	.607	.041
1750.000	-13.134	159.01	.652	.108
1800.000	-14.336	163.22	.686	.079
1850.000	-14.870	151.23	.717	.129
1900.000	-14.709	148.85	.716	.141
1950.000	-16.435	129.17	.806	.193
2000.000	-21.712	127.25	.898	.118

cable to the dipole was made through an Anzac TP-103 transformer. It is clear from this data that the reflection levels are far too great for the dipole to be useful with the mine detection radar. Reflection data were obtained with the transformer terminated in a 220 ohm carbon resistor to verify that the pulse transformer was not damaged. The results are shown in Table 8, and it is apparent that the transformer provides low reflections for frequencies below 1,000 MHz, and its performance is well within the manufacturer's specifications. While the dipole may provide very high pulse fidelity when excited by a well matched source, it would probably cause ringing if it were used with the mine detection radar.

3.5 CONCLUSIONS AND RECOMMENDATIONS

The antenna development effort discussed in this section has resulted in fabrication of the three most promising candidates for an antenna of severely restricted size. If the major constraint is that the size should not exceed twelve inches, and if the antenna must operate down to 300 MHz, the spiral is the strongest contender. However, use of the spiral will necessitate development of new signal processing techniques. The target returns developed through a spiral will not resemble conventional radar returns, where much information is contained in pulse timing and amplitude, but a substantial amount of information seems to be preserved in the spectral distribution of reflected energy.

If the lower end of the operating band is raised to 500 MHz, a good, non-dispersive horn can be developed within the guideline of a 12-inch maximum dimension. Such a horn could be expected to operate well at frequencies as high as 2,000 or 3,000 MHz, and it could possibly go substantially higher. However, raising the low end of the frequency band will severely impair the ability of the radar to penetrate damp earth.

Preliminary tests of the antennas fabricated have been conducted using the frequency domain measurement techniques. These tests suggest that the spiral and the horn have useful sensitivity to the local environment. These tests also suggest that the sensitivity of the radar should be substantially enhanced if the antenna response is removed from radar data by a calibration process similar to that used to provide error correction in automatic network analyzers. It is unlikely that a small antenna can be made to operate satisfactorily without adopting such a calibration process.

TABLE 7. ANA REFLECTION DATA FOR THE GIT/NBS DIPOLE

CORRECTED REFLECTION COEFFICIENTS AND IMPEDANCES

REFERENCE PLANE OFFSET (INCHES TOWARD LOAD) 0.000

MHZ	DB	DEG	Z-REAL	Z-IMAG
200.000	-2.778	-127.96	.195	-.473
250.000	-3.023	-154.50	.181	-.219
300.000	-3.249	-179.57	.185	-.004
350.000	-3.364	158.41	.198	.183
400.000	-3.684	138.33	.238	.362
450.000	-3.764	114.51	.296	.602
500.000	-3.852	96.00	.380	.826
550.000	-4.097	75.08	.572	1.129
600.000	-4.230	53.24	.969	1.533
650.000	-4.082	31.25	1.893	2.014
700.000	-4.399	11.92	3.463	1.353
750.000	-4.272	-14.71	3.278	-1.626
800.000	-3.611	-42.47	1.222	-1.929
850.000	-3.074	-64.15	.576	-1.435
900.000	-3.985	-91.89	.417	-.877
950.000	-4.039	-122.98	.291	-.507
1000.000	-3.317	-142.87	.209	-.383
1050.000	-4.417	-80.13	.552	-1.026
1100.000	-3.822	172.96	.217	.059
1150.000	-3.365	157.53	.199	.191
1200.000	-3.236	143.93	.203	.313
1250.000	-3.439	123.21	.250	.514
1300.000	-3.102	112.47	.252	.639
1350.000	-3.216	99.97	.305	.793
1400.000	-3.117	86.40	.366	.996
1450.000	-3.048	77.64	.422	1.152
1500.000	-3.397	63.63	.633	1.415
1550.000	-3.123	54.78	.752	1.672
1600.000	-3.350	45.30	1.063	1.911
1650.000	-3.549	27.92	2.089	2.329
1700.000	-3.446	25.07	2.341	2.436
1750.000	-3.939	13.66	3.531	1.777
1800.000	-3.967	-1.58	4.439	-.259
1850.000	-4.017	-7.93	4.046	-1.165
1900.000	-4.849	-24.30	2.365	-1.656
1950.000	-4.993	-36.95	1.652	-1.624
2000.000	-5.805	-51.10	1.191	-1.289

AD-A107 752 GEORGIA INST OF TECH ATLANTA ENGINEERING EXPERIMENT --ETC F/G 19/1
ANTENNA CONSIDERATIONS AND SIGNAL PROCESSING TECHNIQUES FOR THE--ETC(U)
JUN 81 W J STEINWAY, J A FULLER DAAK70-78-C-0081

UNCLASSIFIED NL

2 OF 2
AD
A107 752

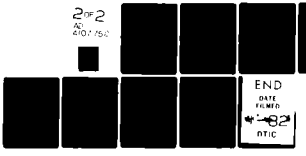

END
DATE FILMED
-82
DTIC

TABLE 8. ANA DATA FOR THE ANZAC TP-103 PULSE TRANSFORMER BALUN WITH A 220 OHM RESISTIVE LOAD

CORRECTED REFLECTION COEFFICIENTS AND IMPEDANCES

REFERENCE PLANE OFFSET (INCHES TOWARD LOAD) 7.750

MHZ	DB	DEG	Z-REAL	Z-IMAG
200.000	-30.959	179.09	.945	.001
250.000	-27.677	167.51	.922	.017
300.000	-25.578	153.39	.909	.043
350.000	-23.666	136.45	.906	.082
400.000	-22.075	119.89	.916	.126
450.000	-20.054	104.61	.934	.181
500.000	-18.257	90.26	.969	.241
550.000	-16.735	79.33	1.012	.296
600.000	-15.537	72.11	1.051	.344
650.000	-15.081	67.50	1.081	.363
700.000	-14.956	64.35	1.104	.367
750.000	-15.875	64.62	1.097	.327
800.000	-17.548	72.83	1.046	.270
850.000	-17.911	91.99	.960	.248
900.000	-17.694	92.79	.955	.253
950.000	-21.943	101.44	.957	.151
1000.000	-23.623	145.90	.894	.066
1050.000	-19.402	167.46	.810	.038
1100.000	-17.062	177.50	.754	.009
1150.000	-14.409	173.25	.681	.032
1200.000	-12.734	161.12	.635	.100
1250.000	-11.142	146.40	.600	.199
1300.000	-10.160	131.87	.598	.306
1350.000	-8.816	116.11	.599	.449
1400.000	-8.459	103.00	.653	.561
1450.000	-6.761	90.15	.650	.757
1500.000	-5.875	83.61	.647	.882
1550.000	-5.183	78.67	.641	.993
1600.000	-4.444	73.60	.628	1.127
1650.000	-4.117	66.43	.688	1.283
1700.000	-3.789	59.23	.770	1.469
1750.000	-3.596	51.64	.913	1.682
1800.000	-3.537	45.36	1.098	1.865
1850.000	-3.717	35.39	1.588	2.085
1900.000	-4.174	27.18	2.189	2.002
1950.000	-4.188	18.99	2.897	1.882
2000.000	-4.267	12.17	3.512	1.448

The antennas fabricated for this program have been optimized through a preliminary phase of frequency domain testing. These antennas work well enough that subsequent time domain tests with the pulse radar should be meaningful. Such tests are needed to make a conclusive assessment of the relative capabilities of these antennas, but the conditions and alternatives reviewed in this subsection are not likely to be changed.

SECTION 4
DISCRIMINATION ALGORITHMS

4.1 BACKGROUND

The discrimination algorithms presented here are based on the assumption that there is a correlation of the frequency spectrum over the spatial extent of a target of interest. For objects that are not of interest, limited correlation results.

The first concept is that all targets have a set of natural resonant frequencies. This stems from the fact that finite size objects have resonances that depend on their physical characteristics such as size, shape, and composition as well as the medium surrounding the object. It has been shown [24] that the backscattered waveforms from the sub-surface targets received by a wide bandwidth (short-pulse) radar system are good approximations to the impulse responses of the target. Furthermore, they appear to be made up of a few exponentially damped sinusoids.

The second concept is that man-made objects have some spatial uniformity of surfaces and shape, as opposed to rocks and other junk which tend to have irregular surfaces. The result is that, although all objects exhibit complex natural resonances, mine-like (man-made) objects will exhibit the same resonances over most of their spatial extent. If methods are used to extract the resonant frequencies using radar measurements made at different spatial points on an object, then a spatial correlation in the frequency domain will result for those man-made objects. It is a reasonable assumption that targets of interest (mine-like) are in this category. Certainly there will be other non-mine targets (a metal plate for example), that will correlate and will result in a false alarm. But, the function of a discrimination algorithm is to be functionally simple and yet screen-out most of the junk from targets of interest.

The third concept is that a means of accurately identifying the natural resonant frequencies of an object is necessary. This can be done by examination of the frequency spectrum obtained by transforming the short data length record of the target area. Problems arise, typically with FFT processes, due to inadequate frequency resolution resulting from short data records. Maximum Entropy Methods [25, 26] provide a possible solution by achieving improved resolution in the frequency domain over that of the FFT process. FFT techniques are well known and algorithmic details are not given in this report. MEM on the other hand is not in widespread usage and the following sub-section supplies some background information.

4.2 MAXIMUM ENTROPY METHODS

Just prior to 1970, a nonlinear procedure for spectral estimation with increased resolution was invented: the Maximum Entropy Method (MEM) by Burg 1967 [25]. The major attraction of the procedure is that it shows considerable promise for estimating spectra when the length of the available data record is short. No use of window function is made; rather, when power is being estimated at one frequency, the method adjusts itself to be least disturbed by power at other frequencies. From this view point, the method is considered data adaptive.

The Maximum Entropy Method is a result of Burg's attempt to derive a procedure for increasing spectral resolution when only a small number of samples of the estimate of the autocorrelation function are available from the observed data. The methods used prior to this data basically calculated the autocorrelation estimates and then windowed the autocorrelation function estimate, appended zeros, and Fourier transformed. The window is usually designed to give as much resolution as possible with little leakage.

The Maximum Entropy Method suggests, instead of appending zeros to increase the length of the estimated autocorrelation function, that the estimated autocorrelation function should be extrapolated (predicted) beyond the data limited range. The principle used for this extrapolation (prediction) process is that the spectral estimate must be the most random or have the maximum entropy of any power spectrum which is consistent with the sample values of the calculated autocorrelation function. The objective is to add no information as a result of the prediction.

It has been shown [25] that the MEM can resolve tones arbitrarily close together for any nonzero time-bandwidth product if the signal-to-noise ratio is sufficiently high. This cannot be achieved with the FFT methods (unless of course, the sampling rate and the record length are increased).

The maximum entropy procedure has proven useful, particularly for short data records. However, interesting problems still remain, e.g., selecting the "proper" value of the prediction filter order, p. If p is selected too small, then the resulting spectral estimate is highly smooth; while if p is too large, then spurious detail is introduced into the spectrum. Another problem is the lack of a variance estimate for the spectral density estimator. Such a variance estimate has been difficult to calculate since the MEM estimate is determined via nonlinear operations on the autocorrelation matrix.

The advantage of the MEM approach is that a formal all-pole model is applied as an estimate of the spectrum. The resolution of the MEM procedure is greater than previous conventional methods, but the estimator is higly sensitive to the signal-to-noise ratio. A Comparison of the features or characteristics of MEM and FFT approachs is given in Table 9.

4.3 DATA RESULTS

Figures 49 illustrates the results of applying the FFT and MEM spectrum transform to the NBS test lane measurements for six targets buried 3" deep in sandy loam with a 7% moisture content. The target areas were time-gated in detection processing and then the short data records of the target areas were transformed. As the figures indicate, six targets are easily detected and their spectra differ upon examination. Note that the MEM results are "spiked" in appearance due to resolution improvement.

The objectives of the discrimination algorithm addressed here are to (1) identify the resonant frequency information given by the spectra (whether it is obtained by FFT, MEM, or other methods), and (2) to correlate that information spatially across an object to determine whether the object is a possible man-made (mine-like) target.

4.4 ALGORITHM SPECIFICATION

In the first step, the peaks of the spectrum are found above a given threshold; their frequency value and amplitude are stored. The second step is to correlate the peaks of two spectra taken sequentially in time (corresponding to ground position).

The family of performance indicies chosen was:

$$P.I.\ (j:p,l,q) = (N_c)^P \sum_{i=1}^{N_c} \frac{\left[(A_i^j + A^{j-1})/2\right]^l}{\left|F_i^j - F_i^{j-1}\right|^q} \qquad (11)$$

where;

N_c = number of correlating peaks

F_i^j = natural resonant frequency peak

A_i^j = corresponding amplitude of peak

TABLE 9. FFT/MEM CHARACTERISTICS

	FOURIER	MAXIMUM ENTROPY
RESOLUTION OF TWO FREQUENCIES	$\propto 1/N$	$\approx 1/N^2$
BANDWIDTH OF PURE TONE	$\propto 1/N$	$\propto 1/(PN)^2$
PEAK POWER OF PURE TONE	$\propto P$	$\propto (PN)^2$
LINEARITY OF SPECTRUM	LINEAR	NON-LINEAR
WINDOW EFFECTS	LEAKAGE AND REDUCED RESOLUTION	NONE

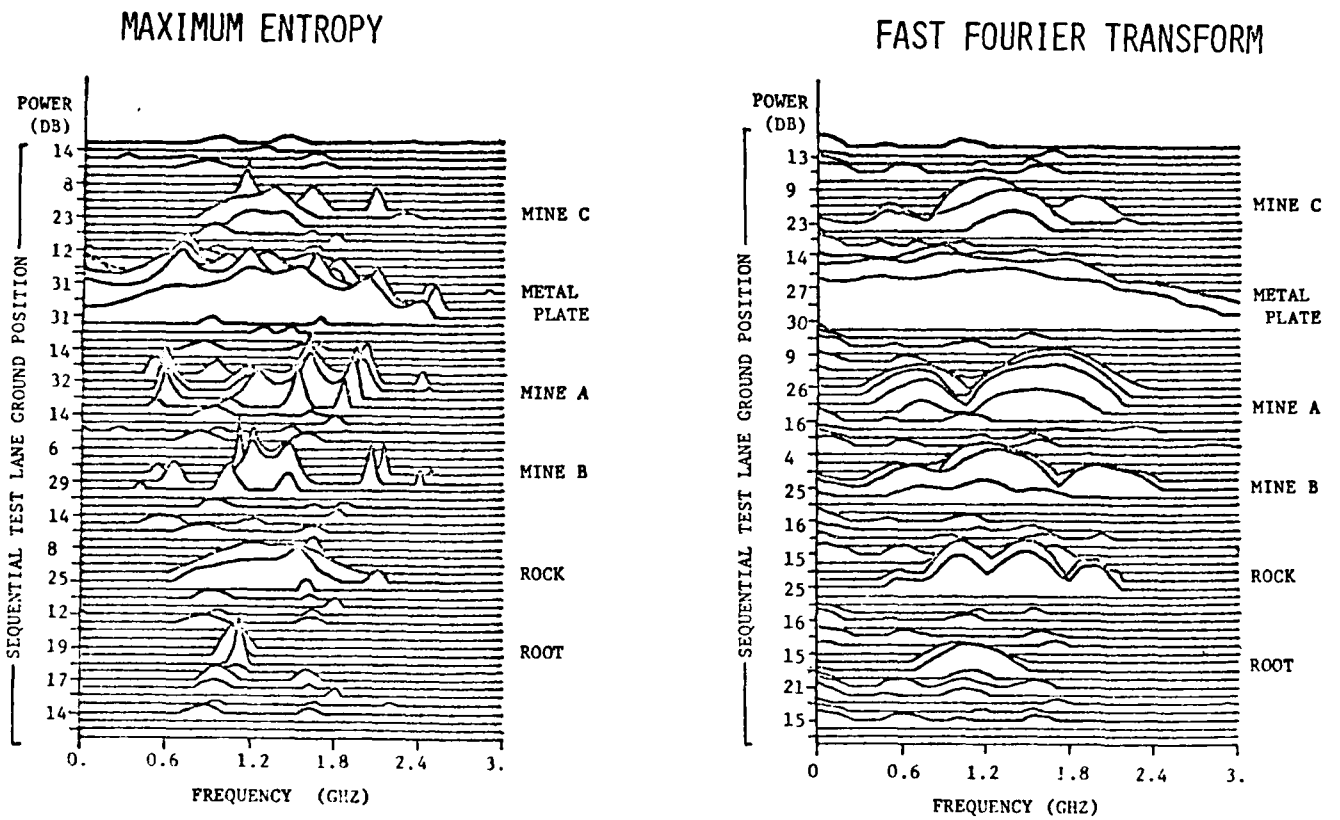

Figure 49. FFT/MEM spectra representation.

i = peak number.

j = spatial position number

p, l = integers, 0, 1, 2

q = integer, 1, 2

This family is a weighted sum of averaged-amplitudes of spatially matched peaks, including a weighting for spectrum complexity by multiplying the sum by the number of correlated peaks.

Strong frequency matching and large amplitudes increase the performance index. In all cases, the difference term in the demoninator is not allowed to be ≤ 1.

4.5 PERFORMANCE COMPARISON

All combinations of the family were evaluated by computer and normalized for comparison. Figure 50 and 51 are the results of this evaluation applied to both the FFT spectra and the MEM spectra. Not all, certainly, are practical algorithms, and the results over many sets of runs indicated an advantage for the particular indices given by

$$P.I.\ (j:0,2,1) = \sum_{i=1}^{N_C} \frac{\left[(A_i^j + A_i^{j-1})/2\right]^2}{\left|F_i^j - F_i^{j-1}\right|} \tag{12}$$

or FFT spectra, and by

$$P.I.\ (j:2,2,2) = (N_C)^2 \sum_{i=1}^{N_C} \frac{\left[(A_i^j + A_i^{j-1})/2\right]^2}{\left|F_i^j - F_i^{j-1}\right|^2} \tag{13}$$

or MEM spectra.

By inspection, it is seen that that number of peaks is important in the MEM case; which is a direct result of the MEM spectra having a large number of identified frequencies. Figure 52 illustrates the value of these two performance indices for both the MEM and FFT spectra over all ground positions for the data of Figure 49. The MEM performs better in both cases, with the best results for P.I. (j:2,2,2). All others

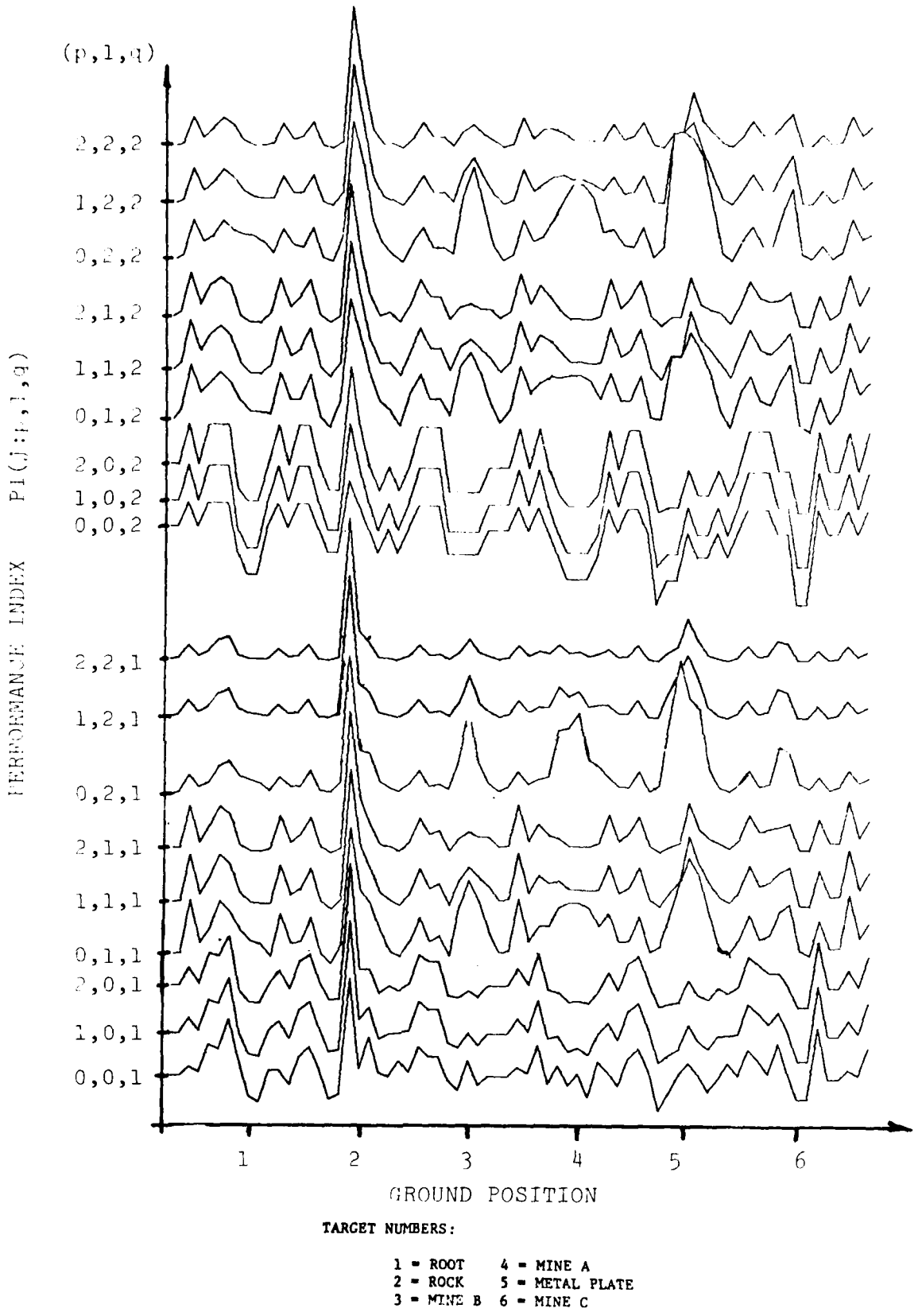

Figure 50. Performance index results: FFT spectra.

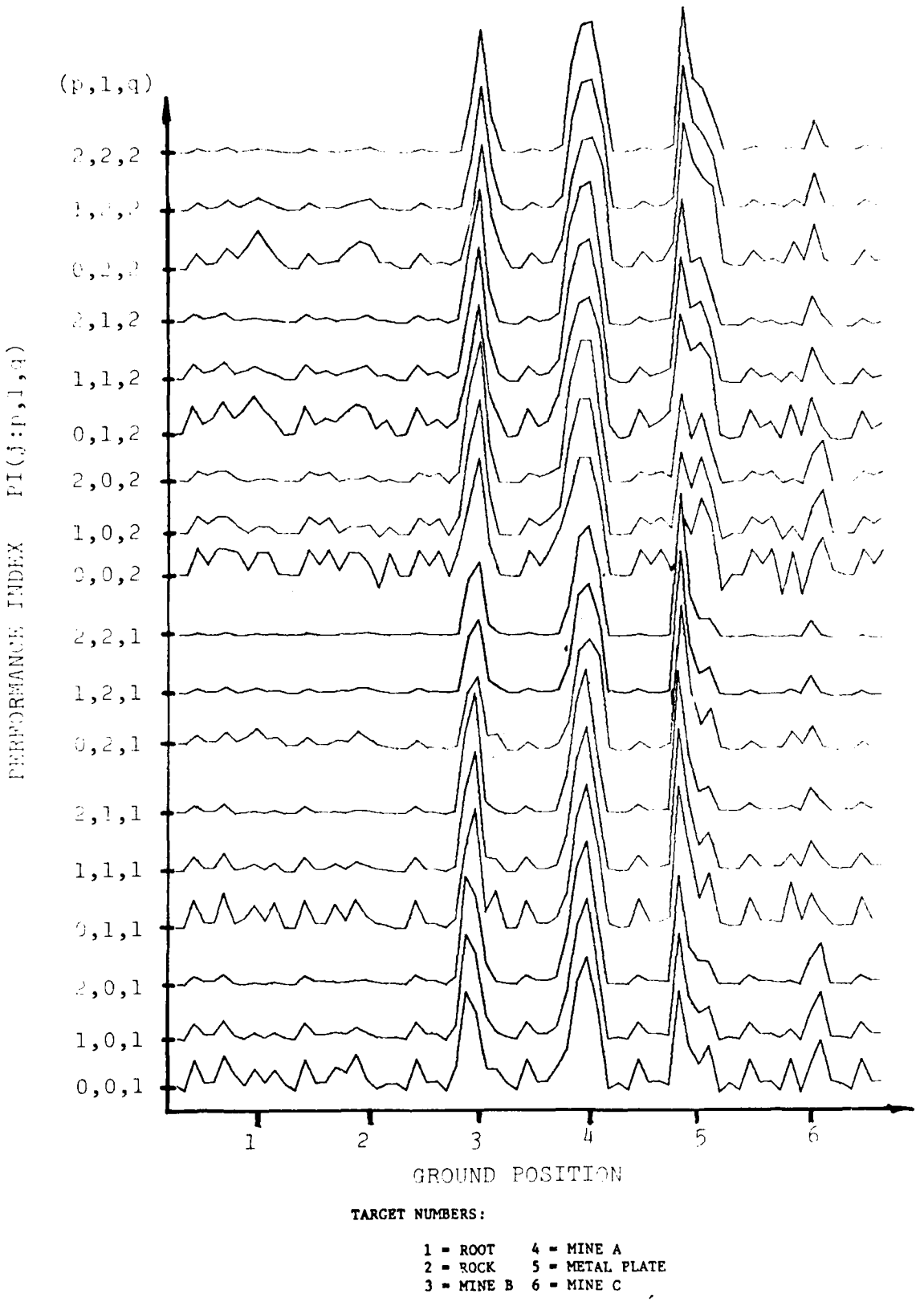

Figure 51. Performance index results: MEM spectra.

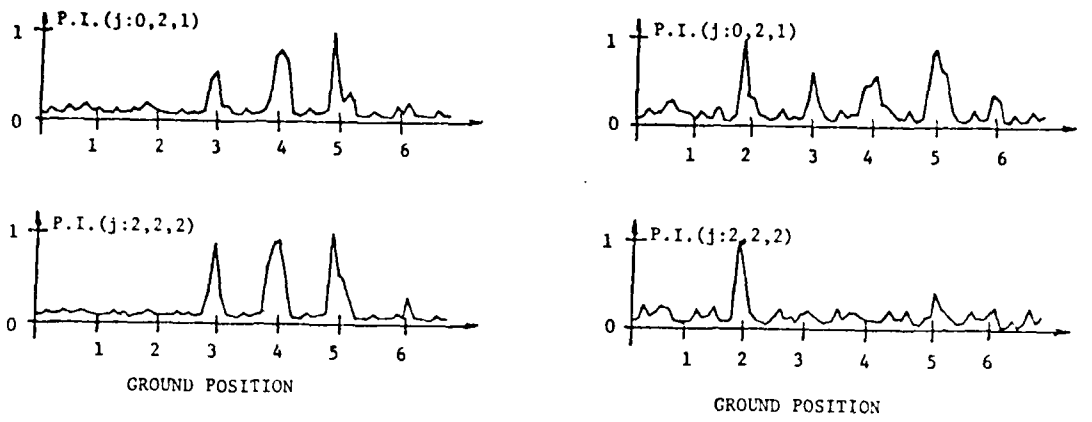

MAXIMUM ENTROPY

FOURIER TRANSFORM

TARGET NUMBERS:

1 = ROOT
2 = ROCK
3 = MINE B
4 = MINE A
5 = METAL PLATE
6 = MINE C

$$P.I.(J:0,2,1) = \sum \frac{(A_I^J + A_I^{J-1})/2}{\left| F_I^J - F_I^{J-1} \right|^2}$$

$$P.I.(J:2,2,2) = N_c^2 \sum \frac{\left[(A_I^J + A_I^{J-1})/2\right]^2}{\left| F_I^J - F_I^{J-1} \right|^2}$$

Figure 52. FFT/MEM best performance.

in the family yielded poorer results. It must be noted that this family is by no means the only, nor has it been completely exhaustive in form. But its simplicity and successful results, thus far, give creedence to its future use and further development.

SECTION 5
CONCLUSIONS

The collection and analysis of data taken with the NBS automatic network analyzer and the MERADCOM short pulse radar for the purposes of verification of equivalency and identification of salient features were completed. Temporal and spectral plots for the NBS data and temporal plots for the SPR data were examined and compared. Visual inspection indicates that both temporal and spectral responses of the buried objects differ sufficiently to allow discrimination of objects of interest. Indications were that new antenna designs to be considered should have low-disperision and wide bandwidth. This will allow the high resolution waveform (very short pulse) measurement capability to be preserved. The high resolution (wide bandwidth) is the key element that will drive the performance of the discrimination/classification algorithms.

Antenna designs were considered, and the results indicated that a TEM horn and a cavity-backed spiral were the best candidates. Fabrication of prototypes of these antennas was completed. Tests provided information as to the reflection and impedance properities. Indications are that both antennas have slightly poorer performance than the Calspan horn, as was expected. But, both the 1/4th the size and man-portable. Processing techniques can be uses to compensate for the loss in performance, so this was not perceived as a problem. The TEM horn incorporates several new design concepts and is an important result of this work. Key aspects of the TEM horn are the tapered resistive loading on the H-plane walls, the feed design, the non-contracting partial sidewalls, and the flare geometry. The TEM horn is an excellent candidate for application to a man-portable mine detection/discrimination/classification system.

The data analyzed during this program indicates that the essential information needed for mine detection and discrimination is contained in the spectral range between 500 and 3,000 MHz. The experience gained during this work and related work at NBS indicates that the resistive TEM horn can be made to function very well with a short pulse radar for signals in this range; but if the MERADCOM radar were used, it might be desirable to remove the low frequency content of the transmitter pulse, to prevent ringing between the radar and the antenna.

A preliminary step was taken in the algorithm development area with the introduction and testing of a frequency-based discrimination technique. The method required high resolution data in the frequency domain. This was best achieved by the use of Maximum Entropy Methods for spectral representation. the discrimination algorithm rejects non-mine objects, such as roots, rocks. Data sets accepted in the discrimination process would then be passed on to a classifier.

As mentioned in the introduction, the funding was cut short on this work and as a result only tasks I, II, and III were completed. Some work was also started on Task V.

The new antennas developed on this project should be fully evaluated as to their performance for the mine detection work. Extensive data should be collected so that an adequate learning set is available. The signal processing algorithm development should then be completed. After evaluating the performance of the algorithms, a processing hardware configuration for implementating the algorithms should be specified.

REFERENCES

1. "Mobile Microwave Test Set Operating and Maintenance Manual," National Bureau of Standards, unpublished manuscript.

2. "S-Parameters ... Circuit Analysis and Design", Hewlett-Packard Application Note 95, September 1968.

3. "Radar Detection, Discrimination, and Classification of Buried Non-Metallic Mines:, J. D. Echard, J. A. Scheer, E. O. Rausch, W. H. Licata, J. R. Moore, and J. A. Neston, Georgia Institute of Technology Engineering Experiment Station, Final Technical Report, February 1978.

4. "Antennas and Pulsers for a Vehicular-Mounted Mine Detector (U)," Calspan Report #MA-5366-E-1, M. E. Bechtel and A. V. Alongi, September 1974.

5. Discriminator and Display for Vehicular-Mounted Mine-Detector Radar (U)," CALSPAN Report #MA-5366-E-2, M.E. Bechtel and A. V. Alongi, June 1976.

6. R. J. Wohlers, "The GW1A, An Extremely Wide Bandwidth Low-Dispersion Antenna," Abstracts of the Twentieth Annual Symposium: USAF Antenna Research and Development Program, Allerton Park, Illinois, October 1970.

7. S. Rehnmark, "On the Calibration Process of Automatic Network Analyzer Systems," IEEE Trans. Microwave Theory and Techniques, Vol. MTT-22, pp. 457-458, April 1974.

8. "Automating the HP 8410B Microwave Network Analyzer," Hewlett-Packard Application Notes 221, 221A, June 1980.

9. M. Kanda, "A Relatively Short Cylindrical Broadband Antenna with Tapered Resistive Loading for Picosecond Pulse Measurements," IEEE Trans. Antennas and Propagation, Vol. AP-26, pp. 439-447, May 1978.

10. M. Kanda, "The Time Domain Characteristics of a Traveling-Wave Linear Antenna with Linear and Non-Linear Loads," NBSIR-78-892, National Bureau of Standards, February 1979.

11. M. Kanda, "The Effects of Resistive Loading on TEM Horns," NBSIR-79-1601, National Bureau of Standards, August 1979.

12. M. Kanda, "Transients in a Resistively Loaded Linear Antenna Compared with Those in a Conical Antenna and a TEM Horn," IEEE Trans. Antennas and Propagation, Vol. AP-28, pp. 132-136, January 1980.

13. C. Gerst and R. A. Worden, "Helix Antennas Take a Turn for the Better," Electronics, pp. 100-110, August 1966.

14. G. A. Deschamps and J. D. Dyson, "The Logarithmic Spiral in a Single-Aperture Multimode Antenna System," IEEE Trans. Antennas and Propagation, Vol. AP-19, pp. 90-96, January 1971.

15. G. A. Deschamps, "Impedance Properties of Complementary Multiterminal Planar Structures," IRE Trans. Antennas and Propagation, Vol. AP-7 (Supplement), pp. S371-S.378, December 1959.

16. B. R. S. Cheo, V. H. Rumsey, and W. J. Welch, "A Solution to the Frequency-Independent Antenna Problem," IRE Trans. Antennas and Propagation, Vol. AP-9. pp. 527-534, November 1961.

17. E. K. Miller and J. A. Landt, "Short-Pulse Characteristics of the Conical Spiral Antenna," IEEE Trans. Antennas and Propagation, Vol. AP-25, pp. 621-626, September 1977.

18. B. R. Mayo, P. W. Howells, and W. B. Adams, "Generalized Linear Radar Analysis," Microwave Jour., pp. 79-84, August 1961.

19. D. L. Sengupta and C. T. Tai, "Radiation and Reception of Transients by Linear Antennas," Chapter 4 in Transient Electromagnetic Fields, L. B. Felsen, Ed., New York: Springer-Verlag, 1976.

20. T. T. Wu and R. W. P. King, "The Cylindrical Antenna with Non-reflecting Resistive Loading," IEEE Trans. Antennas and Propagation. Vol. AP-13, pp. 369-373, May 1965.

21. L. C. Shen and T. T. Wu, "Cylindrical Antenna with Tapered Resistive Loading, "Radio Science, Vol. 2, pp. 191-201, February 1967.

22. D. E. Isbell, "Log-Periodic Dipole Arrays," IRE Trans. Antennas and Propagation, Vol. AP-8, pp. 260-267, May 1960.

23. R. J. Blum, "Analysis of an Orbiting Low-Frequency Radio Telescope," Abstracts of the Twentieth Annual Symposium: USAF Antenna Research and Development Program, Allerton Park, Illinois, October 1970.

24. "A Characterization of Sub-Surface Radar Targets", Luen Chan, David Moffatt, and Leon Peters, Proceedings of the IEEE, Vol. 67, No. 7, July 1979.

25. Modern Spectrum Analysis, Donald G. Childers, IEEE Press, John siley & Sons, Inc., 1978.

26. "Linear Prediction and Maximum Entropy Spectral Analysis for Radar Applications", S. B. Bowling, MIT Lincoln Laboratory Project Report RMP-122, 24 May 1977.